SPATIO-TEMPORAL MODELLING AND ANALYSIS OF EPILEPTIFORM EEG

A THESIS SUBMITTED TO THE UNIVERSITY OF MANCHESTER
FOR THE DEGREE OF DOCTOR OF PHILOSOPHY
IN THE FACULTY OF ENGINEERING AND PHYSICAL SCIENCES

2011

By
Marc Goodfellow
School of Chemical Engineering and Analytical Science: Doctoral Training Centre
Integrative Systems Biology: From Molecules To Life

Contents

Word count: 43,128

List of Tables

List of Figures

Abstract

"Spatio-temporal modelling and analysis of epileptiform EEG".
A thesis submitted to the University of Manchester for the degree of
Doctor of Philosophy by Marc Goodfellow, 2011.

In this thesis we investigate the mechanisms underlying the generation of abnormal EEG rhythms in epilepsy, which is a crucial step towards better treatment of this disorder in the future. To this end, macroscopic scale mathematical models of the interactions between neuronal populations are examined. In particular, the role of interactions between neural masses that are spatially distributed in cortical networks are explored. In addition, two other important aspects of the modelling process are addressed, namely the conversion of macroscopic model variables into EEG output and the comparison of multi-variate, spatio-temporal data. For the latter, we adopt a vectorisation of the correlation matrix of windowed data and subsequent comparison of data by vector distance measures.

Our modelling studies indicate that excitatory connectivity between neural masses facilitates self-organised dynamics. In particular, we report for the first time the production of complex rhythmic transients and the generation of intermittent periods of "abnormal" rhythmic activity in two different models of epileptogenic tissue. These models therefore provide novel accounts of the spontaneous, intermittent transition between normal and pathological rhythms in primarily generalised epilepsies and the evocation of complex, self-terminating, spatio-temporal dynamics by brief stimulation in focal epilepsies.

Two key properties of these models are excitability at the macroscopic level and the presence of spatial heterogeneities. The identification of neural mass excitability as an important processes in spatially extended brain networks is a step towards uncovering the multi-scale nature of the pathological mechanisms of epilepsy. A direct consequence of this work is therefore that novel experimental investigations are proposed, which in itself is a validation of our modelling approach. In addition, new considerations regarding the nature of dynamical systems as applied to problems of transitions between rhythmic states are proposed and will prompt future investigations of complex transients in spatio-temporal excitable systems.

Declaration

No portion of the work referred to in this thesis has been submitted in support of an application for another degree or qualification of this or any other university or other institute of learning.

Copyright

i. The author of this thesis (including any appendices and/or schedules to this thesis) owns certain copyright or related rights in it (the "Copyright") and s/he has given The University of Manchester certain rights to use such Copyright, including for administrative purposes.

ii. Copies of this thesis, either in full or in extracts and whether in hard or electronic copy, may be made **only** in accordance with the Copyright, Designs and Patents Act 1988 (as amended) and regulations issued under it or, where appropriate, in accordance with licensing agreements which the University has from time to time. This page must form part of any such copies made.

iii. The ownership of certain Copyright, patents, designs, trade marks and other intellectual property (the "Intellectual Property") and any reproductions of copyright works in the thesis, for example graphs and tables ("Reproductions"), which may be described in this thesis, may not be owned by the author and may be owned by third parties. Such Intellectual Property and Reproductions cannot and must not be made available for use without the prior written permission of the owner(s) of the relevant Intellectual Property and/or Reproductions.

iv. Further information on the conditions under which disclosure, publication and commercialisation of this thesis, the Copyright and any Intellectual Property and/or Reproductions described in it may take place is available in the University IP Policy (see
http://www.campus.manchester.ac.uk/medialibrary/policies/intellectual- property.pdf), in any relevant Thesis restriction declarations deposited in the University Library, The University Librarys regulations (see
http://www.manchester.ac.uk/library/aboutus/regulations) and in The University's policy on presentation of Theses

Acknowledgements

Chapter 1

Introduction

Epilepsy mechanisms and dynamic EEG state transitions

Epilepsy is a prevalent neurological disorder which manifests as a predisposition for the brain to undergo transient seizure periods (Fisher et al., 2005) caused by abnormal neuronal activity. The predominant means of imaging neuronal activity in epilepsy is the electroencephalogram (EEG) due to its favourable time resolution, low cost and non-invasiveness. The EEG measures electrical field potentials (see Chapter 5) via a series of electrodes placed on the scalp (scalp EEG), or implanted inside the skull (ECoG or depth electrodes), and acts as a biomarker for different normal brain states such as waking, sleep, stimulus processing, as well as pathological states such as epileptic seizures. Often, these states are distinguished on the EEG by the presence or absence of certain rhythms, i.e. repetitive or periodic time evolving signals. Since clinical EEG consist of recordings from multiple electrodes, these projections of the abnormal processes of epilepsy are spatially distributed, multi-variate time series, or equivalently, dynamic spatio-temporal patterns. Thus, the problem of understanding the mechanisms of clinical epilepsy is inseparable from the problem of understanding transitions between dynamic, spatio-temporal states of the EEG. Improving our understanding of the spatio-temporal mechanisms responsible for EEG transitions in epilepsy is a key problem we wish to investigate in the current thesis.

Temporal properties

EEG rhythms associated with epileptic processes (epileptiform rhythms) can be revealed, in most cases, by visual inspection. Some of the key temporal features distinguishing epileptiform rhythms from "background" EEG are waveform, frequency, amplitude and stereotypy. Observations or analyses of temporal, as well as spatial aspects reveal a rich diversity in the EEG manifestation of seizures, which are associated with a range of physical symptoms. However, certain features of the data

observed as well as the symptoms experienced during seizure support a classification of different seizure types (ILAE, 1981). In turn, patients experiencing seizures with certain characteristics may be classified as having a particular epilepsy syndrome when combined with other information such as the age of the patient and the potential cause of the seizure (ILAE, 1989).

A classic example of salient temporal features during an epileptiform rhythm can be seen in the EEG during absence seizures (see Figure 4.2), which are accompanied clinically by a brief period of impaired consciousness and often minor motor manifestations such as eye lid fluttering. In this case, seizures are identifiable on the EEG by a sudden onset and offset of high amplitude slow rhythms with a characteristic multi-modal morphology, known as the spike-wave discharge (SWD). Other common features, seen in different seizure types, include a possible high frequency and low amplitude onset to seizure activity, high amplitude rhythms during seizure, and a slowing of rhythms towards the end of a seizure. Patients with certain epilepsies can also present transient inter-ictal abnormal activity, such as inter-ictal spikes or slow waves. Others might be susceptible to initiation of abnormal EEG rhythms due to stimulus, for example in the photo-paroxysmal response.

EEG abnormalities are visually identifiable because of their contrast to "normal", or "background" EEG. The normal waking EEG of the adult is characteristically low amplitude, and of an apparently random nature. Investigation of the frequency spectrum reveals a predominantly $1/f$ distribution of power, often with excess contribution in the alpha frequency band at around 10Hz.

Spatial properties

The spatial characteristics of epileptiform EEG are other important, variable features, and as such form a high level classification of seizure types as *focal* versus *generalised* events. Generalisation here refers to the appearance of abnormal activity on all (or at least the majority of) recording electrodes, and can apparently occur with the onset of seizures in the case of primary generalisation (e.g. absence seizures, or idiopathic generalised seizures (IGE)), or can more obviously evolve from an initially focal distribution in the case of secondary generalisation. Abnormal activity on the EEG during focal seizures, on the other hand, initiates in, and remains restricted to, isolated regions of brain tissue. Improving our understanding of the mechanisms of focal onset (even in the case of primary generalisation, see Chapter 4 and e.g. Meeren et al. 2002) and spreading or restriction of abnormal activity, at the level of the EEG, is another important motivating factor for the current thesis. Clearly, in order to address the spatio-temporal dynamics of epileptiform rhythms, one must consider the influence of connectivity in the brain. The general aim of the current thesis is therefore to investigate the mechanisms of epileptiform rhythms

using spatially extended mathematical modelling. In addition to presenting models for epileptiform rhythms and transitions (Chapters 3 and 4), the problems of comparing model output to clinical EEG (Chapters 5 and 6) are also discussed.

Structure of the thesis

In Chapter 2 the question of which modelling strategy to pursue is discussed, and leads to the conclusion that spatially extended neural mass models will be the focussed approach. In the two chapters that follow, two applications of this strategy are described which provide insight into two different epileptic phenomena, namely the repetitive response to stimulation (Chapter 3, (Valentin et al., 2002; Valentín et al., 2005; Flanagan et al., 2009)) and the spontaneous occurrence of absence seizures (Chapter 4, e.g. (Snead, 1995)). This latter chapter provokes further considerations of the generation of epileptiform EEG, which are discussed in Chapter 5. The problem of quantification and comparison of spatio-temporal patterns via multi-variate time series analysis is introduced in Chapter 6. In Chapter 7, the implications of the work are discussed and the main conclusions are summarised.

The main results of Chapters 3 and 4 are presented in an article in press (Goodfellow et al., 2011b) and in the publication Goodfellow et al. (2011a), respectively.

Chapter 2

Macroscopic modelling of brain dynamics

2.1 Overview

Observations and statistical analyses can help catalogue properties of neurological data and allow us to compare output under different conditions. However, understanding the mechanisms that *cause* our data observations requires mathematical models of dynamical systems (Breakspear and Jirsa, 2007). There is a long history of mathematical modelling (i.e. using systems of coupled ordinary differential equations to observe the effect of plausible mechanistic interactions) in relation to problems in neuroscience (e.g. references in Gerstner and Kistler 2002; Deco et al. 2008). Indeed, the pioneering work of Hodgkin and Huxley, who made quantitative models of action potentials in the giant axon of the squid (Hodgkin and Huxley, 1952), is often cited as an early example of quantitative modelling in complex biological systems (Crampin et al., 2004; Hunter and Nielsen, 2005), and can therefore be considered a forebear of systems biology or computational physiology.

In attempting to understand brain dynamics, models are typically formulated at one of two different scales, roughly speaking. At the *microscopic* scale, the activity of individual neurons is the observation of interest. In this case, a mathematical system is formulated based upon the components and mechanisms that influence the dynamics of a single neuron, for example ion concentrations, membrane potentials and voltage dependent conductances. The classical model formulation of these processes was described by Hodgkin and Huxley (1952). The microscopic level of modelling can also be extended to include networks of individually modelled neurons, and in this case can also incorporate further abstractions regarding the exact mechanisms leading to neuronal dynamics. One of the major features of neuronal activity is the action potential spike, and this feature has been abstracted in certain reduced forms of the Hodgkin-Huxley model, such as the Fitzhugh-Nagumo model (Fitzhugh, 1961; Nagumo et al., 1962; Gerstner and Kistler, 2002), which retain the

important feature of *excitability* (see Chapter 3) to generate action potential spikes. At the microscopic level, the mechanisms of synchronisation in neural networks is a fundamental question in investigations of the mechanisms of epilepsy (Traub and Wong, 1982; Destexhe, 1998; Bazhenov et al., 2008).

It is clear that modelling at the microscopic scale is particularly appropriate when data observations reside at the level of recordings from single cells or relatively small networks of cells. The goal of modelling in this case is to account for observations in the microscopic data by relating them to appropriate variables in a microscopic model, in which the mechanisms are known. However, as described in Chapter 1 our observations of the mechanisms of epilepsy in humans most often reside at the level of EEG recordings, and these derive from current sources due to (post-synaptic) activity in large regions of nervous tissue (for more details refer to Chapter 5 and e.g. Nunez 1981). Thus, mechanistic modelling of human epileptiform EEG at the microscopic scale presents a number of important problems. Firstly, the specific microscopic mechanisms have to be described in detail for a large region of nervous tissue. Since there are approximately 10,000 neurons and as many synapses per neuron in the cortical column, this represents a major challenge (Markram, 2006). Difficulties in the application of such a model are due to the complexity of i) the description of the underlying physiological system and ii) the way in which it can be analysed in terms of perturbations of its many parameters in order to uncover the mechanisms for generation of abnormal activity.

Thus it is clear that, in order to address the mechanisms underlying epileptiform EEG rhythms, a modelling strategy based at the *macroscopic* scale is important. At this level, state variables represent the activity of *populations* of neurons (see e.g. Wilson and Cowan 1973; Deco et al. 2008; Coombes 2010). From the systems biology point of view, it is interesting to note that both *bottom up* and *top down* approaches have been employed to account for the dynamics of populations of neurons.

An example of the bottom up approach is the continuum formulation of Wilson and Cowan (1973), and later that of Amari (1977). These models are derived from several important assumptions. Firstly, cortex is assumed to be effectively two-dimensional, with local populations of neurons being approximated by activity within a vertical column. In these formulations, tissue is continuous, with activity described at each spatial location on the continuum. The dynamics of local activity is assumed to be due to the influence of inhibitory and excitatory afferents from other locations in the brain. Thus one of the main components of the evolution equation for a point on the continuum relates to a weighted sum over the activity at other regions in the model, with negative weighting for inhibition. The other crucial component in this formulation is a non-linear, sigmoid curve into which the afferent activity is placed in order to determine the activity (population firing rate)

at the current location. This non-linearity is based upon there being an underlying Gaussian distribution of states or membrane thresholds, above which individual neurons in the mass will fire. The density of neurons whose threshold is below the current population membrane potential is given by the cumulative probability over the Gaussian curve, which results in a sigmoid function (see section 2.3).

Pioneering top down approaches have been introduced by Freeman (Freeman, 1975). Although several features of models resulting from top down and bottom up formalisms coalesce, it is important to identify a distinction here between the two approaches. Whilst Wilson-Cowan and subsequent researchers place an emphasis on the derivation of the activity of neural masses from properties of interactions amongst neurons, Freeman emphasises the neural mass as a new entity in the nervous system, which we might expect to have emergent properties. Thus a tenet of his work is to catalogue the response of neural masses to stimulation, and then use these observations in conjunction with considerations on the underlying physiological aspects of the mass. It is important to consider that neural mass activity might not be entirely attributable to neuronal or afferent activity, especially given that the constituents of the cortical mass are not only neuronal (Liley et al., 2002). However, it is often the properties of neurons, such as spiking, excitatory and inhibitory processes, membrane and axonal delays etc., that constitute our population or neural mass theories. Indeed, a different approach to modelling populations of neurons is the "mean field" model which explicitly accounts for statistical properties of the distribution of states of neurons in a population (Deco et al., 2008). Determining the degree to which population activity can be derived bottom up, and exactly which emergent aspects are important will be crucial in the future for making truly multi-scale models of brain activity.

A different perspective on the modelling of activity of populations of neurons was introduced by Lopes Da Silva et al. (1974). In this work, a network of microscopic level neurons was simulated in an investigation of the alpha rhythm. In an important step towards accounting for the local field potential (LFP) rather than the *activity* of a population of neurons, the time course of post-synaptic potentials was explicitly incorporated, in a simple way. The network of neural elements in this study was referred to as a *distributed* model. In tandem, the authors also proposed a *lumped* version of their model. The lumped model assumed that the post-synaptic potential dynamics were representative of a population of neural elements, or a neural mass. This allowed the complexity of the explicit (distributed) neuronal network to be significantly reduced, and therefore allowed a systems analysis on the population dynamics over changes in lumped parameters.

There are thus pros and cons associated with the use of *continuum* or *neural mass/ lumped parameter* approaches. An advantage of the continuum type of model is that they are explicitly derived in terms of spatial interactions in nervous tissue.

However, since they in general do not provide time courses of post-synaptic potentials, and are formulated from theoretical rather than empirical considerations, it is unclear in what way they relate to the generation of the EEG. This is in contrast to neural mass approaches which either account for post-synaptic activity or are derived from observations of modulations in cortical output under certain changes of input.

The above models represent a local view of the generation of brain rhythms. That is, they assume that temporal oscillations seen on the EEG can be accounted for by local circuitry with oscillatory capability. An alternative view to this is the possibility that certain brain rhythms are the result of global wave properties of the brain as a conducting medium (Nunez 1981, Chapter 11). In this context, Nunez emphasises several important perspectives with respect to the generation of EEG activity. In particular, it is recognised that the activity at a macroscopic scale can be formed as the average of activity at spatial scales below this (Nunez 1995, Chapter 1). In addition, the dynamics of EEG are captured in a spatially extended wave equation based on inherent delays and spatial scales of cortico-cortical interactions. This emphasis on spatio-temporal generation of travelling or standing waves highlights several limitations of models accounting for EEG rhythms in the output of a spatially localised neural mass. In particular, that a neural mass model can generate a certain rhythm does not imply that this will persist in the obvious spatial extension to that system. Coupled oscillators can introduce new modes, other than those inherent in the individual oscillators (Nunez, 1981). A further complication to an account of EEG waves based on a local mass with a single oscillatory mode is that time scales are likely to be heterogeneous so that it is unclear whether averaged activity at the level of the EEG is likely to reflect this oscillatory mode (Nunez, 1981). However, epileptic rhythms present a richer spatio-temporal dynamics than simple standing or travelling waves. For example, heterogeneous oscillations can be seen in focal onset seizures, as can localised slow waves, spikes or SWD. In addition, the spatial scale of recordings can determine whether abnormal rhythms are present at all (Stead et al., 2010).

It is clear that there are a wide range of tools with which to tackle the problem of understanding macroscopic mechanisms of epileptiform rhythms. Many of the previous studies into the EEG dynamics of epileptic tissue have utilised neural mass models (see e.g. Wendling et al. (2002); Breakspear et al. (2006)). Therefore, the spatially extended interactions between neural masses is a good starting point for our investigation into spatio-temporal dynamics of epilepsy, and thus will form the basis for the modelling aspects of this thesis. The reasons for this approach are elucidated in the following section, which forms a more in depth review of this type of model and its application to epilepsy.

2.1.1 Neural mass models

In terms of the fundamental principles of network communication in the nervous system, neurons can be thought to behave as input to output converters (Freeman, 1975). In this model, afferent pulse trains of action potentials provide input by causing a temporally smeared propagation of membrane potential change down to the soma. At this juncture, the neuron will fire an action potential if the soma membrane potential is above threshold, therefore producing output. The neural mass framework abstracts this model to the population level by utilising two conversion operators. The first is "pulse to wave", in which incoming population pulse densities are temporally filtered by the action of post-synaptic potentials in the dendrites and by the cable properties to induce a change of membrane potential at the soma. These waves are then summed at the soma, and the population output is determined by the second conversion operator, the "wave to pulse". The principle of these two conversion operations are conserved in many different derivations of neural mass models. Often, the sigmoid function is used to convert wave to pulse, and is assumed to represent a gaussian distribution of underlying states or firing thresholds within the population. Crucially it captures a non-linear property of neural masses in providing saturation of their output in networks of connected populations. In the pioneering study of of Lopes Da Silva et al. (1974), the pulse-to-wave conversion was mediated in the lumped system by the time profiles of post-synaptic potentials. These delays, together with temporal smearing of activity due to cable properties are often described as the physiological basis for this component of the system (Robinson et al., 1997). With this interpretation, the neural mass can be viewed as a "grey box" model, as its dynamics can be related in some way to physiological mechanisms (Ortega et al., 2008).

The neural mass is often used to examine the possible role of interactions between different neural populations for the generation of rhythms (Lopes Da Silva et al., 1974; Freeman, 1975). In this way, a notation was introduced by Freeman to describe the complexity of the resulting network. The isolated mass, in its "open loop" form is denoted $K0$, whereas two connected $K0$ sets form a $K1$ set, etc. These networks of neural masses have been investigated extensively in relation to the activity of the olfactory bulb (Freeman, 1975).

A famous example of the neural mass model, which has been used in a wide range of applications is the model proposed by Jansen et al. (1993); Jansen and Rit (1995). This model was derived to provide a mechanistic account for the generation of sensory evoked potentials, and is based upon an important canonical circuit in the brain. The circuitry modelled is the network of principal (pyramidal) neurons, which incorporates both excitatory and inhibitory feedback. Its three components are, explicitly, i) pyramidal cells, ii) inhibitory interneurons and iii) excitatory interneurons

(stellate cells). In the Jansen model the inhibitory and excitatory post-synaptic potentials on pyramidal neurons are explicitly modelled (motivated by the lumped parameter model of Lopes Da Silva et al. (1974)). Since these processes operate on time scales equivalent to processes that contribute to the EEG, this model is an obvious starting point for an investigation of clinical data in epilepsy. Further considerations on the ways in which neural mass models can be used to account for epileptic EEG are given in Chapter 5.

Indeed, an investigation of the dynamics of the Jansen model revealed the presence of spiking solutions, as well as lower amplitude oscillations (Jansen and Rit, 1995). This led to the incorporation of mass modelling to investigate the mechanisms underlying epileptiform EEG by Wendling et al. (2000). In these early studies it was noted that a noise driven system could produce inter-ictal spiking like waveforms, and that periodic spiking could be seen under the same noise driving with different parameters (Wendling et al., 2000). This was an important demonstration of the way in which neural mass models could be used to account for the transition between different rhythms observed on recordings from epileptic patients, and has sparked much subsequent interest. Importantly, Wendling also used this model to investigate whether connectivity between different spiking regions could be inferred from the measured signals (Wendling et al., 2001). This provided a first insight into the effect of connectivity in these spiking neural masses, for example in the transference of spiking between regions. We expand on this idea in our model proposed in Chapter 3.

The mathematics behind Wendling's observations were formalised in bifurcation analyses by Grimbert and Faugeras (2006) and later by Spiegler et al. (2010). This latter paper accounted for the interim expansions of the Jansen model to incorporate additional important physiological aspects. These expansions are in the spirit of the formation of higher "Ki" sets by Freeman. In one such study, it was shown that many features of the dynamic transitions in focal epilepsies could be modelled by changing parameters in an extended neural mass model (Wendling et al., 2002). Other, more recent developments include the incorporation of a forward model to better account for the generation of spikes and infer on the size of the required region of activity (Cosandier-Rimélé et al., 2008) as well as the development of whole brain, hierarchical extensions to the neural mass framework (Sotero et al., 2007; Babajani-Feremi and Soltanian-Zadeh, 2010).

Alongside these models of focal epilepsies, neural mass models have also been used to investigate transitions into absence seizures in thalamocortical networks (Suffczynski et al., 2004; Breakspear et al., 2006). Suffczynski et al. (2004) found that a model of the thalamocortical system of the rat could support a bistability between steady state and oscillations, which when perturbed by noise could produce spontaneous transitions from background into high amplitude rhythms. An

alternative mechanism for seizure onset was given by Breakspear et al. (2006), who mapped the global bifurcation structure of the thalamocortical neural field model of Robinson et al. (1997) and showed that certain parameter sets could display absence seizure-like rhythms. Interestingly, this model could also display rhythms associated with generalised tonic-clonic seizures. Thus, a unified model of generalised epilepsies was proposed in which pathological oscillations could occur if deviations were made in the parameter set of a fixed model structure (thalamocortical system).

These two different modelled routes into seizure highlight one of the major endeavours in epilepsy research, which is to search for the mechanisms of the onset and offset of seizure activity. They also demonstrate the potential of the analysis of macroscopic, non-linear dynamical systems to frame this problem in a concise and useful way. The formalisation of these ideas has been provided in a number of studies (see e.g. Lopes da Silva et al. (2003a); Milton (2010)), and will be discussed in greater detail in the introduction and discussion of Chapter 4.

2.2 Spatially extended macroscopic models

Robinson et al. (1997) provided a major advance by introducing a wave equation for propagation of activity in the cortex, based on previous considerations by Jirsa and Haken (1996) and Wright et al. (1994). This synthesised the mass modelling framework into a tractable spatially continuous system, known as a *neural field.* Another feature of the works of Robinson, and of Wright and Liley (see e.g. Wright et al. (1994)) has been to emphasise the physiological plausibility of macroscopic models. Wright et al. (1994) aimed to make quantitative estimates of connectivity parameters in their model whilst Robinson et al. (1997) emphasise the characteristic length scale of synaptic connectivity, for example. However, it is clear that these parameters, and even the concept of neural masses or neural fields retain an abstract quality and that their exact nature demands further investigation in the future.

An important contrast between neural mass and neural field models is that the latter model EEG by the excitatory field which propagates in the cortex. This is in contrast to the mass models of, for example, Lopes Da Silva et al. (1974); Jansen and Rit (1995), which relate the EEG directly to the net depolarisation due to post-synaptic membrane changes, i.e. a net post-synaptic potential. Neither of these methods rely on a mechanistic derivation of the EEG in relation to model variables, for example in terms of induced current flow, which, if addressed, may represent an important advance (Avitan et al., 2009). Currently used mass models therefore assume the EEG to be proportional either to the activity of pyramidal neurons or their net depolarisation at the soma. Though this may be adequate in cases where frequency properties are the features of interest, and therefore the choice of model output matters less, in the case of epilepsy we are often concerned with the task

of elucidating mechanisms for distinctive multi-modal waveforms such as the spike wave discharge (SWD). In this case it is clear that one should, in addition, take into account the contribution of inhibitory PSPs and also the depth at which afferent activity arises. Current source density analysis has shown that these laminar profiles of activity can be complex and time varying in animal models of generalised seizures (Kandel and Buzsáki, 1997). These matters are discussed further in Chapter 5.

The question of the origin of spatio-temporal patterns in EEG and ECoG during epileptiform events is difficult but crucial in advancing our understanding of epilepsy. One of the key questions is whether it is appropriate to examine spatially continuous systems or interacting, discretised local masses, where discrete network structure is a facet of interest in the latter. In any case, the computational simulation of models derived from a continuum approach requires a discretisation at some arbitrary resolution. It is plausible that epilepsy is characteristic of a state of the brain in which assumptions regarding continuity of connectivity or homogeneity are no longer valid. In particular, isolated epileptiform rhythms have been observed at a variety of spatial scales, including those of the order of micrometres (on micro-electrodes) (Stead et al., 2010). Recent work has demonstrated that these rhythms are likely not attributable to volume conduction, which highlights the importance of considering local mechanisms for the production of epileptiform rhythms, and their subsequent spreading (Schevon et al., 2010). It will be the aim of the current thesis to begin an investigation of the effects of spatial interactions between *local neural masses*, in particular those that are capable of displaying epileptic dynamics.

Motivated by this discussion, we will focus upon simulating discrete networks of connected neural masses in order to increase our understanding of the mechanisms of epileptiform rhythms.

2.3 The neural mass model of Jansen and Rit

Throughout the thesis, we use the model of cortical neural mass activity of Jansen (Jansen et al., 1993; Jansen and Rit, 1995). The structure of this model is therefore described in this section. The model follows the lumped parameter formulation employed by Lopes Da Silva et al. (1974). The system under study in the Jansen model is a cortical circuit of three neuronal populations, namely i) pyramidal neurons, ii) inhibitory interneurons and iii) excitatory interneurons. It thus describes a salient cortical network (Douglas and Martin, 2004).

Activation of neural populations within the model is given by a *pulse-to-wave* conversion. Incoming pulse afferents are convolved in time in a second order impulse response of the following formulation:

$$\ddot{y}(t) = Aa\{Q(t)\} - 2a\dot{y}(t) - a^2 y(t) \tag{2.1}$$

22
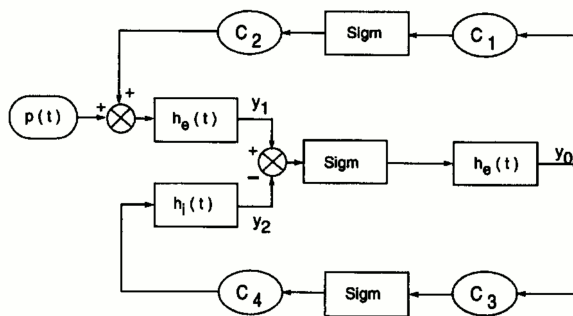
Figure 2.1: Schematic of the neural mass model. "Sigm" represents the static non-linear wave-to-pulse conversion. Blocks represent impulse responses (pulse-to-wave conversions). p(t) is the time varying input, which throughout this thesis is denoted I. Recreated from Figure 1 of Jansen and Rit (1995).

Here, Q is the input to the impulse response. This formulation arises from the time convolution of input, Q as follows (see also Robinson et al. (1997)):

$$y(t) = \int_{-\infty}^{t} w(t - t')Q(t')dt' \tag{2.2}$$

with

$$w(u) = Aaue^{-au} \tag{2.3}$$

In the Jansen model, activation of both excitatory and inhibitory interneurons is given by a single impulse response, driven by excitatory synaptic kinetics (Jansen et al., 1993). However, the pyramidal neuron population has two impulse responses, one each for excitatory and inhibitory PSPs. This allows a rough approximation to the contribution of both sources and sinks in the EEG output (an expanded use of this idea is given in Chapter 5).

The *activity* of each neural population is given as the output of the static non-linear sigmoid curve (wave-to-pulse conversion):

$$S[v] = 2e_0/(1 + \exp(r(v_0 - v))) \tag{2.4}$$

Here, e_0 represents the maximum firing rate, v_0 is the mid-point of the distribution of membrane thresholds for action potential firing at the population level, and r represents the steepness of the sigmoid (Jansen and Rit, 1995).

A schematic of the network and its conversion operators is given in Figure 2.1. It can be seen that the connectivity between each population is parameterised by C_1, C_2, C_3 and C_4. The ratios for these parameters are assumed to remain fixed (as defined in Jansen and Rit (1995)), such that the extent of internal connectivity can be lumped into a single parameter, C.

The equations for the neural mass model are therefore:

$$\dot{y_0}(t) = y_3(t)$$
$$\dot{y_3}(t) = Aa\{S[y_1(t) - y_2(t)]\} - 2ay_3(t) - a^2 y_0(t)$$
$$\dot{y_1}(t) = y_4(t)$$
$$\dot{y_4}(t) = Aa\{I + C_2 S[C_1 y_0(t)]\} - 2ay_4(t) - a^2 y_1(t) \qquad (2.5)$$
$$\dot{y_2}(t) = y_5(t)$$
$$\dot{y_5}(t) = Bb\{C_4 S[C_3 y_0(t)]\} - 2by_5(t) - b^2 y_2(t)$$

A and B represent the excitatory and inhibitory gains, respectively. a and b are the time scales (inverse duration) of the excitatory and inhibitory PSPs, respectively. It can be seen from these equations and the schematic of Figure 2.1 that the net output of pyramidal neurons that is passed through the sigmoid to generate activity is the net depolarisation $y_1(t) - y_2(t)$. This is traditionally also taken to represent a model of the EEG, though we re-examine this assumption in Chapter 5.

Several recent studies, particularly in the context of epilepsy, have used extended formulations of the system above (Wendling et al., 2002; Labyt et al., 2006). In this way, further important interactions and important mechanisms can be accounted for in the mass model. In Wendling et al. (2002), for example, a second, fast inhibitory population was incorporated into the model, whereas in Labyt et al. (2006) several different time scales of inhibition were included. Such extensions have also been made in model studies of normal brain rhythms (Ursino et al., 2010). The general extension to the model above is to introduce further populations as additional wave to pulse conversions and incorporate their effect on the principal cells by including their output as a term in the summation for net PSP on these cells (see e.g. Spiegler et al. (2010)). In Chapter 4 an extension to the neural mass model along these lines will be described and investigated.

In the next two chapters (Chapters 3 and 4) the extension of the neural mass model into networks of connected nodes will be considered. It will be shown that this approach can provide insight into the mechanisms of spontaneous transitions into seizure as well as the macroscopic response of nervous tissue to stimulation.

Chapter 3

Spatial extensions of a neural mass model: excitable media and stimulus response

3.1 Abstract

In this chapter we begin our investigation of the dynamics of spatially extended neural mass models in the context of epilepsy. Following the discussion in the previous chapters, our starting point is the neural mass model of Jansen and Rit (1995), which has been used as a model for epileptic spiking. We use this model to construct an excitable medium of locally coupled compartments and investigate the response of this system to perturbation. This is an attempt to provide new understanding of the macroscopic mechanisms of the response of nervous tissue to stimulation which is a fundamental open question in epilepsy.

In particular, stimulation of human epileptic tissue can reveal complex, self-terminating, transient oscillatory responses on the EEG or ECoG. These responses play a potentially important role in localising tissue involved in sustained seizure activity, yet the mechanisms underlying their generation are still unknown. However, in vitro evidence suggests that oscillations in nervous tissue are underpinned by non-trivial spatio-temporal dynamics in an excitable medium.

Here, we demonstrate that our spatially extended model, in one and two dimensions, displays propagating travelling waves but also more complex transient dynamics in response to perturbation. Crucially, the neural mass framework allows the incorporation of spatially distributed, functional abnormalities, such as regions of reduced inhibition. Such spatial heterogeneities are fundamental to epileptic processes, though their effect on macroscopic dynamics are currently unknown. It is demonstrated that the incorporation of regions of reduced inhibition in our model can lead to self-terminating reverberating responses to a single pulse perturbation, depending upon the location at which the stimulus is delivered. We thereby provide

a hypothesis for the generation of space dependent, transient responses to perturbation at the macroscopic scale in the epileptic brain.

3.2 Introduction

Excitability

A fundamental feature of the brain which enables the processing of environmental information is its ability to provide a response to external stimuli in normal working states. The output of the brain's processing of stimulation can be measured in controlled conditions as an evoked response on the EEG. In this way one can consider the entire brain in terms of input to output conversion, similarly to the conceptualisation of the dynamics of neural masses, as presented by Freeman (Freeman, 1975). Aside from natural stimuli, it can also be shown that electrical (or magnetic) stimulation can evoke a response in the brain that can be seen on the EEG (the electrical evoked response). An important means by which this stimulus response is mediated in nervous tissue is by the *excitability* of neurons, which enables information to be conferred across large regions of nervous tissue. Indeed the functional units of the brain, the neurons, are archetypal biological excitable units. Intuitively this means that a small perturbation to the neuron (for example the activation of an afferent excitatory synapse) can cause a large deviation in its activity (the action potential spike).

Excitability is an important concept in non-linear dynamics and is used to describe many important processes in physical systems, for example certain chemical reactions and biological processes. Formally speaking, an excitable dynamical system is characterised by a large amplitude trajectory in the near vicinity of a resting state, such that a perturbation can cause a large deviation in its dynamics (Strogatz, 1994; Izhikevich, 2006). Traditionally, the rest state is considered to be a stable equilibrium, though as we shall see in Chapter 4, excitability from a resting oscillatory state is also important and the existence of a deviating trajectory behind some separator in phase space can imbue spontaneous synchronising capabilities.

There are a number of dynamical system structures (in the geometric or global bifurcation sense) that can lead to excitability as defined by Izhikevich (2006). These structures exist because the excitable system resides close to a bifurcation into limit cycle dynamics. In general, these bifurcations are due to the disappearance or loss of stability of the stable equilibrium, as shown in Izhikevich (2006) (figure 7.3 page 217). The large excursion evoked by perturbation may be replaced by a stable limit cycle due to different bifurcations such as a saddle-node on invariant circle or a supercritical Hopf. Alternatively the limit cycle can emerge via intermediate bistable systems as is the case in a saddle-homoclinic orbit bifurcation followed by a saddle node bifurcation.

In Neuroscience, the concept of excitability arose due to empirical observations by Hodgkin (1948), who identified different classes of excitability for cells of the nervous system. In the first two such distinctions, *Class 1* and *Class 2*, the important observation was made that an injection of current can cause periodic spiking with arbitrarily low spiking frequency (*Class 1*) or with a robust, fixed frequency (*Class 2*). Crucially, these observations have direct analogues in bifurcation theory. *Class 1* dynamics relate to a bifurcation in which the birth of a limit cycle occurs with a saddle node on the limit cycle, which therefore can lead to long period (low frequency) oscillations. *Class 2* dynamics on the other hand occur when a limit cycle appears due to the disappearance of a stable equilibrium (off the limit cycle), or a change in stability of the equilibrium (Hopf bifurcation). In addition, *Class 3* neurons exhibit a single spike in response to perturbation but then maintain a plateau through the duration of the injected current. *Class 3* dynamics, therefore, relate to the preservation of a stable equilibrium.

The concept of excitability has profound importance in spatially extended systems, wherein network connectivity between excitable nodes can produce the effect of conferred excitation. Such systems, known as *excitable media* are of particular importance in neuroscience, and indeed the brain can be referred to as an excitable medium due to its excitable components (neurons) and network (synaptic) connectivity. Mathematical and physical (for example in chemistry and biology) excitable media display some characteristic spatio-temporal dynamics due to the transmission of threshold excitation across the system. For example, such systems may display travelling waves and spiral waves (Winfree, 2001).

Stimulus response and excitability in epilepsy

There is a long standing notion that epileptic tissue (or the epileptic brain) is somehow "more excitable" than its "normal" equivalent. However, we can appreciate from the previous section that in the mathematical sense, the notion of "more" or "less" excitable is perhaps not well defined. One might suggest that a stable equilibrium closer to the start of its deviating excursion (in the sense that a "smaller" perturbation can take it there), could be considered more excitable than an equilibrium "farther" from its equivalent point.

In the context of epilepsy, this use of the term "excitability" most likely stems from the fact that abnormal rhythmic activity, as well as clinical symptoms, can be elicited by stimulation. Stimulation can either be sensory (for example by visual stimulus in the case of the photo-paroxysmal response (Parra et al., 2003)), or electrical. The latter was explored to a great extent in humans in the seminal work of Penfield and Jasper (1954), and has also been explored in animal models (see e.g. Lüttjohann et al. (2011) for a recent, pertinent example and the extended discussion below). In this context, a lengthy elicited period of abnormal rhythmic activity is

often termed an *afterdischarge* (see e.g. Blume et al. (2004)).

It seems that the invocation of an afterdischarge, defined at the level of macroscopic recordings, does not fit immediately into the context of excitability as defined for neurons, or more generally as discussed above. However, the concept might extend if one considers that the long trajectory onto which a system at rest is perturbed is in this case represented by a long lasting, rhythmic transient. This transient is then the analogue of the high amplitude spike trajectory that epitomises excitability in single neurons. Indeed it has been demonstrated that the afterdischarge length has a threshold relationship to various stimulation characteristics (Pinsky and Burns, 1962) which are reminiscent of the plots of frequency of spiking against input current for single neurons (Izhikevich, 2006).

It is worth noting that a more traditional dynamical systems perspective of the afterdischarge, since it is characterised by a lengthy period of oscillatory dynamics (Blume et al., 2004), would be that the system has deviated onto an "abnormal" attractor due to stimulation. In this sense, a distinction between epileptic and control nervous tissue might be made by the strength or duration of the perturbation required to push the system onto this attractor, or the length of time the system stays there before returning to its "normal" state (Penfield and Jasper, 1954; Lüttjohann et al., 2011). Since it is unclear what effect would push the system away from this attractor and back towards its "normal" state, the transient concept seems more appealing. Considerations regarding different dynamical regimes for the rhythmic transitions of epilepsy have been the subject of previous work, most notably by Lopes Da Silva (Lopes da Silva et al., 2003b). This will be expanded upon in Chapter 4. To summarise, the notion of excitability in relation to elicited macroscopic responses demands clarification and extension to the level of the neural mass. This will be addressed in the context of the current work in the discussion of the current chapter.

Stimulation in human epilepsy and considerations for therapy

The response of human cortex to electrical stimulation has historically been the source of much research. Penfield and Jasper (1954), for example, described detailed case studies of afterdischarges evoked in several patients. They produced a categorisation of the kinds of responses that can be seen, which was subsequently reorganised by Blume et al. (2004). The morphologies were reported to contain a good degree of overlap, and some non-trivial evolution, but they were grouped as i) rhythmic waves, ii) rhythmic waves evolving into spike-waves, iii) polyspike bursts and iv) spike-waves (Blume et al., 2004). These responses were elicited via subdurally implanted electrodes, and stimulation was used to locate *eloquent cortex*, which is the part of cortex indispensable for important normal function (Rosenow and Lüders, 2001).

Mapping the eloquent cortex is an important consideration in pre-surgical evaluation for intractable epilepsies in which a region of nervous tissue is targeted for resection. The aim of surgery is to remove the *epileptogenic zone*, which is the hypothetical region of tissue necessary for the generation of seizures (Rosenow and Lüders, 2001). An additional motivation for studies such as Blume et al. (2004) is that stimulation might be used to localise the region of tissue responsible for the initiation of spontaneous seizures, namely the *seizure onset zone* (Rosenow and Lüders, 2001). Although early studies reported a correlation between aspects of afterdischarges, such as their length, and the seizure onset zone (Penfield and Jasper, 1954), Blume et al. (2004) found evidence for the contrary and highlighted the potential mis-localisation of seizure generating tissue as judged by features of stimulus evoked afterdischarges.

The discussion above introduces several key concepts to motivate the work in this chapter. Firstly, it is clear that in focal epilepsies (and in epilepsy in general) we are presented with spatial heterogeneities. These are specified by their capability to influence epileptic and ongoing activity, and are referred to in the case of focal epilepsy as different *zones*. For example, the seizure onset zone, introduced above, is a spatially localised region of nervous tissue that influences the onset of spontaneous seizure activity. It is worth noting that this does not correspond directly to the epileptogenic zone, so that information regarding the onset of seizure activity on the EEG or ECoG is not sufficient to determine which region of tissue to remove. The major goal in epilepsy surgery is to accurately locate the epileptogenic zone and remove it, whilst minimising the impact to eloquent cortex. This is the method by which patients will be rendered seizure free with minimal impact on essential cognitive function, or equivalently the intervention that maximises a gain in quality of life for the patient. Clearly a greater understanding of the spatially distributed, functional abnormalities of nervous tissue in focal epilepsy will provide advances in the treatment of epilepsy. The spatially varying response to stimulation is an intriguing and promising candidate for exploration in this direction.

The aforementioned afterdischarges are often evoked in response to prolonged stimulation, which also produces substantial post-stimulus artefact (Penfield and Jasper, 1954; Blume et al., 2004). It is therefore possible that this kind of stimulation initiates substantial interim changes in local brain dynamics, rather than being the kind of threshold excitation response alluded to from the dynamical systems perspective. However, shorter stimulus protocols have also produced interesting and potentially useful spatially dependent responses. Single pulse stimulation has recently been shown to produce space dependent responses in epileptic patients with intractable epilepsy (Valentin et al., 2002; Valentín et al., 2005; Flanagan et al., 2009). In this case, "abnormal" responses are delayed or repetitive, rhythmic responses, whereas the "normal" response is a single deflection (examples of these are

shown in Figure 3.11). There is some evidence that these different types of response may aid the spatial localisation of epileptogenic tissue (Valentin et al., 2002). However, although an imbalance between excitatory and inhibitory processes is expected to contribute to the excitability of epileptic cortex, and thereby convey an ability to display abnormal responses (Valentin et al., 2002), the mechanisms underlying macroscopic responses to stimulation in human epilepsy remain essentially unknown, despite their potential clinical importance.

Spatio-temporal dynamics: insights from animal models

Afterdischarges have been investigated in feline models (Pinsky and Burns, 1962) and insight into the excitability of epileptic tissue has been provided by electrical recordings from *in vitro* slice models of partially disinhibited cortex (Chervin et al., 1988; Pinto et al., 2005) as well as the imaging of spatio-temporal patterns of voltage sensitive dyes (Bai et al., 2006; Wu et al., 2008). It has been shown in these *in vitro* models that stimulation can induce the propagation of simple or more complex wave patterns, with propagation found to be mediated by synaptic excitation (Pinto et al., 2005). The study of Pinto et al. (2005) provided a highly resolved set of one-dimensional recordings from a widely studied *in vitro* preparation, the partially disinhibited neocortical slice. In this study, a series of 25 μm electrodes placed 100 μm apart were used to measure the spatial evolution of local field potentials (LFPs) across the slice in response to a bipolar stimulation. As expected for excitable media, the cortical slice could propagate simple travelling waves in response to local perturbation. Interestingly, more complex patterns, which incorporated reflected waves could also be evoked. The invocation of travelling activity was found to be a threshold event in which the threshold depended upon pharmacologically manipulated excitatory and inhibitory efficacy.

Several other studies (e.g. Chervin et al. (1988)) have also observed travelling waves in response to stimulation in nervous tissue. In addition, more complex dynamics attributable to excitable media such as spiral waves have been observed (Huang et al., 2004; Schiff et al., 2007). These studies highlight the need to understand normal and pathological brain rhythms in terms of their spatio-temporal dynamics. The imaging of voltage sensitive dyes has provided insight in this direction. Bao and Wu (2003), for example, observed simple (single travelling wave) and complex spatio-temporal patterns underlying a theta oscillation in a slice preparation. Interestingly, this study demonstrates that the relationship between local field potential recordings and underlying spatio-temporal activity (as imaged by voltage sensitive dyes) may be non-trivial. For example, irregular oscillations in the LFP could be seen to coincide with complex travelling waves on the voltage dye image. Non-trivial and spatially heterogeneous dynamics have also been observed in an evoked response in rat neocortical slice (Bai et al., 2006). A review of results

concerning propagating wave activity in neocortex is given by Wu et al. (2008).

Mathematical models of excitable media

In the paradigm of the cortex as an excitable medium, it is clearly imperative to examine stimulus response dynamics in spatially extended mathematical models, as will be the case in this chapter. This kind of approach has been very fruitful in investigation of the activity of the heart which is another important excitable system in Biology and Medicine. Bub et al. (2003), for example, investigated the role of the density of cells in culture and its effects on spatio-temporal dynamics and found that low densities could support spirals and wave-breaks.

There are many examples of spatio-temporal mathematical models in the context of neuroscience and epilepsy. In fact, an archetypal excitable medium can be formed by connecting Fitzhugh-Nagumo neurons. In general, networks of connected models at the neuronal level have been extensively investigated. In the context of epilepsy a particular point of interest is their synchronisability (see, for example, Destexhe (1998)). On a more abstract level, cellular automata are another important type of spatio-temporal dynamical system which incorporate nearest neighbour connectivity and discrete state transitions. They have been used in the context of epilepsy by Traub et al. (2010) to investigate pattern formation in high frequency local field potential oscillations.

The spatio-temporal dynamics of nervous tissue have also previously been modelled at the macroscopic level, most often in the Wilson-Cowan framework (Wilson and Cowan, 1973), and have been demonstrated to be capable of producing single and multiple propagating waves (Pinto and Ermentrout, 2001; Troy and Shusterman, 2007) and spiral dynamics (Huang et al., 2004; Laing, 2005). Although often formulated without inhibitory components in line with conditions leading to experimentally observed spatio-temporal dynamics, sustained synchronous responses to stimulation have also been shown to form in models incorporating inhibition (Shusterman and Troy, 2008). Neural field formulations also include a spatial dimension (see Chapter 2) and have been used to study travelling oscillatory activity in epilepsy (Kramer et al., 2005; Kim et al., 2009).

Despite its repeated use in studies of epileptic rhythms (Wendling et al., 2000, 2001, 2002; Labyt et al., 2006; Cosandier-Rimélé et al., 2008), no extensive examination of the dynamics of spatial extensions to the neural mass model of Jansen and Rit (1995) has been undertaken. Of particular importance in this type of model, as utilised extensively in the context of epilepsy (e.g. Wendling et al. (2002); Breakspear et al. (2006)), is the opportunity to relate dynamics to physiologically meaningful parameters such as gain and time scale of inhibitory and excitatory PSPs. This implies the opportunity to explicitly model spatial heterogeneities and also allows to study the response to perturbation of networks of neural masses, connected via

explicitly modelled excitatory synapses.

Excitability in the neural mass model

The dynamics of a single neural mass in the standard parameter set suggested by Jansen and Rit (1995), have been previously explored (Jansen and Rit, 1995; Grimbert and Faugeras, 2006; Spiegler et al., 2010) and shown to have a structure of particular interest for the study of epilepsy (Wendling et al., 2000), which we briefly review here. The bifurcation structure for changes in the input parameter, I, presents two branches: a lower branch, corresponding to relative quiescence (low firing output of principal cells) and an upper branch, corresponding to increased activity (high output of principal cells and oscillatory activity). When starting at the lower branch and increasing I, there is a saddle node on invariant circle bifurcation (SNIC) which eliminates the stable fixed point on the bottom branch. The system, when placed at rest at the stable equilibrium for low I, has implicitly been shown to be excitable (Wendling et al., 2000) and as such has been used as a model for inter-ictal spiking. The bifurcation structure is in line with the *Class 1* excitability described above.

This SNIC bifurcation reveals a high amplitude limit cycle which has previously been used to model epileptic EEG spiking (Wendling et al., 2000). The upper branch is a saturated high output fixed point for high I and undergoes a Hopf bifurcation into a small-amplitude oscillation when I decreases. For intermediate I there is a region of bistability between the large limit cycle and the Hopf oscillation. The small-amplitude oscillation generated via Hopf bifurcations was previously suggested as a model for (background) alpha rhythm (Jansen and Rit, 1995). However, previous mass modelling studies of epileptic transitions (Wendling et al., 2000, 2002; Breakspear et al., 2006; Marten et al., 2009a) would suggest the lower branch fixed point as a model for background activity.

Aims of this chapter

Motivated by the foregoing discussion we aim to explore the dynamics of spatially extended networks of coupled neural mass models. In particular, it is important to investigate the excitability of these systems in order to progress our understanding of the potential mechanisms underlying macroscopic responses to perturbation in the epileptic brain. It will also be crucial to begin to examine spatially structured heterogeneities in order to progress a theoretical framework for the investigation of the hypothetical epileptogenic zone (Rosenow and Lüders, 2001).

3.3 Methods

The neural mass model used in this chapter is that proposed by Jansen (Jansen et al., 1993; Jansen and Rit, 1995), and presented in detail in Chapter 2. Here, we describe how this model is extended into a spatially extended system.

N interacting neural masses are connected and communicate via excitatory output from principal neurons. In this thesis we focus predominantly on *local* connectivity, and so explicit time delays are not considered. However, future extensions to the method presented will account for these effects. Each neural mass, defined by superscript i, is modelled by a system of six differential equations representing the interaction of excitatory and inhibitory cortical processes (Jansen et al., 1993; Jansen and Rit, 1995), with model equations given by:

$$\dot{y}_0^i(t) = y_3^i(t)$$
$$\dot{y}_3^i(t) = Aa\{S[y_1^i(t) - y_2^i(t)]\} - 2ay_3^i(t) - a^2 y_0^i(t)$$
$$\dot{y}_1^i(t) = y_4^i(t)$$
$$\dot{y}_4^i(t) = Aa\{I + P^i + C_2 S[C_1 y_0^i(t)]\} - 2ay_4^i(t) - a^2 y_1^i(t) \qquad (3.1)$$
$$\dot{y}_2^i(t) = y_5^i(t)$$
$$\dot{y}_5^i(t) = Bb\{C_4 S[C_3 y_0^i(t)]\} - 2by_5^i(t) - b^2 y_2^i(t)$$

Inter-compartment connectivity is defined by a homogeneous connectivity constant, R, representing coupling between different local populations. Previous neural mass models have employed nearest neighbour (Wendling et al., 2000, 2001; David et al., 2005) or distance dependent connectivity (Sotero et al., 2007; Babajani-Feremi and Soltanian-Zadeh, 2010), whereas neural field models couple via diffusion terms (Kim et al., 2009) or by distance dependent integration over the output of a spatially extended continuum (Kramer et al., 2005; Shusterman and Troy, 2008). Here we begin a systematic investigation of the dynamics of spatial extensions by opting initially for a nearest neighbour connectivity scheme. Thus, larger systems are formed as open ended chains in 1-d, and ultimately an open ended sheet in 2-d. In addition, we study an alternative connection scheme and, briefly, the impact of long-range connections on the dynamics, but leave considerations of inhibitory coupling, more complex connection topology and the effect of different boundary conditions for future studies. The input to each population, P^i ($i = 1, .., N$) is given by the weighted contribution of nearest neighbours, as shown below, where R indicates the strength of connectivity and δ_{ij} indicates the presence of connections:

$$P^i = \sum_{j=1}^{N} \delta_{ij} R S[y_1^j - y_2^j] \qquad (3.2)$$

As discussed in Chapter 2, model output for the i_{th} compartment is given by the net PSP on principal neurons in that compartment $(y_1^i - y_2^i)$. Within the model a net post-synaptic potential (PSP) is transformed via the sigmoidal activation function $S[v]$ (Marreiros et al., 2008) into neuronal activity or firing rate:

$$S[v] = 2e_0/(1 + \exp(r(v_0 - v)))$$ (3.3)

Within compartment connectivity is governed by a parameter, C, which provides an overall weight for parameters C_1, C_2, C_3 and C_4 (see Table 3.1). In order to simplify the dynamics, we reduce the extent of bistability in the model by slightly increasing the internal connectivity parameter, C, from 135 to 140 (Grimbert and Faugeras, 2006). In this configuration, $I{=}50$ is chosen to represent the lower branch fixed point dynamics (henceforth referred to as "fixed point"). We summarise the values for system parameters in Table 3.1. The reader is referred to Grimbert and Faugeras (2006) and Spiegler et al. (2010) for a detailed examination of the single compartment model.

The presence of oscillations in large systems was determined by calculating the variance over time for the mean output over all compartments. A threshold of variance ≤ 0.0001 was found adequate to reliably distinguish fixed point from out of phase oscillations. The length of transient responses to perturbation was found by comparing the mean output over all compartments one second before stimulus to the mean post stimulus. The length was given by the time taken to return to within 0.001 of the pre-stimulus mean value.

Two dimensional figures and corresponding supplementary movies (which are available from the supplementary material of Goodfellow et al. (2011b)) are colour coded by amplitude on a blue to red scale, with deep blue representing the lowest amplitude. The resolution of these figures was improved by inserting additional compartments and interpolating over their values.

3.3.1 Model perturbations

The effect of stimulation was investigated by delivering a short, rectangular pulse in the input parameter, I, to the EPSP (of the principal neuron population) of a single compartment either at the centre of the system, or at different locations. Square wave pulses of duration 0.1 seconds were considered in this study, though the amplitude was varied. This follows previous investigations of the effects of stimulation on the dynamics of neural masses in the context of epilepsy (Suffczynski et al., 2004; Adhikari et al., 2009), and provides an abstract notion of the fact that stimulation introduces a local excitatory perturbation to the system. However, we note that, in experimental settings, bipolar stimulation is delivered via implanted electrodes (Valentin et al., 2002), with current flowing between anode and cathode and with

Parameter	Description	Value
A	Average excitatory gain	3.25mV (is varied)
B	Average fast inhibitory gain	22mV (is varied)
a	Average excitatory time constant	$100s^{-1}$
b	Average fast inhibitory time constant	50s^{-1}
C, C_1, C_2	Connectivity constants	$C = 140, C_1 = C, C_2 = 0.8C$
C_3, C_4		$C3 = C4 = 0.25C$
I	External input to pyramidal neurons	$I = 50$
R	Matrix of connectivity constants	R is varied though is homogeneous.
v_0	Parameters of the sigmoid function	$v_0 = 6mV$
e_0, r		$e_0 = 2.5s^{-1}, r = 0.56mV^{-1}$

Table 3.1: Parameter values for all model output in Chapter 3.

strongest impact (highest current density) at the tip of an electrode. In addition, the action of direct stimulation is complex, and not completely understood, with excitation probably targeting axons rather than dendrites, remote effects (David et al., 2010) and also the possible activation of inhibitory neuronal populations. Thus, future studies will need to account for greater bio-physical detail of nervous tissue stimulation, for example as implemented in the models of Anderson et al. (2007, 2009). However, in the current study we focus on the macroscopic propagating activity due to a short time dependent "activation". In future, this principle might therefore extend to localised pharmacological stimulation, where the details of an applied electrical field would not need to be considered.

Propagation of activity to the extremes of a system was detected by whether the maximum of the EEG output variable in one of the compartments at the edge of the system exceeded a value of 2, which is above the range of output seen in non-oscillating compartments. The threshold stimuli to elicit such a response was found by sequentially incrementing the stimulus strength in successive simulations proceeding from the background fixed point.

3.4 Results

We explore the transition from background activity to abnormal spiking in progressively larger systems, beginning with two coupled compartments and moving onto one and two-dimensional spatially extended systems. In the penultimate subsection we investigate the effect of adding a spatial heterogeneity to a two dimensional system, simulating a patch of abnormal tissue in the epileptic brain. In the final subsection we relax the assumption of strict nearest-neighbour coupling and show how the current scheme can be extended to include long range connections.

3.4.1 Bifurcations and excitability in two coupled compartments

Each model compartment is representative of a salient cortical circuit with excitatory and inhibitory influences at the level of populations of neurons (for example a cortical column (Jansen and Rit, 1995; Mountcastle, 1997)) and is referred to as a neural mass. Thus the effect of excitatory connectivity between neural masses can be explored by connecting compartments in the model framework described in section 3.3. This introduces an additional parameter into the model, R, which represents the strength of excitatory influence between one neural mass and another. The effect of changes in this parameter on the model dynamics are explored in the bifurcation diagram of Figure 3.1 (a) (for details on bifurcations in neural mass models see e.g. (Grimbert and Faugeras, 2006; Breakspear and Jirsa, 2007; Spiegler et al., 2010)).

The system of two coupled compartments shows fixed point behaviour for values up to R=135, which is characterised by a low (resting) activity of the neural mass. Between $R \approx 135$ and $R \approx 147$, there is a window of oscillatory activity which resembles the periodic spiking of a single compartment (see example time series in Figure 3.1 (b)). The spiking frequency is variable and depends on the coupling strength; for R=139 it is around 1/s, but by $R = 143$ the oscillation has a faster frequency of around 6/s and a slightly smaller amplitude (see example time series in Figure 3.1 (c)). Beyond R=148, the system settles into a fixed point with permanent high activity of principal neurons in the neural mass.

In Figure 3.1 (d) we demonstrate the excitability of this system of two coupled compartments by delivering a sub- or supra- threshold pulse stimulus to both compartments. This threshold response to stimulus defines excitability and it can be seen in the coupled compartment model over a large range of coupling strength, R. Interestingly, certain stimuli could also lead to a prolonged response in both compartments mediated by faster oscillations. An example of this behaviour is shown in Figure 3.1 (e). The initial excitation is followed by a number of oscillations with small amplitude, but at an elevated level of excitation, before the return to basal activity. This indicates that the coupling of compartments creates complex transients due to the mixing of the two oscillatory modes present in the uncoupled system (c.f. the description in section 3.3).

3.4.2 Simple and complex propagating activity in one-dimension

The consequences of excitatory connectivity in larger systems of interacting neural masses, and its impact on the model's excitability, were explored by connecting 21 compartments in a nearest neighbour coupled chain. This provides a one-dimensional approximation to an extended region of cortical tissue. The choice here of 21 compartments allows an initial exploration of the dynamics of a larger system
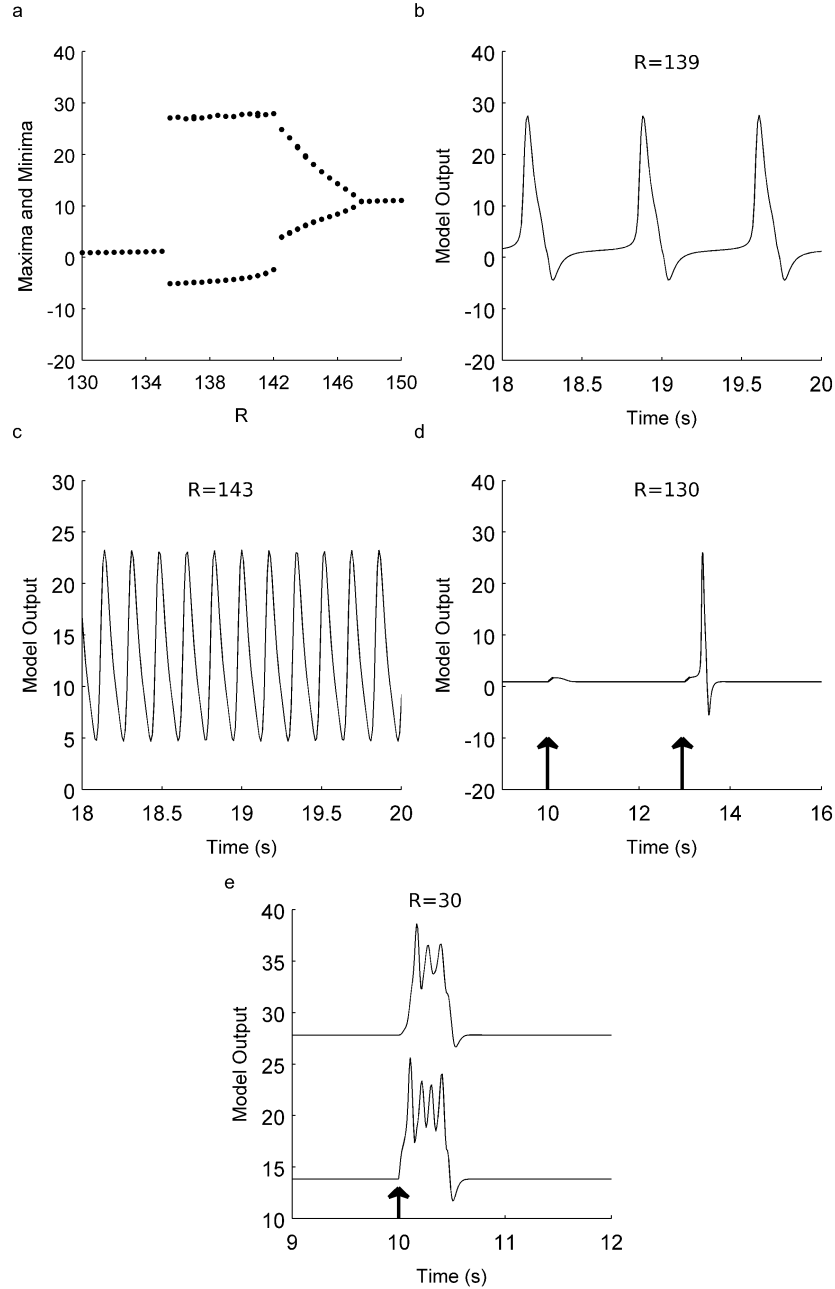
Figure 3.1: Dynamics of two coupled compartments under changing connectivity strength. a) bifurcation diagram for changing R. Maxima and minima for compartment 1 are shown. The dynamics of compartment 2 are equivalent. b) spiking solution, $R=139$, c) faster oscillations, $R=143$, d) response to perturbation with R = 130. Stimulus strength at t=10 seconds is 62 and at t=13 seconds is 62.5. e) response to stimulus of strength 150 at t=10 seconds, $R=30$. Time series in e) are plotted with an offset on the vertical axis. Arrows indicate stimulus times.

with symmetry about a central compartment that will receive a stimulus. Larger systems were also explored and allowed qualitatively similar results (i.e. regarding

the nature of oscillations and the response to stimulation) under alternative parameter choices. For example, under the default parameter settings employed for the simulations in Figure 3.2, increasing the size of the system causes the fixed point to become unstable and leads to permanent oscillations, due to reverberating, travelling activity. However, the lower steady state and the travelling wave response to stimulation can be recovered in larger systems by adjusting, for example, the inhibitory gain parameter, B. In addition, the generalisation of these results to larger two dimensional systems is explored in subsequent sections. As in the previous section, the effect of varying strengths of connectivity between masses was examined as a function of the coupling strength, R. These results were additionally tested for stability by introducing a small heterogeneity (random distribution around the value given in Table 3.1) in each of the parameters in the first two compartments.

In this spatially extended system with N=21, the coupling strength required to produce sustained oscillatory activity is lower than in the two compartment case, as can be seen in the bifurcation diagram of Figure 3.2 (a). In this case, the onset of oscillatory activity is at $R \approx 68$, initially as regular propagating spikes, similar to those observed in Figure 3.1 (b). For a small region, approximately $68 \leq R \leq 68.7$, this spiking solution is bistable with the background steady state. The simple spiking solution is replaced by complex oscillations for $70 \leq R \leq 74$, with reverberating activity across the range. An example of complex oscillations (henceforth referred to as "mixed oscillations") is shown in Figure 3.2 (b).

It can be seen that activity is heterogeneous across the range apart from a brief refractory period which is conserved across all compartments. As R is increased within the region of mixed oscillations, these global refractory periods become more sparse. An important feature of this complex dynamic regime is that the spatial symmetry of the model is broken and a given variable varies in amplitude and phase at different locations for any given time point. Note that the spatially symmetric oscillatory state still exists as a solution when initiated in a spatially symmetric state (i.e. when all compartments and coupling parameters are identical). However, this solution is unstable and would therefore be unobservable under physiological conditions, where fluctuations are unavoidable.

As R increases beyond 70, the amplitude of oscillatory activity at the centre of the system becomes smaller until it appears saturated at high output, though until $R \approx 85$ there are oscillations at the periphery of the system, as can be seen in Figure 3.2 (a). The region of bistability apparent in Figure 3.2 (a) around R=75 is mediated by the amplitude of oscillations at the periphery. For $R \leq 72$ the periphery oscillates with spiking dynamics of variable amplitude. For $72 \leq R \leq 77$, the peripheral compartments are either both oscillating with high amplitude spikes, or one of them is oscillating at the smaller amplitude, faster oscillations, which give the lower amplitude maxima and minima seen in Figure 3.2 (a). In the region
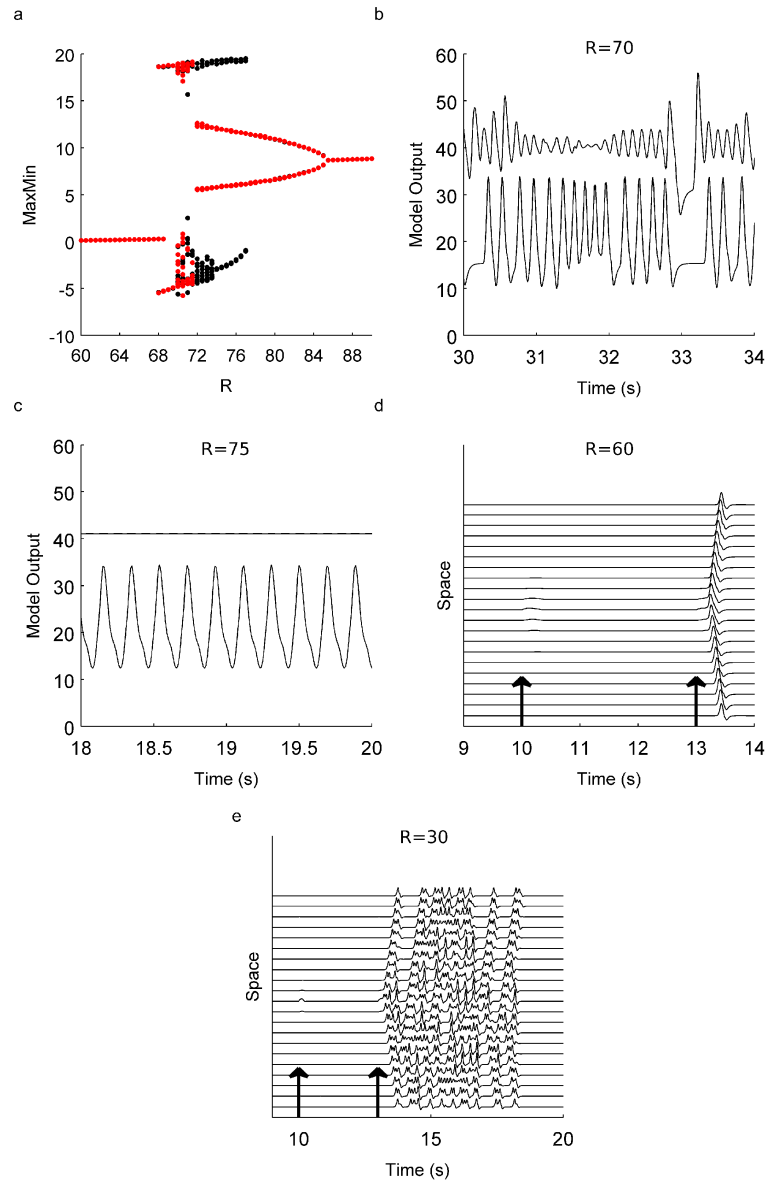
Figure 3.2: Dynamics of 21 compartments coupled in a one dimensional chain. a) bifurcation diagram for changing R (remaining parameters are default values as in Table 1). Maxima and minima are plotted for compartment 1 at the end of the chain. Forward scan is plotted in black, backwards scan is in red. b) solution with mixed oscillations at R=70. Note the refractory period at t=33. c) solution with central saturation, R=75, d) response to perturbation of the central compartment with R=60, strength = 87 at t=10 seconds and strength = 88 at t=13 seconds, e) response to perturbation of the central compartment with R=30, strength = 120 at t=10 seconds and strength = 121 at t=13 seconds. In b and c, time series for the central compartment and a peripheral compartment (compartment 1) are plotted, with an offset on the vertical axis. Arrows indicate stimulus times.

$74 \leq R \leq 77$, the maxima and minima of oscillations at the periphery fluctuate less. An example of this activity is given in Figure 3.2 (c), for R=75.

If the one dimensional system is set in the fixed point state a single stimulus to

the model elicits a single propagating wave of activity, as shown in Figure 3.2 (d), where the elicited spike propagates uniformly from the central compartment to the periphery. If the system is prepared in the fixed point state near the onset of the periodically spiking solution, long initial transients of mixed oscillatory activity can be observed.

Over a large region of R (for example, $25 \leq R \leq 50$), a non-trivial response of the background, fixed point state to single perturbations was found for the system with N=21. An example of this behaviour is shown in Figure 3.2 (e). The complexity is due to so-called "backfiring" (Bär et al., 1994) which occasionally sparks new propagating oscillations starting from locations other than the perturbed compartment.

As shown in Figures 3.2 (d) and (e), propagation of activity depends upon the size of the stimulus to the central compartment, with an approximately all or none threshold for propagation. That is, the system can either show only a damped response with small amplitude in its neighbours, whilst leaving the periphery unaffected, or actively propagate high amplitude activity throughout the entire chain of compartments, with a sharp threshold for onset of propagation. Following previous *in vitro* experiments regarding the effect of changes in inhibitory and excitatory strength on propagation of activity in epileptic tissue (Pinto et al., 2005), we explored the effect of changes in excitation and inhibition on the stimulus threshold in our model. This was achieved by altering the gain parameters in the PSP equations, A and B, the results of which are documented in Figure 3.3. It was found that, for fixed parameter B, decreased excitation leads to an increase in the stimulus intensity required to elicit a spreading response (Figure 3.3 (a)), whereas for constant A, decreasing inhibition has the reverse effect (Figure 3.3 (b)). In the case of low inhibitory gain, propagation is of the form of the previously described complex transients as e.g. in Figure 3.2 (e), rather than simple wave propagation as e.g. in Figure 3.2, (d)). This latter result suggests that responses reminiscent of epileptic afterdischarges can be modelled in the spatially extended system with low inhibitory gain, whereas these reverberating responses to stimulus can be eliminated by increasing the inhibitory gain in the system. In the system with 21 compartments, increasing B shifts the onset of oscillatory activity to higher values of R (results not shown).

3.4.3 Propagating activity in two dimensional excitable media

The cortex can be approximated by a two-dimensional system of interacting neural masses if it is assumed that the vertical direction is redundant, as is the case when considering the local activity of neural masses (Wilson and Cowan, 1973; Mountcastle, 1997). This induces an additional spatial degree of freedom compared to the one-dimensional case, which must be investigated in model systems arranged
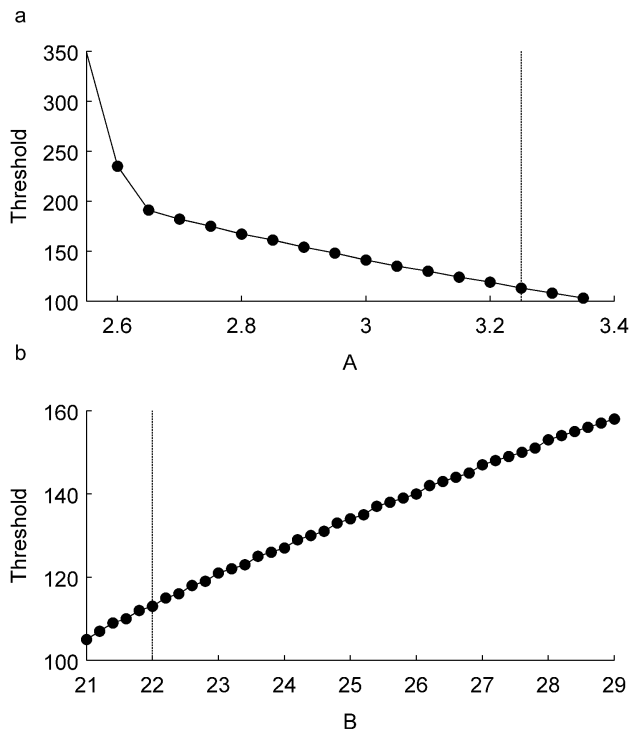
Figure 3.3: Effect of changes in excitatory a) and inhibitory b) gain on the threshold required to propagate activity to the edge of the 21 compartment system. In a), $R=60$, $B=22$. In b), $R=60$, $A=3.25$. Vertical lines indicate previously used default values of these parameters (Jansen and Rit (1995)).

in two-dimensions. Here, we examined these systems in a hexagonally arranged, nearest neighbour coupled scheme. The central compartments have 6 neighbours each, whereas the peripheral compartments have 3 neighbours.

We start with a model of one central compartment surrounded by 6 symmetrically coupled compartments, which represents the simplest such 2 dimensional configuration (c.f. the arrangement of grey hexagons in Figure 3.8). The dynamics of this model of 7 coupled compartments are characterised by the bifurcation diagram in Figure 3.4 (a). It can be seen that these dynamics follow a similar structure to those of the one dimensional chain, in that the fixed points are interrupted by a region of oscillations. However, the critical value for onset of oscillations is lower (compare Figure 3.2 (a)) due to each compartment communicating with more neighbours and therefore receiving an increased net contribution for equivalent R.

For $R \leq 32$ the fixed point background solution persists. At $R=32.5$, the system enters a region of bistability between fixed point and oscillatory dynamics. The oscillatory activity in this region is around 8 Hz, with phases distributed across the 7 compartments. Figure 3.4 (b) shows that whilst the amplitude of the peripheral compartment can be relatively stable, the amplitudes in other compartments (here, the central compartment) may vary, leading to sub-harmonic components in the Fourier spectrum. Between $R=36$ and $R=40$, the system is in a region of bistability between large amplitude spiking activity, occurring at around 1 spike per second, and

oscillations of smaller amplitude at around 8Hz, with phases distributed across the 7 compartments. The dynamics of the former are shown in Figure 3.4 (c), and the smaller amplitude oscillations are shown in Figure 3.4 (d). The effect of increasing R beyond 40 was i) to bring into closer alignment the phases of the oscillations in the peripheral compartments, and ii) to produce an offset between the central compartment, which oscillated at a higher mean value, and the rest of the system, which oscillated around a lower mean.
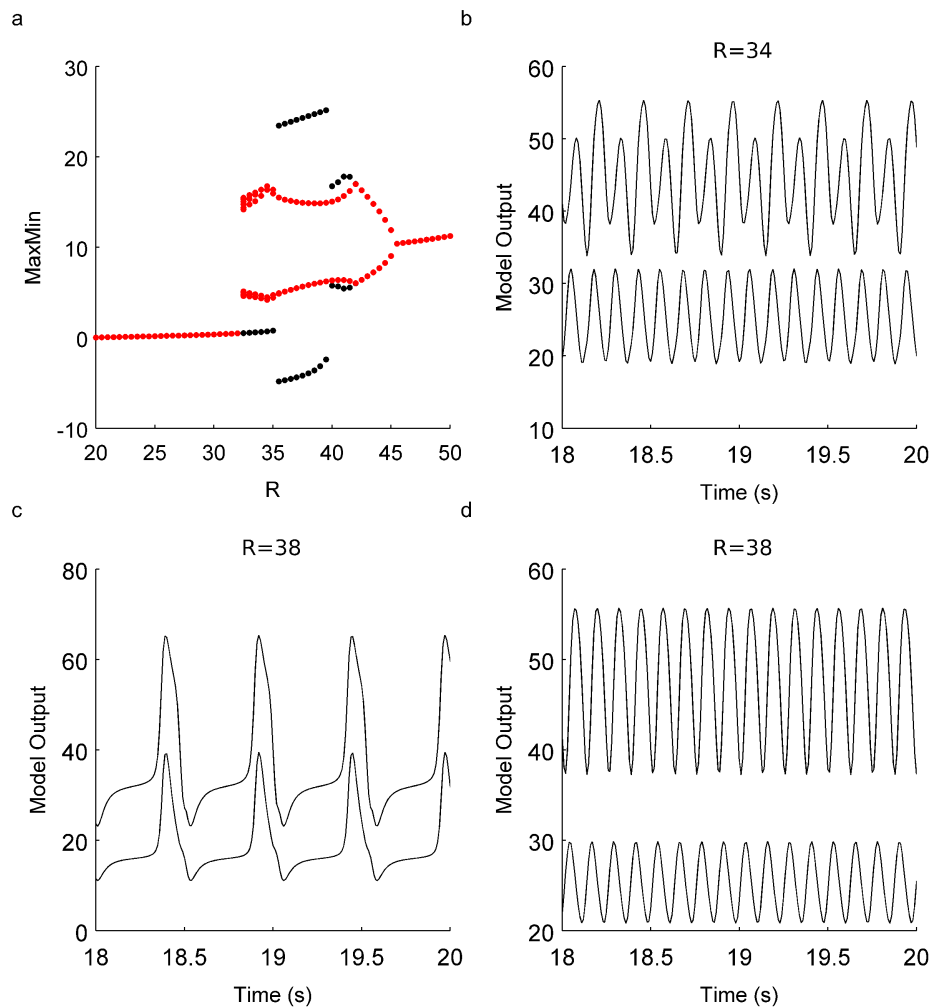
Figure 3.4: Dynamics of 7 compartments with hexagonal nearest neighbour coupling. a) bifurcation diagram for changing R. Maxima and minima are plotted for a peripheral compartment. The forward scan is plotted in black and the backward scan is plotted in red. b) mixed oscillations at $R=34$, c) spiking solution at $R=38$, , d) oscillatory solution at $R=38$. In b-d, time series for the central compartment and an outer compartment are plotted with an offset along the vertical axis.

A larger region of cortex was modelled by an extended two-dimensional sheet of connected model compartments. At the default value of $B=22$, low values of R in large two dimensional systems typically lead to sustained mixed oscillations. For example a 15×15 grid with $R=20$ outputs heterogeneous oscillations with apparent

frequency components ranging from 5 to 10 per second and heterogeneous amplitudes and phases, somewhat reminiscent of mixed oscillations in the one dimensional case. As in the one dimensional case, these oscillations can be replaced by the fixed point solution if B is increased for a given coupling strength. In such a case, a stimulus applied to the system in the background fixed point can evoke a travelling wave, as shown in Figures 3.5 (a) and (b). A movie of this response is given in supplementary file "SFigure5a.mp4", which can be obtained from Goodfellow et al. (2011b).

In contrast, at different values of coupling strength R, more complex responses can be observed (Figures 3.5 (c) and (d)). Here, the system is identical to that in Figures 3.5 (a) and (b), but $R = 35$, i.e. coupling is stronger. The initially induced wave activity evolves with a tail of higher amplitude compared to that observed for $R=20$, and causes the evolution of two subsequent travelling fronts. Collision of wavefronts then eliminates further activity leading to a total duration of around 1 second for this transient. A movie of this response is given in supplementary file "SFigure5c.mp4", which can be obtained from Goodfellow et al. (2011b).

In addition to travelling waves, it is expected that a two dimensional excitable system can propagate spiral activity (see e.g. Winfree (2001)). Indeed, our two dimensional, excitable system is capable of generating complex spiral waveforms, as shown in Figure 3.6 (a) and (b), for a $N=421$ square arrangement of hexagonally coupled compartments with $B=35$ and $R=50$. A movie of these dynamics is given in supplementary file "SFigure6.mp4", which can be obtained from Goodfellow et al. (2011b).

The effect of changes in inhibitory gain, B, and connection strength, R, on the dynamics of a cortical patch modelled by the 421 compartment system were explored with random initial conditions over different combinations of these two parameters. Figure 3.7 (a) maps the presence of fixed point versus oscillatory dynamics and therefore indicates the region appropriate for examining stimulus induced transitions from the lower steady state. It can be seen that fixed point activity is generally found for extremely low or high B. The fixed point region to the left of the oscillatory band is saturated in a higher state, though peripheral compartments still oscillate for smaller R. The band to the right of the oscillatory region resides at the lower steady state and is therefore the starting point for the investigation of responses to stimuli.

The response to stimuli in the region of the lower steady state solution (white region to the right of Figure 3.7 (a)) was found to vary depending upon the value of R and B, the effects of which are explored in Figure 3.7 (b). Figure 3.7 (b) is colour coded by length of activity evoked by stimulation, with darker colours indicating longer transients, and displays approximately three regions of differing activity. In the very light grey region at the top right (approximately $R \leq 18$ and
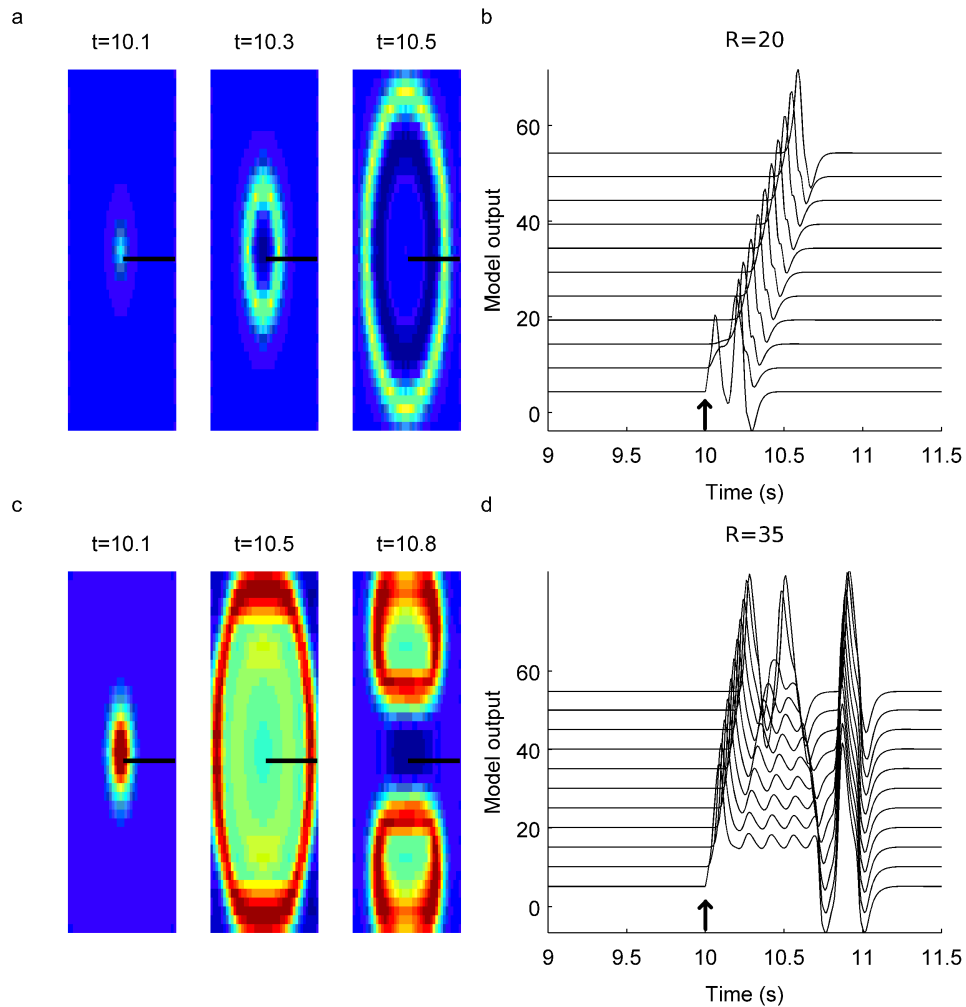
Figure 3.5: The effect of perturbation to a central compartment in the two dimensional, homogeneous system. a) snapshots of wave propagation due to stimulus, $R=20$ and $B=28$, at t=10.1, 10.3 and 10.5 seconds The black line indicates a one dimensional projection for the time series plotted in b), which are plotted with an offset on the vertical axis. c) more complex transient due to stimulus, snapshots shown at t=10.1, 10.5 and 10.8 seconds. $R=35$ and $B=28$, time series for compartments along the black line in c) are plotted in d) with an offset on the vertical axis. The duration of these responses can be seen in supplementary files "SFigure5a.mp4" and "SFigure5c.mp4", respectively, which can be obtained from Goodfellow et al. (2011b).

$B \geq 22$) a stimulus evokes no travelling response and therefore the duration of the perturbation to model output is of the order of the length of stimulation. In the darker grey region (approximately $18 \leq R \leq 40$ and $B \geq 25$), the stimulus evokes at least one travelling wave. In general, for constant R, the responses are more complex for smaller B, i.e. near the boundary of the oscillatory domain.

The darker squares within this region, including those coloured black, elicit more than one travelling wave or more complex responses. We note that the number of compartments stimulated, as well as their position in the system, affects activity
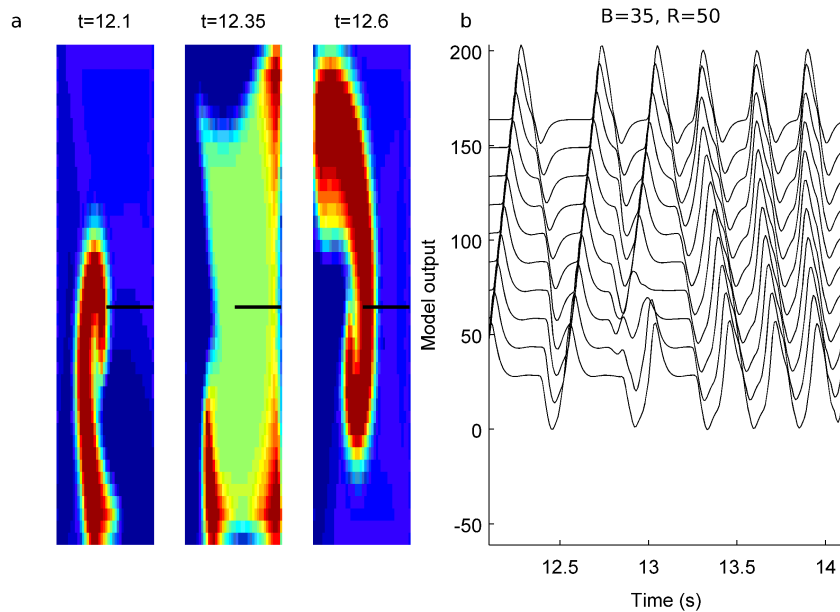
Figure 3.6: Example of complex spiral waves in a system with N=421, B=35, R=50. Images in (a) represent t=12.1, 12.35 and 12.6 seconds. Time series for the compartments along the black line in (a) are plotted in (b) with an offset along the vertical axis. A movie of these dynamics is provided in supplementary file "SFigure6.mp4", which can be obtained from Goodfellow et al. (2011b).

post-stimulus. For instance, if stimulation of a single compartment does not elicit a response, the stimulation of multiple compartments occasionally can. The response of the system to stimulus at the centre and at the edge of the system is often not equivalent.

3.4.4 Reverberating activity in a stimulated model of heterogeneous cortex

It is expected that there are spatial heterogeneities in normal cortical tissue, as well as in the case of focal epilepsies. In particular, in cases of intractable epilepsy, often there exist deformations, such as dysplasias, which are capable of conveying abnormal activity (Fauser and Schulze-Bonhage, 2006; Fauser et al., 2009). In addition, a recent modelling study highlighted the importance of considering heterogeneity in a spatially extended neural mass model of epileptic dynamics (Goodfellow et al., 2011a). We investigated the effect of spatial heterogeneities in cortical tissue by forming a two-dimensional extended system with a central region containing diminished inhibition. A 421 compartment system (21 x 21 hexagonally coupled compartments, i.e. with symmetry around the central compartment) was formed with R=20. In the central hexagon of 7 compartments, B was set to 22 ("disinhibited"), whereas in the surrounding compartments, B was set to 28 ("normal"). The layout of this system is illustrated in Figure 3.8.
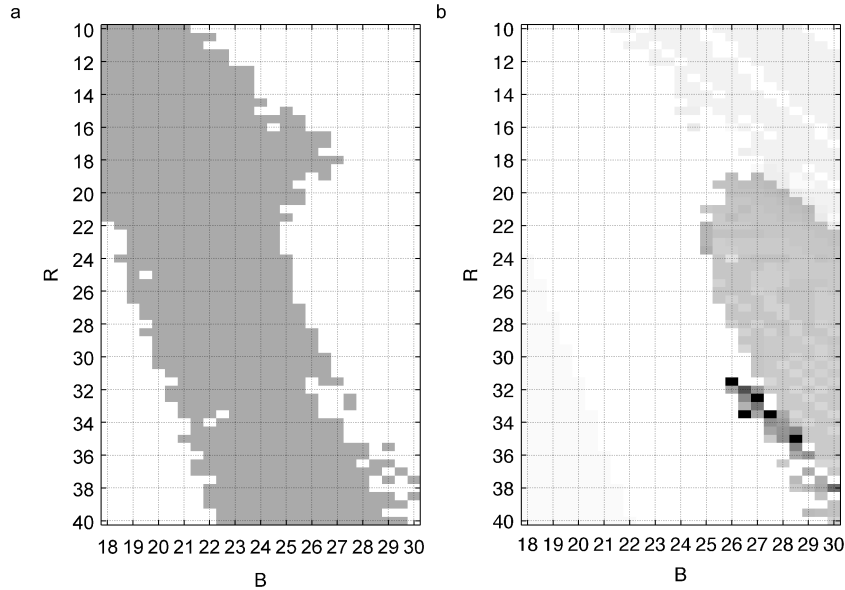
Figure 3.7: Investigation of the dynamics and stimulus response of the homogeneous two dimensional system with $N=421$. a) Map of fixed point versus oscillatory dynamics over changes in B and R (other parameters are default values as in Table 3.1). Systems with fixed points are coloured white. The region of grey represents oscillatory dynamics. Fixed point solutions to the left of this region are at the high steady state, whereas those to the right are at the lower steady state. b) shows the length of response to stimulus, with the system initially in the lower steady state, and stimulus of strength 300 applied for 0.1 seconds to the central compartment. Darker colours indicate longer responses, with black representative of transients longer than 3 seconds. Very light grey squares in the top right corner indicate a response only in the stimulated compartment.

Following our previously described results, it might be expected that the surrounding tissue is more likely to propagate single waves, whereas the compartments of the centre might generate more complex oscillatory activity. From random initial conditions, the system was left to settle into a background fixed point, to which a stimulus was applied. The response to a stimulus of duration 0.1 seconds and size 300 applied to 8 different locations was investigated, with results shown in Figures 3.9, 3.10 and 3.11.

Depending upon the location of the stimulus, the system can display different responses, consisting of i) a simple propagating wave (Figure 3.9, (a)), ii) two waves propagating from the centre (Figure 3.9, (b)) or iii) more complex and longer lasting transients (Figure 3.9 (c, d, e)). In the latter case, the oscillatory waveform at each compartment is heterogeneous, similar to the results reported previously in evoked oscillations in cortical slices (Bai et al., 2006). Example spatial patterns for stimuli 1 (a) and 8 (e) are shown as snapshots in Figures 3.10 (c) and (e), respectively. Movies showing these responses are given in supplementary files "SFigure10c.mp4" and "SFigure10e.mp4", respectively, which can be obtained from Goodfellow et al. (2011b).
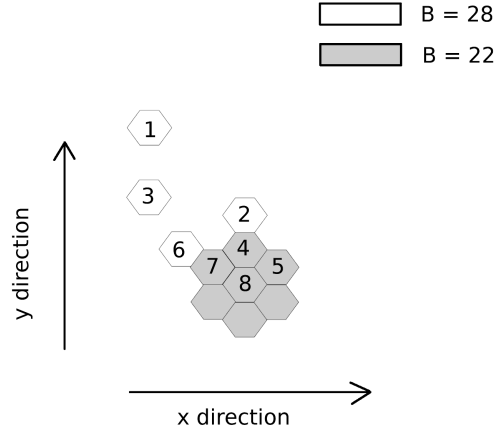
Figure 3.8: Schematic of the heterogeneous system with a central hexagonal region of diminished inhibition. Also shown are the locations of 8 compartments which were subjected to a single pulse perturbation.

In order to compare this behaviour to observations from repetitive responses in humans, we must consider the size of the modelled system in relation to brain tissue. A previous whole brain model based on the neural mass framework employed a single compartment as a model for a voxel of diameter 1-3mm (Sotero et al., 2007). These dimensions are in line with the original formulation of the neural mass model as a model for a cortical column (Jansen and Rit, 1995). Thus we proceed with the assumption that each compartment represents a $1mm$ diameter column, which implies a size of $421mm^2$ for the entire 421 compartment model. Each quadrant of this model can therefore be assumed to represent activity recorded by a single electrode of diameter $2.3mm$, separated by $10mm$, as used in Valentin et al. (2002).

Figure 3.10 (d) and (f) each show four mean field time series representing the averaged activity of each of the four corners of the heterogeneous system in Figure 3.8 under stimuli 1 and 8, respectively. The mean field of the response of the heterogeneous system to stimulation 8 (see Figure 3.8) shows a repeated series of irregular waves, as in the abnormal "repetitive response" described by Valentín et al. (2005) (recreated here in Figure 3.11 (b)). This is in contrast to activity propagated in the homogeneous system, the mean field of which is a single wave lasting approximately half a second, as observed in the "early response" presented in Valentín et al. (2005) (recreated here in Figure 3.11 (a)). For direct comparison, we re-create in Figure 3.11 some features of the spatially varying response to perturbation observed in humans.

The time series of a mass adjacent to the stimulated compartment is shown
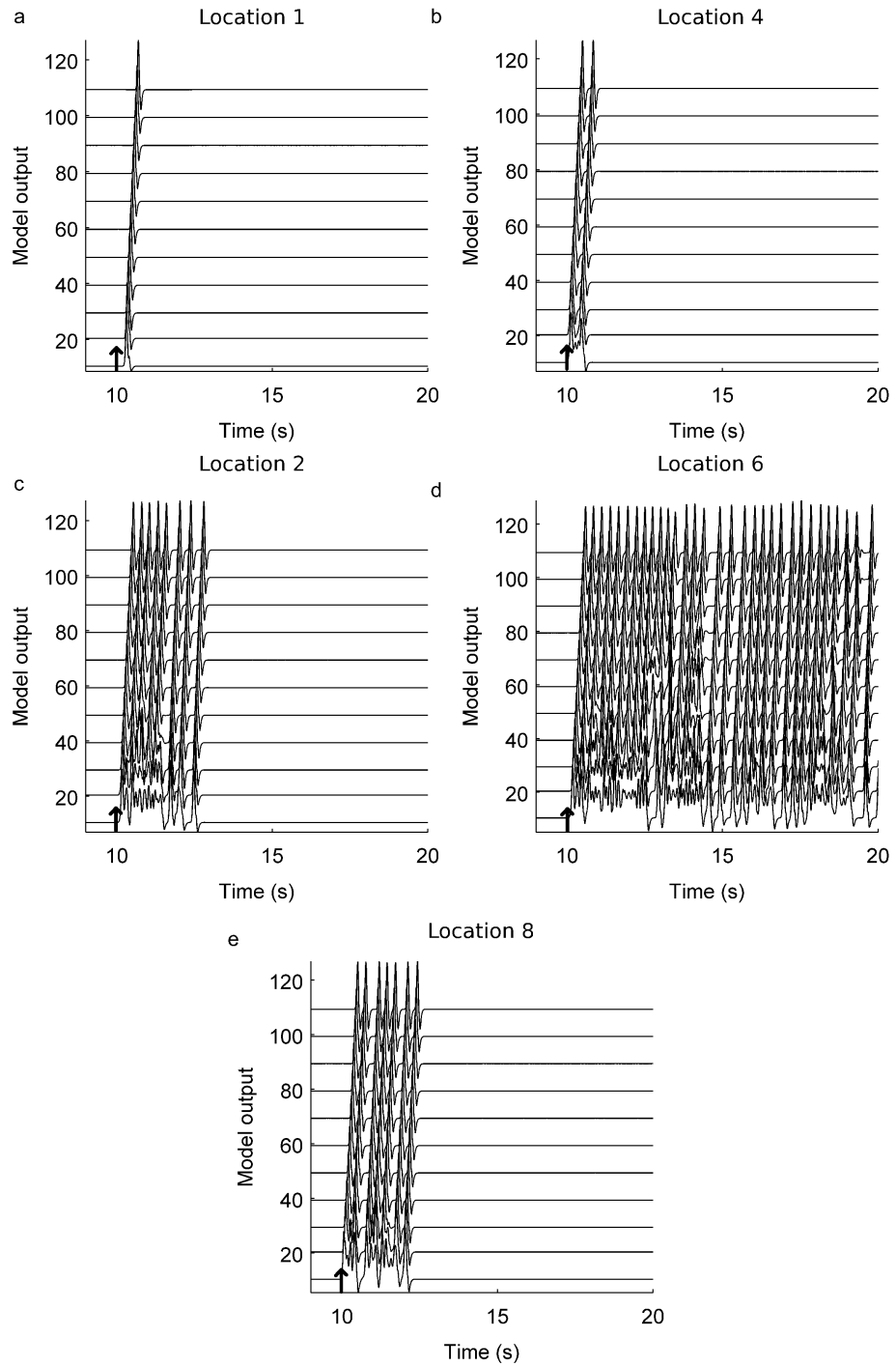
Figure 3.9: Time series for response to stimulus at a selection of the different locations marked in Figure 3.8. Shown are responses for positions 1 (a), 4 (b), 2 (c), 6 (d) and 8 (e) in Figure 3.8. Time series are plotted with an offset on the vertical axis. Stimuli were delivered at 10 seconds for a duration of 0.1 seconds and with strength 300.

for the homogeneous and heterogeneous cases in Figure 3.12. It can be seen that
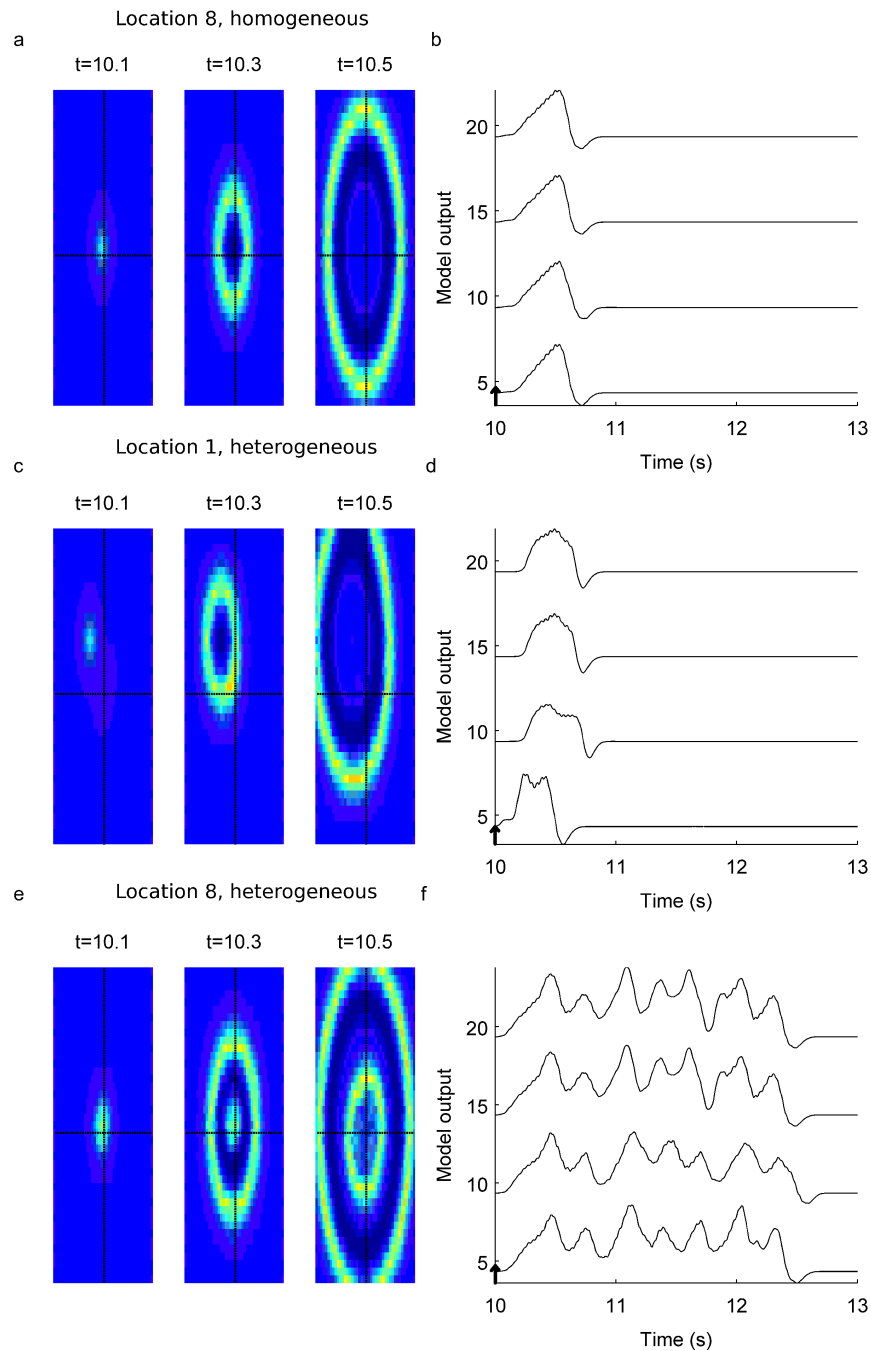
Figure 3.10: Comparison of spatiotemporal patterns and model mean field in the case of wave propagation in the homogeneous system (a and b), stimulus 1 in the heterogeneous system (c and d) and stimulus 8 in the heterogeneous system (e and f) (see Figure 3.8 for the location of these stimuli). The four channels in b), d) and f) represent averages of activity in the 4 corners of the system, indicated by broken black lines in (a, c, e). These are plotted with an offset on the vertical axis. Movies for the responses shown in c) and e) are given in supplementary files "SFigure10c.mp4" and "SFigure10e.mp4", respectively, which can be obtained from Goodfellow et al. (2011b).
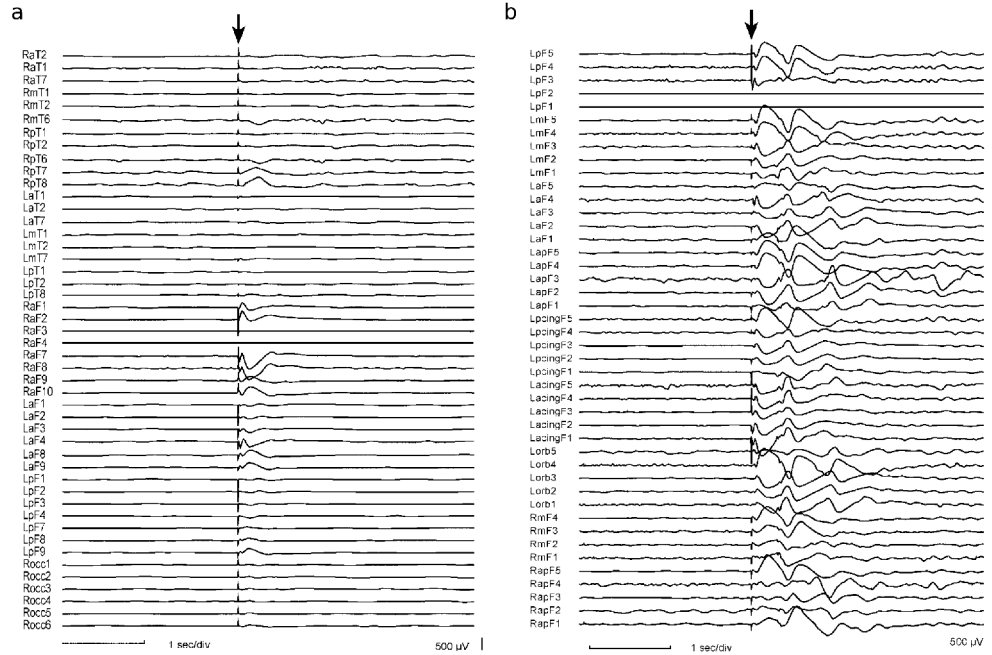
Figure 3.11: Examples of (a) "early" and (b) "repetitive" responses observed in human tissue in response to single pulse perturbation. (a) recreated from Valentín et al. (2005), Figure 2A and (b) recreated from Valentín et al. (2005) Figure 4A. A key feature in relation to the present modelling study is the difference in transient length due to single perturbation, which is space dependent in the epileptic brain. The repetitive response, seen in retrospectively determined epileptogenic tissue is a complex spatio-temporal transient.

in the case of simple single wave propagation, there is a strong hyperpolarisation immediately following the large amplitude spike, whereas in the case of the more complex transient, there are varying degrees of hyperpolarisation throughout the transient. We note that in the case of the heterogeneous model, the steady state of the compartments with reduced inhibition are at a higher level than those in the heterogeneous system. The depth of the hyperpolarisation in the heterogeneous compartment becomes closest to that of the homogeneous system only during the hyperpolarisation preceding termination of the oscillation.

3.4.5   Beyond nearest neighbour coupling

The model we presented is governed by nearest neighbour connectivity in order to examine the effect of transmission of neural mass spiking due to local connections. In this section we demonstrate how this assumption can be relaxed in order to investigate more complex connectivity patterns, which will be an important feature of future work. We note that, in this section specific examples are provided to guide the reader in the ways that the model can be extended in future, rather than providing a thorough description of system dynamics, which will be left to future
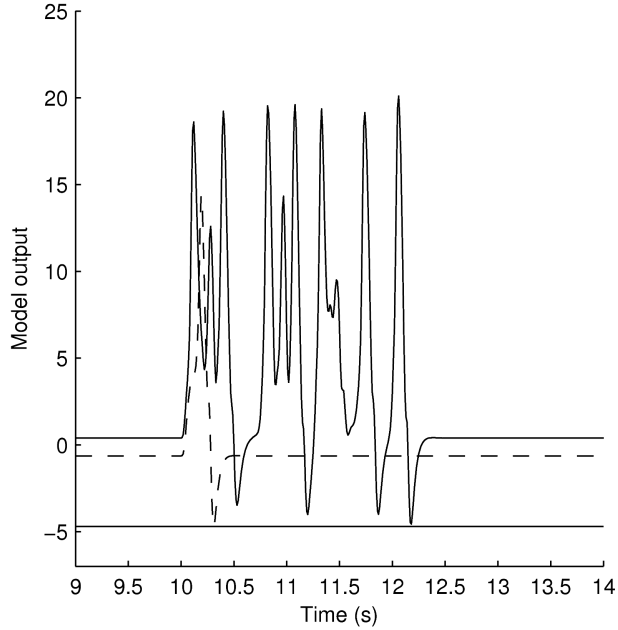
Figure 3.12: Time series of a compartment adjacent to the stimulated electrode in the homogeneous system with propagating wave (dashed line, compare Figure 3.9 (a) and Figure 3.10 (a)) and the heterogeneous system with complex transient (solid line, compare Figure 3.9 (e) and Figure 3.10 (c)). The solid horizontal line indicates the minimum value reached by the homogeneous system.

work.

Here, we persist with the notion that, at the level of connectivity between neuronal populations, connections to local regions predominate (Boucsein et al., 2011). This has been modelled in large scale neural mass formulations of brain connectivity by an exponential, distance dependent function (Jirsa and Haken, 1996; Sotero et al., 2007). In the model presented here, applying such a function smoothes the coupling to include contributions from beyond the first neighbour. Connectivity in this scheme is given by:

$$R_{ij} = r \cdot \frac{1}{2\sigma} e^{-\frac{|x_i - x_j|}{\sigma}} \tag{3.4}$$

where R_{ij} is the resulting connectivity between two compartments, r is a scaling factor common to all network edges, σ is a parameter determining the spatial extent of connectivity and x_i, x_j denote the position of nodes i and j in the square lattice. $|x_i - x_j|$ denotes the Euclidian distance given by:

$$\sqrt{(x_i(1) - x_j(1))^2 + (x_i(2) - x_j(2))^2} \tag{3.5}$$

With this extended connectivity, the homogeneous system can display complex spatio-temporal patterns and also steady state dynamics depending on its parameters. For example $\sigma = 0.5$ and $r = 146$ leads to a fixed point in a square system

of 31×31 compartments, and the evocation of a single travelling wave due to stimulation (data not shown). Adjusting σ leads to changes in the size of travelling wave fronts (as well as parameters required for steady state). Thus, in exploring the parameters of the model in future studies, one will need to consider the size of the system and its boundary conditions in relation to the variance of connectivity.

This extended coupling scheme also allows the study of additional long-range connectivity (Boucsein et al., 2011), since the propagation of activity is not dependent only on nearest neighbours. We demonstrate how the system might be used in the context of the current study by once again introducing a region of diminished inhibition at the centre of the system (here a 4×4 square). With $r = 100.7$ the heterogeneous system settles into its steady state, in which stimulus response is space dependent (results not shown).

We now provide an initial demonstration of the capability to explore more complex connectivity patterns. The distance dependent connectivity was supplemented by randomly drawn long-range connections of strength equivalent to that connecting closest neighbours. This was achieved by first constructing the distance dependent adjacency matrix, then scanning over entries and adding connections with a specified probability (with probability given by the parameter p). An image of the top left corner of the resulting connectivity matrix is given in Figure 3.13 (a).

Interestingly, with p=0.001, the steady state, under the parameter settings previously employed, is often difficult to recover under random initial conditions. Thus, we can speculate that in this regime, the system is more likely to reside in an oscillatory state due to the distribution of connectivity. If long range connections are restricted to nodes outside this central region, the steady state can be more easily recovered from random initial conditions, and stimulating a central compartment elicits a prolonged reverberating response, as shown in Figure 3.13 (b).

Also of interest is that when the probability of long-range connectivity is increased to 0.002, the steady state is also recovered even when the central region is included in the long-range structure. In this case, the response to stimulation has interesting dynamics, with increased synchrony in bursting across the range. This response is shown in Figure 3.13 (c).

3.5 Discussion

In this study we explored spatial extensions to a previously proposed neural mass model of epileptic spiking (Jansen and Rit, 1995; Wendling et al., 2000, 2001, 2002; Grimbert and Faugeras, 2006; Spiegler et al., 2010). It was demonstrated that this model, under the assumption of excitatory nearest neighbour connectivity, is an excitable system which can propagate activity induced in a single stimulated compartment. We found that the system could display complex reverberating responses
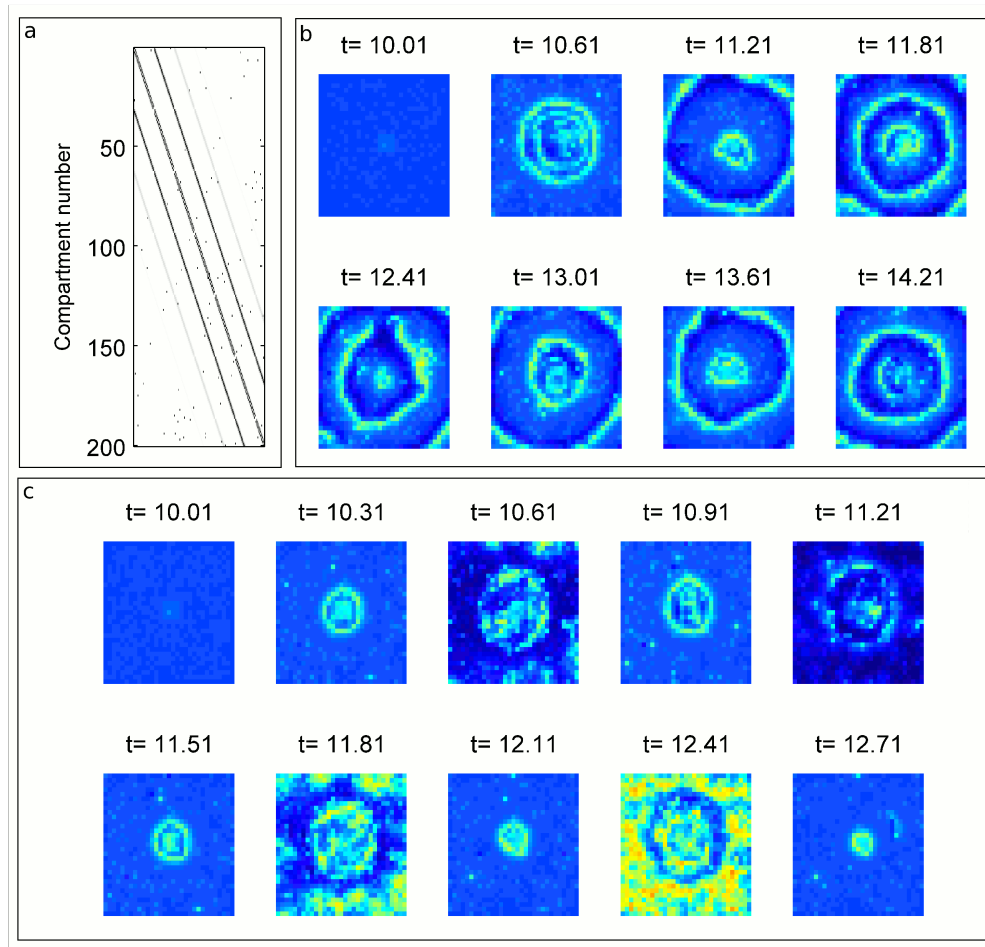
Figure 3.13: Dynamics of a system with non-local connections. a) shows the top left corner of the adjacency matrix (nodes 1 to 200) when σ=0.5 and p=0.002. Notice the scattering of long range connectivity in combination with distance dependent connectivity. b) shows snapshots of the dynamics of the system with σ=0.5, r=100.7. In this case long range connectivity is restricted to nodes outside the central region of diminished inhibition. c) shows snapshots of the same system, but with p=0.002 and long range connectivity allowed also with the central region. See section 3.4.5.

to a single pulse perturbation and is therefore relevant to the mechanisms underlying macroscopic epileptiform responses *in vitro* (Pinto et al., 2005) as well as in the human brain (Valentin et al., 2002; Valentín et al., 2005; Flanagan et al., 2009).

Specifically, we predict the existence of complex rhythmic responses in excitable media formed by interacting excitatory and inhibitory neural populations, as assumed for the neocortex. This is due to excitability in the vicinity of a saddle-node on limit cycle bifurcation and the (co-)existence of either a fast oscillation or a corresponding saddle-focus. We demonstrate that this framework allows the investigation of the dynamic consequences of spatial heterogeneity and that this can result in the formation of long lasting rhythmic transients in response to single-pulse perturbations. This allows us to combine insight from smaller scale properties (cortical

excitability) with macroscopic clinical observations to propose the specific hypothesis that long EEG transients derive from the spatially transmitted self-activation of regions of diminished inhibition.

3.5.1 Complex spatio-temporal responses to stimulation are underpinned by neural mass excitability

An important correlate of epileptiform activity at the *neuronal* level is the paroxysmal depolarising shift (PDS), characterised by an overt depolarisation of neurons (Elger and Speckmann, 1985; McCormick and Contreras, 2001). Certain epileptiform events on the EEG are caused by the synchronous activation of PDSs in local neuronal populations. Thus, at the level of the *neural mass*, we propose that the spiking dynamics observed in the neural mass model can be regarded as representative of locally synchronous paroxysmal depolarising shifts. Accordingly, the neural mass makes a transition from relative quiescence to a brief period of high activity, causing a spike in the output of the mass, with subsequent hyperpolarisation.

This framework assumes a resting state of the neural mass with a low output of principal neurons, which from the dynamical systems perspective is modelled by a fixed point. This state can be perturbed by surrounding tissue undergoing abnormal spiking, or stimulation delivered from an external source. The model of a fixed point at the level of the neural mass is a scheme often employed in models of the transition to epileptic activity (Wendling et al., 2000; Breakspear et al., 2006; Marten et al., 2009a) and the apparently random nature of background EEG can be approximated by applying a time dependent noise to the fixed point. Although it might be a reasonable assumption that, at the level of the neural mass in an asynchronous state, activity is averaged out and relatively quiescent, other models of non-quiescent background activity have also been proposed (Shusterman and Troy, 2008; Goodfellow et al., 2011a). In order to better understand the nature of the production of epileptic rhythms in neural masses, the equations governing the dynamics of background EEG demand more attention in the future.

The response of epileptic tissue to local perturbations as well as the spontaneous initiation, spreading and termination of seizure activity is represented by transient spatio-temporal rhythms. Complex spatio-temporal transients have been described in excitable media (Zimmermann et al., 1997; Jung and Mayer-Kress, 1995; Tel and Lai, 2008) and we here specifically introduce a dynamic mechanism for the generation of rhythmic transients following a single-pulse stimulus as used in pre-surgical evaluation of epileptic neocortex. We find that a description at the macroscopic level requires excitatorily coupled spiking mass models. By considering spatially extended systems of population PDS, we offer a framework with which to investigate the transmission of abnormal activity over large regions of cortex, mediated by local, excitatory interactions. The role of these mechanisms in the spreading

of epileptiform rhythms is an important unanswered question in epilepsy research (Elger and Speckmann, 1985).

3.5.2 Spatially extended models of rhythmic activity: benefits of the current model

Previous mathematical models have offered insight into the formation of spatio-temporal patterns and the spreading of activity in nervous tissue. Nervous tissue based excitable media have been demonstrated to be capable of producing propagating waves (Pinto and Ermentrout, 2001) and spiral dynamics (Huang et al., 2004; Laing, 2005), which are in line with experimental results (Chervin et al., 1988; Huang et al., 2004; Pinto et al., 2005; Bai et al., 2006; Schiff et al., 2007; Wu et al., 2008). Mathematical models have also been shown to propagate single and multiple travelling waves (Troy and Shusterman, 2007) or sustained synchronous responses to stimulation (Shusterman and Troy, 2008).

In addition to these disinhibited systems, cellular automata-like models have been used to investigate the spreading of activity. Kaiser et al. (2007), for example demonstrated that a hierarchical structure is capable of producing a critical state for the contained propagation of activity in a network. Traub et al. (2010) presented a cellular automaton model for the appearance of patches of activity in relation to very fast oscillations observed in epileptic tissue. Examination of the activation of neuronal networks in epilepsy has also been addressed at the microscopic level of modelling, for example in the work of Lytton et al. (2008).

The model we present here, based on interconnected neural masses, provides several important advances compared to these previous models. First of all, it is important to address the mechanisms of clinical epileptic data at the macroscopic level (Wendling et al., 2000; Suffczynski et al., 2006b; Goodfellow et al., 2011a). By forming spatially extended systems at this level in the form of neural mass models, with physiologically interpretable parameters, the macroscopic propagation of activity, and its dependence on local excitatory and inhibitory processes (Wendling et al., 2000) as well as network interactions (Goodfellow et al., 2011a) and heterogeneities can be explored. A key feature relating to the spreading or suppression of epileptiform activity is the presence of local "surround" and "vertical" inhibition (Elger and Speckmann, 1985) and the modulation of inhibitory processes has been demonstrated to affect the ability of synchronous activities to form and spread (Trevelyan et al., 2006). It is therefore important to consider the role of inhibitory processes, which are preserved in the mass model presented in this study. The model might be extended to include inhibitory nearest neighbour connections, which, when diminished, might then support the spreading of activity, as suggested by Trevelyan et al. (2006). The physiological interpretability of parameters in the mass model allow us to make more meaningful models of functional deficiencies, such as diminished

inhibition, and assess their impact on network dynamics.

Another crucial aspect of the framework presented here is that we consider the transition into epileptiform rhythms as invoked spatio-temporal dynamic transients. This marks a shift in emphasis away from a time dependent modulation in system parameters (bifurcations) to explain epileptiform EEG (Breakspear et al., 2006; Marten et al., 2009a; Kramer et al., 2005; Kim et al., 2009; Lopour and Szeri, 2010) and places more weight on the self-organising capabilities of spatio-temporal networks in the brain.

3.5.3 Network connectivity and dynamics

There is much work regarding network connectivity in nervous tissue and its relation to epilepsy. Morgan and Soltesz (2008), for example, used a detailed neuronal model of the dentate gyrus to show that the inclusion of hubs in the connectivity network could lead to an enhanced susceptibility of the network to seizure activity. Hierarchical connectivities have been shown to be important for the spreading of activity (Kaiser et al., 2007). Though we focussed here initially on nearest neighbour connectivity and the properties of excitable media, we also demonstrated an extension of the system into more complex network structures through the addition of long range connections. The future investigation of stimulus response dynamics in the model framework presented here must consider different model connectivities. Indeed, our model framework will allow the investigation of the role that network connectivity plays in the formation of complex responses to stimuli at the macroscopic level, and in combination with spatially structured heterogeneities.

The incorporation of different connectivity structures, including hierarchical and long range connectivity, must be supplemented by considerations regarding time delays in transmission between different neuronal populations separated by increased distances in the brain. Several previous formulations of large scale brain dynamics in the neural mass framework have taken into account delays between compartments (Jansen and Rit, 1995; Wendling et al., 2000; David et al., 2004; Sotero et al., 2007). Indeed, the value of an explicitly modelled time delay has been shown to affect the frequency of rhythmic dynamics in a heterogeneous coupled neural mass model (David and Friston, 2003). Future investigations of the dynamics of the system presented here can incorporate transmission delays in the ODE framework by modelling delayed transmission as an additional temporal convolution, as proposed initially by Jansen and Rit (1995).

3.5.4 Local inhibition and excitation balance determines stimulus response dynamics in connected neural masses

Excitatory coupling induced new types of behaviour in the model composed of compartments set into a region of parameter space conferring fixed point dynamics. In the system composed of two compartments, for example, coupling led to spiking or faster oscillatory activity for certain values of coupling strength, R (see Figure 3.1). In larger systems, the region of oscillatory activity for the default value of inhibitory gain, B, was extended, although the fixed point was recovered for increased inhibition. This is in agreement with the notion that a modulation of inhibitory processes is important for the generation of rhythmic activity in epileptic tissue.

Three important features of the experiment of Pinto et al. (2005) can be recreated by our model of stimulus response in brain tissue, namely i) the all or none response depending on the size of perturbation (Figures 3.1 (d) and 3.2 (d)), ii) the dependence of this threshold on the regulation of excitatory and inhibitory activity in the slice (Figure 3.3) and iii) the demonstration of simple waves or more complex activity (Figure 3.2 (d,e), Figure 3.5). Thus our model provides evidence for the generation of propagating activity due to proximal excitatory coupling in a model with threshold excitability. In addition, many aspects of our model are also in agreement with analyses of spatio-temporal patterns imaged by voltage sensitive dyes. In particular, the study of Bai et al. (2006) reported the propagation of activity in a slice preparation with heterogeneous oscillations at different locations in the slice (see Figure 3.7 A in Bai et al. (2006)). This is reminiscent of our model activity close to the disinhibited region during reverberating activity (see our Figure 3.9 (e), bottom 2 traces). However, certain other observations cannot at present be recreated by our model, such as the potential delay, both temporally and spatially, from the onset of stimulation to the propagation of activity. Such effects have also been observed in humans (Valentín et al., 2005; Lesser et al., 2008). Future improvements to the model in terms of more complex spatial coupling may help to uncover potential mechanisms underlying these phenomena.

3.5.5 Modelling the implications of functionally heterogeneous regions: a hypothesis for the prolonged transient response to brief stimulation

The effect of introducing a localised region of diminished inhibition was the production of long and complex responses to perturbation (Figures 3.9, 3.10 and 3.11), which on the mean field were reminiscent of repetitive responses seen in human recordings (Valentin et al., 2002; Valentín et al., 2005; Flanagan et al., 2009). Our investigation of travelling wave and complex transient responses to pulse stimulation

therefore lead us to the following mechanistic hypothesis for the formation of repetitive responses. Local neural masses capable of generating spiking responses are modelled by the bifurcation structure inherent to the Jansen model framework, i.e. the presence of excitability from a low output state to a high amplitude "spike" orbit ("population PDS") due to a perturbation of the excitatory input (EPSP). These local masses are connected by nearest neighbour coupling. A spatially contiguous region of "reduced inhibition" within this system can then confer the capability to produce long lasting transient responses to short pulse perturbations due to i) a reverberation within the region of reduced inhibition and ii) the propagation of non-trivial wave activity from this location, which can then break and cause subsequent activity. Cessation of these transients is autonomous and relies on the system propagating a trivial wave away from the region of reduced inhibition, thus causing no further reverberation.

Thus we provide a demonstration of the putative mechanism proposed by Valentín et al. (2005), i.e. a "re-entry of neuronal activity" after the initial stimulation. This is supported, in our model, by a local region of reduced inhibition. Thus we predict that the complex space varying, transient responses to perturbation seen in epileptic tissue derive from a spatially localised diminished inhibition. This prediction is open to experimental testing *in vitro* and comparison to human stimulus responses in the future, and suggests that in understanding the mechanisms of epileptic processes, one should investigate in neural mass models not only the properties of tissue at a single location, but also the effect of spatial variation on pathological dynamics. The use of mechanistic modelling of the stimulus response in heterogeneous, macroscopic systems may in future provide a valuable tool with which to specify the neurophysiological features of the epileptogenic zone in focal epilepsy, which is defined as the brain area that has to be removed to render a patient seizure free (Rosenow and Lüders, 2001). Comparison to clinical stimulus responses in pre-surgical testing could then aid the localisation of the epileptogenic zone.

3.5.6 Modelling spatially dependent stimulus response dynamics

That single pulse perturbation might aid in the localisation of ictogenic tissue is of great interest clinically (Valentin et al., 2002; Valentín et al., 2005; Flanagan et al., 2009), where resection of epileptic tissue is an important therapeutic option for pharmacologically intractable cases. However, the mechanisms for spatially heterogeneous responses that depend on distance from ictogenic tissue are unknown. Applying perturbations to different regions in our heterogeneous model suggest that a stimulation in and around the region of diminished inhibition can cause an "activation" of this region in terms of subsequent generation of long lasting transients

(see Figures 3.9, 3.10 and 3.11). On the other hand, stimulating further from this region elicited a simple travelling wave, which on passing through the diminished inhibition region did not spark prolonged activity. These contrasting dynamics displayed waveforms on the mean field similar to those of the "repetitive" and "normal" responses seen post-stimuli in humans with epilepsy (Valentin et al., 2002; Valentín et al., 2005; Flanagan et al., 2009). Interestingly, stimulating a compartment directly adjacent to the region of diminished inhibition could evoke a longer transient than a stimulation inside this region (compare Figures 3.9 (b) and (c)). This offers an initial demonstration of the potential mis-localisation of ictogenic cortex. Future investigation of the mechanisms underlying these phenomena in mathematical models may aid our understanding of the processes relevant to repetitive responses, and therefore inform as to what responses are expected from various locations around an ictogenic region. Assisting the processes of accurately identifying appropriate tissue for surgical resection must be a long term goal for modelling studies such as the one presented here.

The observed time varying response to stimulation (Lesser et al., 2008) suggests the possible involvement of *ictogenic* processes at a variety of different time scales. A more complete understanding of the processes underlying epileptiform activity would therefore consider, in models of epileptic tissue, the contribution of long term, *epileptogenic* processes as well as short time scale and longer time scale *ictogenic* processes. Such considerations might be appreciated in Figure 3.7 (c) where the boundary between fixed point and oscillatory dynamics with respect to two of the system parameters can present regions of longer transient activity. In this kind of framework one might suggest that epileptogenicity presents the system with the capability to demonstrate such bifurcation structures, whereas ictogenicity presents a movement in this structure towards regions of oscillatory activity. In our model, as the system moves closer to the oscillatory region over *time*, longer transients due to stimulation can be observed.

However, we also showed in the heterogeneous system the effect of moving closer in *space* to an ictogenic region. In this way we demonstrated the potential importance of considering spatial heterogeneities in models of epileptic tissue, and therefore in the tissue itself. Indeed, it is known that spatial heterogeneities are associated with epileptogenicity. In models of post-trauma epilepsy, for example, it has been suggested that mechanisms leading to an enhancement of local excitatory connectivity (e.g. sprouting) or an impairment of inhibition (reduced effectiveness of inhibitory interneurons) are important epileptogenic processes (Prince et al., 2009). These mechanisms have been shown to contribute to the propagation of rhythmic activity in our model.

3.5.7 Perspectives on the measured speed of propagation of epileptic activity

The peak to peak time of transmission of spikes from one compartment to its neighbour in our two-dimensional system with $R=35$ was 0.02 seconds, which means that a distance of $1mm$ between compartments gives a velocity of $0.05ms^{-1}$. This is of the same order of magnitude as that reported by, for example, Pinto et al. (2005) and Chervin et al. (1988). However, it is important to note that many different propagation velocities for travelling spiking activity have been reported in the literature. In addition to the aforementioned values, which were derived from slice experiments, Meeren et al. (2002) reported propagation velocities of $1ms^{-1}$ in local field potentials recorded from epileptic activity *in vivo*. Kramer et al. (2005) reported speeds of $0.5ms^{-1}$ in ECoG recordings from human epileptic seizures. The differences in these reported velocities raise several important points. The first point is with regards to the scale at which measurements of spatio-temporal patterns are made. In the study of Meeren et al. (2002), activity was recorded bilaterally in the cortex of WAG/Rij rats using $100\mu m$ diameter electrodes separated by $2mm$. In the study of Kramer et al. (2005), ECoG recordings were made from electrodes with $2.3mm$ exposed surface and with $10mm$ spacing between discs. Thus, neither of these recordings allow to map the transmission of spiking activity between neighbouring cortical columns in the same way as the experiment of Pinto et al. (2005). In addition, we demonstrate in Figure 3.10 that transmission velocities in an excitable medium may not be conserved across scale. The underlying travelling wave, when averaged at the macroscopic scale appears synchronous between the four electrodes due to the location of the initiation of the wave at the centre of the system. Further discrepancies relate to whether propagating activity is conserved between *in vivo* and chemically treated *in vitro* recordings, between spontaneous and evoked activity, and also by the different techniques used to measure time delays. Each of these issues will need to be studied in order to resolve the spatio-temporal mechanisms of responses to stimuli in nervous tissue in the future.

3.5.8 Future perspectives on oscillations in the EEG and travelling wave activity

In this model we showed that macroscopic oscillatory activity might be underpinned by travelling waves at a smaller spatial scale (for example in the average waveforms observed in Figure 3.11). This raises an important issue regarding the origin of EEG waves and their relation to underlying "activity" of populations of neurons. In this sense, activity refers to a population level representation of the output of neuronal populations, or equivalently the entity that will be synaptically transmitted between locations in the networks of the brain. Importantly these two attributes

do not always coalesce, as will be outlined in greater detail for the case of SWD, in Chapter 5, and as can be seen directly in simultaneous recordings of neuronal activity and local field potentials (Truccolo et al., 2011). In this sense, one might therefore consider that there is a hidden variable in studies of LFPs (EEG), which is the activity output of the local mass. Indeed, since the EEG or LFP is thought to represent post-synaptic activity, it can be considered to represent the *input* into a local population rather than the *output* or activity of that population.

As mentioned in the description of spatially extended models in Chapter 2, and in the implementation of the model in the current chapter, the input to a neural mass is considered to be a spatially weighted average of connected activity. In this way, one might suggest that a locally recorded LFP wave represents the rise and fall of weighted afferent activity. The spatially extended neural mass model used in this thesis captures these dynamics by using the afferent post-synaptic potentials as the output of the mass at a given location. In future it will be important to ascertain the spatio-temporal dynamics of epileptic activity *in vivo* at the mesoscopic scale, in which the output of functional units such as cortical columns are visualised.

3.5.9 Outlook

In addition, future work will be needed to more systematically clarify the dynamics of the system, for example in comprehensive bifurcation and sensitivity analyses. Sensitivity in the current context will be most informative if it relates stimulus response dynamics to changes in the structure of the system, the spatial distribution of heterogeneities and the location of stimulation relative to heterogeneities (i.e. when specifying the concept of the "epileptogenic zone"). It is anticipated that these will be some of the most prominent patient and experiment specific features. However, this raises a number of non-trivial and currently unexplored details, for instance the quantification of spatio-temporal dynamic transients, and methods by which to systematically evolve heterogeneous topologies and assess spatial patterns, parameter distributions and network connectivities. It is therefore expected that future investigations of systems such as the one presented here will require advances in the study of dynamical systems and their computational implementation.

3.5.10 Summary

In conclusion, we have demonstrated a spatially extended neural mass model of complex, self-terminating, transient responses to perturbation. The systems creating these responses are excitable media based upon the excitatory transmission of epileptic activity at the level of the neural mass. The model gives potential new insight into the creation of complex reverberating responses due to perturbation in epileptic tissue, the propagation of complex oscillations in *in vitro* preparations,

and introduces new considerations regarding the spatio-temporal manifestations of epileptiform activity in the human brain. From the non-linear dynamics perspective, new emphasis is placed on transients to explain epileptiform activity, rather than the traditional analysis of asymptotically stable phase space structures.

In the following chapter (Chapter 4) the spatially extended neural mass model framework is extended to investigate the network mechanisms underlying *spontaneous* transitions into epileptiform EEG.

Chapter 4

Intermittent state transitions in a spatially extended neural mass model of SWD

4.1 Abstract

Generalised epileptic seizures are frequently accompanied by sudden reversible transitions from low amplitude irregular background activity to high amplitude, regular spike-wave discharges (SWD) in the EEG. The underlying mechanisms responsible for SWD generation and for the apparently spontaneous transitions to SWD and back again are still not fully understood. Specifically, the role of spatial cortico-cortical interactions in ictogenesis is not well studied. In this chapter we investigate the nature of this transition in spatially extended neural mass models.

Following previous investigation into the mechanisms of absence epilepsy, a simple extension is made to the neural mass model in the form of an additional slow inhibitory component. Spatial extensions to this model are explored and reveal bistability between two different oscillatory modes, one of which is a high amplitude spike-wave discharge (SWD). Further spatial extensions reveal intermittent transitions between background and SWD oscillations on the mean field. The deterministic model is therefore capable of producing absence seizure-like events without any time dependent adjustment of model parameters.

The emergence of such mechanisms due to spatial coupling demonstrates the importance of spatial interactions in modelling ictal dynamics, and in the study of ictogenesis. That these dynamics arise in heterogeneous systems highlights the role of focal abnormalities. In addition, a new model of the dynamics of transitions in epilepsy in neural mass models is introduced.

4.2 Introduction

The spike wave discharge

Spike and wave discharges (SWD) are electrographic features commonly recorded on the EEG during a variety of generalised epileptic events, including absence seizures, myoclonic seizures and seizures of the Lennox-Gestaut syndrome (see e.g. Hrachovy and Frost 2006). They can also be observed in stimulus induced afterdischarges (Blume et al., 2004). The term "spike-wave" gives an intuitive description of the multi-modal nature of this rhythm in that there is a fast component (the spike) followed by a slow component (the wave), although the exact morphology can be variable (Weir, 1965). In idiopathic generalised epilepsy (IGE), there is a characteristic, though variable frequency range for the rhythm at approximately 3Hz (Niedermeyer and Lopes da Silva, 2005), with slowing towards the end of seizures. In line with its importance in epilepsy, SWD dynamics and resulting spatio-temporal distributions are investigated in the remainder of this thesis.

A thorough investigation of the waveform of the SWD was given by Weir (1965). It was noted that "SWD" might be too simplistic a description, and that SWD are actually composed of at least four important components, namely "spikes" 1 and 2, a "positive transient" and the "wave". Weir (1965) also demonstrated some of the potential variable waveforms of the SWD. These are discussed in greater detail in Chapter 5. In addition to the variability in individual SWD waveforms, there is also much variability in spatial distribution of SWD even in the prototypically most homogeneous case of absence epilepsy. These spatial patterns are discussed further in Chapter 6.

Animal models of epilepsy with SWD

The importance of SWD in brain dysfunction has led to intense investigation of the underlying neuronal mechanisms in a number of different animal models of SWD seizures (Gloor et al., 1977; Marescaux and Vergnes, 1995; Steriade and Contreras, 1998; Coenen and Van Luijtelaar, 2003). Perhaps the most prominent results have been gained in studies of feline and murine models. Differences in findings between the models has meant that many controversies remain regarding the mechanisms of SWD seizures as observed, for example, in absence epilepsy. In addition, the exact morphological characteristics of abnormal rhythmic EEG activity in animal models often is not directly comparable to recordings made during human seizures. For example, two of the modern genetic murine models, namely the WAG/Rij (Coenen et al., 1992) and the genetic absence epilepsy rats from Strasbourg (GAERS) (Marescaux et al., 1992), display spontaneous, brief "absence" like seizure events accompanied by appropriate behavioural signs (i.e. they display behavioural arrest which appears similar to the impairment of consciousness observed in humans). The

equivalent EEG recording shows high amplitude rhythmic activity reminiscent of the sudden onset high amplitude activity observed in humans. However, the frequency of activity recorded in rats (8-10Hz) is often much faster than the equivalent observed in humans ($\sim$3Hz). Indeed, these waveforms have previously been referred to as high voltage spindles (Kandel and Buzsáki, 1997). Thus one of the grand challenges in uncovering the mechanisms of SWD resides in translating results from animal models into inference regarding human epilepsy. In future, there will almost certainly be a role for systems biology and mathematical and computational neuroscience in making these links.

Many different hypotheses regarding the mechanisms of absence seizures have resulted from studies in animal models. One of the persistent controversies has been the role of the thalamus in their generation, although it is now commonly accepted that absence seizures are disorders of thalamocortical networks (Blumenfeld, 2005), and much work has investigated the role of the thalamic processes (for example Cope et al. (2009) and Meeren et al. (2009)). However, it is also becoming clearer that the term "generalised" may mask the underlying heterogeneity of involvement of local networks (Holmes et al., 2004; Blumenfeld, 2005). Indeed, one of the major recent advances has been a shift in emphasis towards the view that a focal, cortical onset might be responsible for the generation of seizure activity (Meeren et al., 2002). This highlights the importance of spatial heterogeneities and spatially distributed networks throughout the brain. The apparently ubiquitous, large amplitude activity observed on scalp recordings during absence seizures perhaps led to the initial theories regarding the involvement of sub-cortical structures to either produce or propagate seizure activity in primarily generalised epilepsies. Although recent findings have reinforced the concept of focal, cortical abnormalities in absence epilepsy (Polack et al., 2007, 2009; Lüttjohann et al., 2011), the mechanisms by which seizure events arise and spread via macroscopic cortical and thalamic networks remain largely unknown. It is therefore an aim of the current chapter to advance our understanding of the potential mechanisms for spontaneous seizure onset in spatially extended, heterogeneous networks.

Despite the many differences between animal models of SWD, a ubiquitous finding is that of increased synchronous firing of cortical neurons during the "spike", followed by relative quiescence during the "wave". Thus, with the SWD comes a notion of increased synchrony and burst firing of neurons. One can assume, therefore, that synaptic connectivity and inhibitory and excitatory processes are crucial to the generation and propagation of seizure activity. However, another controversy that remains is the exact role of inhibitory post-synaptic activity, in particular in relation to the hyperpolarisation phase of the 3/s bursts which may rather be a product of aberrant potassium concentrations (Bazhenov et al., 2008).

Mathematical models of epilepsy with SWD

(Electro-) physiological investigations of animal models have been supplemented by mathematical modelling studies of the processes underlying SWD generation, particularly with respect to the putative thalamo-cortical network interactions thought to underlie the 3/s SWD of typical absence seizures, or the 9/s correlate in rat models (Destexhe, 1998; Suffczynski et al., 2004; Traub et al., 2005; Breakspear et al., 2006; Sargsyan et al., 2007; Marten et al., 2009a). Such approaches allow the investigation of SWD generating mechanisms at the systems level, i.e. at the level of complex interactions between the diverse range of processes known to underlie brain (dys-) function. In this way one can test hypotheses about the relative importance of these different processes for the generation of pathological macroscopic brain activity. For example, epileptic rhythms are underpinned by hyperpolarising and depolarising mechanisms (McCormick and Contreras, 2001) including, but not restricted to, synaptic interactions between excitatory and inhibitory neurons. These interactions have been incorporated into mathematical models of both focal onset seizures (Wendling et al., 2002; Labyt et al., 2006) and generalised seizures with SWD (Destexhe, 1998; Breakspear et al., 2006; Suffczynski et al., 2004; Marten et al., 2009b). In particular, the inclusion of different time scales of synaptic inhibition (Thomson and Deuchars, 1997) in these models has been important, although controversy remains over the relative importance of synaptic inhibitory processes in determining the rhythmic firing observed to underlie scalp SWD (Charpier et al., 1999; Timofeev et al., 2004; Bazhenov et al., 2008).

The role of cortico-cortical interactions

Models of thalamocortical network interactions underlying the generation of SWD represent an examination of a restricted set of the important mechanisms that may underlie ictogenesis and the emergence of epileptic SWD. In particular, the majority of connectivity within the cortex is of cortico-cortical origin (Douglas and Martin, 2007) and therefore one can assume that this connectivity plays an important role at least with respect to propagation of epileptic rhythms in the cortex. In addition, the mechanisms of SWD events in certain animal models are known to be predominantly of a cortical origin (Steriade and Contreras, 1998). Thus a more complete understanding of ictogenic processes will come from mathematical models incorporating these connections. However, the complex nature of neuronal connectivity in the cortex makes this a difficult task. In particular, a detailed characterisation of neuronal interactions over an extended region of cortex will result in an extremely large model in terms of number of variables and parameters (Markram, 2006). Drawbacks of such an approach include vast computational demands, difficulties in parameterisation and an inability to characterise system dynamics over changes in parameters.

These drawbacks can be overcome by modelling at the macroscopic level, with variables and parameters accounting for averages over large local networks of neurons, thus providing a parsimonious way with which to study spatially extended interactions (see Chapter 2).

Previous macroscopic models of SWD generation or ictogenesis in generalised seizures (Suffczynski et al., 2004; Breakspear et al., 2006) have not accounted explicitly for extended cortico-cortical connectivity. The model of Breakspear et al. (2006) was derived from spatially extended interactions in the cortex (a cortical field approach), though the transition to SWD was examined in a globally homogeneous mode. In the model of Suffczynski et al. (2004), a single thalamocortical network was studied, with no spatial extension in the cortex besides the local population of cortical neurons. However, macroscopic models incorporating cortico-cortical connectivities at a variety of scales do exist (Wilson and Cowan, 1973; Amari, 1977; Jansen and Rit, 1995; David and Friston, 2003; Sotero et al., 2007; Babajani-Feremi and Soltanian-Zadeh, 2010; Ursino et al., 2010). In particular, the model of Jansen and Rit (1995) incorporates a means to connect different cortical compartments and has been exploited as such in the study of mechanisms underlying rhythm generation in focal epilepsies (Labyt et al., 2006) and in Chapter 3.

Dynamic transitions in epilepsy

Transitions in EEG activity in epilepsy in general, and particularly in the case of absence epilepsy are clear candidates for the application of ideas from non-linear dynamical systems theory. In absence seizures, one observes a sudden transition into a brief epoch of rhythmic, non-linear EEG spike-waves, with sudden termination into background activity. The waveform observed, as well as the increase in synchrony assumed for underlying firing patterns (Neckelmann et al., 1998), has suggested the presence of a low-dimensional non-linear attractor, which has been supported by measures of non-linearity (Breakspear et al., 2006).

The idea that dynamical systems theory can help to conceptualise and investigate the dynamics of transitions in epilepsy has been forwarded explicitly by Lopes da Silva et al. (2003a,b) and Milton (2010). This relates more generally to the concept of "Dynamical Diseases" first proposed by Mackey and Glass (Mackey and Glass, 1977). In the case of epilepsy, Lopes da Silva et al. (2003a) proposed three explicit models for transitions from background to seizure activity. Each of these models relies on the existence of a "normal" and a "background" attractor (i.e. a bistable system), separated in phase space by an unstable structure (separatrix). The three models then relate to the process by which the brain might transit between these two attractors, and these can then clarify a concept of what constitutes a "normal" or "epileptic" brain from the perspective of the global structure of dynamical systems. In *Model 1*, the epileptic brain displays a short enough distance between normal

and abnormal attractors such that it can be perturbed between the two by noise. In contrast, the attractors are separated by a greater distance in the non-epileptic brain, and so the abnormal attractor is not likely to be reached due to perturbation of the dynamics by intrinsic noise processes in the brain. This has been proposed as a model for absence epilepsy, and demonstrated in a bistable, thalamocortical, neural mass model (Suffczynski et al., 2004).

Model 2 and *Model 3* on the other hand, propose that the two attractors are separated sufficiently in both the epileptic and normal brains. In these cases however, a time dependent parameter variation (endogenous, *Model 2*, or exogenous, *Model 3*) can cause the distance between the attractors to lessen, bringing the system into the epileptic state. Clearly, the differences in these conceptual frameworks carry implications for the question of whether a detectable pre-ictal state exists. In the latter two models it might be expected that the time dependent shift in phase space might be projected onto the EEG, rendering it detectable. In *Model 1*, however, no such time dependent change exists. However, in this case, one might test the hypothesis of closeness of attractors by perturbing the system, as has been carried out recently in WAG/Rij rats (see Lüttjohann et al. (2011), and the introduction to Chapter 3). Thus the idea that one can probe the "closeness" to an epileptic state is very appealing (Suffczynski et al., 2008; Kalitzin et al., 2010). However, the question of whether one requires the explicit feature of a separate dynamic attractor is open for debate (see for example the discussion regarding transient dynamics in Chapter 3). Milton et al. (2011), for example, has proposed that seizures can occur as transient dynamics due to the emergence of bistability at the onset of state transitions in the brain.

In this chapter we forward an alternative mechanism in the case of absence seizures, namely that in the epileptic brain, abnormal rhythms may actually be part of a single, complex attractor in a spatially extended system. In this case, the abnormal rhythms emerge spontaneously due to intermittent excursions into the apparently "abnormal" region of the attractor. The consequences of this idea are discussed further in the discussion of the current chapter and also in Chapter 7.

Aims of this chapter

In this chapter we aim to asses the consequences of interactions between local neural masses capable of producing SWD dynamics. Following previous studies regarding the importance of inhibitory processes at different time scales, a slow inhibitory process is incorporated into the model of Jansen and Rit (1995) and is shown to produce different dynamics relevant for the transitions observed in absence seizures. The dynamics of this model are explored in coupled systems in order to gauge the effect of spatially extended excitatory connectivity on the dynamic repertoire of the system.

4.3 Methods

4.3.1 Model

As in Chapter 3, we begin with the neural mass model of Jansen (Jansen et al., 1993; Jansen and Rit, 1995), which is described in detail in Chapter 2. We note here that the original form of the mass model has evolved recently to include many other physiologically relevant aspects of neuronal activity. In particular, versions of this model designed to account for ictal dynamics in partial seizures have included different time scales of inhibitory activity in the hippocampus (Wendling et al., 2002) and cortex (Labyt et al., 2006), with the latter model incorporating a slow inhibitory time scale mediated by $GABA_b$ inhibition. In this study we introduce a simple extension to the original Jansen model by including a second, slow inhibitory post-synaptic potential (IPSP) on the pyramidal neurons. The model structure is therefore close to that used by Wendling et al. (2002), though we omit the interactions between inhibitory processes that were inferred specifically for hippocampal activity. Controversy exists regarding the exact nature of the mechanisms for the hyperpolarising phase of bursting seen in neuronal recordings during the wave of SWD, with intrinsic membrane currents and potassium ion concentrations recently proposed to contribute (Bazhenov et al., 2008). Although the neural mass formulation used here is based upon synaptic interactions between populations of neurons, it can also encompass a more abstract notion of the delayed activation of excitatory and inhibitory processes. In this way, the model can be used to explore the dynamic effects brought about by coupling neural masses which incorporate relevant dynamic processes.

In the current study we also incorporate N interacting local populations of neurons, with inter-compartment connectivity as described in Chapter 3 . However, in this case, rather than examining nearest neighbour coupling, we investigate a small local region of cortical tissue by assuming all to all local coupling. Thus, the scale of the model might relate to a single node as described in Chapter 3. Again, we therefore do not consider here specific time delays. Investigations of inhibitory connectivity, longer range interactions and considerations of multiple recording scalp electrodes are also left to further studies.

In this chapter, each neural mass, defined by superscript i, is modelled by a system of 8 differential equations representing the interaction of excitatory and inhibitory cortical processes (Jansen et al., 1993; Jansen and Rit, 1995), with model equations given by:

$$\dot{y}_0^i(t) = y_4^i(t)$$

$$\dot{y}_4^i(t) = AaS[y_1^i(t) - 0.5y_2^i(t) - 0.5y_3^i(t)] - 2ay_4^i(t) - a^2y_0^i(t)$$

$$\dot{y}_1^i(t) = y_5^i(t)$$

$$\dot{y}_5^i(t) = Aa\{I + P^i + C_2S[C_1y_0^i(t)]\} - 2ay_5^i(t) - a^2y_1^i(t) \qquad (4.1)$$

$$\dot{y}_2^i(t) = y_6^i(t)$$

$$\dot{y}_6^i(t) = B_f b_f\{C_4S[C_3y_0^i(t)]\} - 2b_f y_6^i(t) - b_f^2 y_2^i(t)$$

$$\dot{y}_3^i(t) = y_7^i(t)$$

$$\dot{y}_7^i(t) = B_s b_s\{C_4S[C_3y_0^i(t)]\} - 2b_s y_7^i(t) - b_s^2 y_3^i(t)$$

Inter-compartment connectivity is defined by a homogeneous connectivity constant, R, representing coupling between different local populations. The input to each population, P^i $(i = 1, .., N)$ is therefore given by the weighted contribution of all other populations, as shown below:

$$P^i = \sum_{j=1, j \neq i}^{N} \frac{R}{N-1} S[y_1^j - 0.5y_2^j - 0.5y_3^j] \qquad (4.2)$$

We therefore use 4 blocks of impulse response equations (see e.g. Jansen and Rit (1995) and Chapter 2) to represent changes in the membrane potential of interneurons (1 block, output variable y_0) and pyramidal neurons (3 blocks, output variables y_1, y_2 and y_3). Within the model a net post-synaptic potential (PSP) is transformed via the sigmoidal activation function as described in Chapters 2 and 3.

4.3.2 Model parameters

The excitatory post-synaptic potential (EPSP) has the same time scale and amplitude parameters as the original model (Jansen and Rit, 1995). For the inhibitory processes, we set a fast and a slow time scale and tune the amplitude using the original parameter ratios (Jansen and Rit, 1995) as utilised in David and Friston (2003) and Spiegler et al. (2010). We note the use of different time scale and gain parameters for the inhibitory processes in this study compared to Wendling et al. (2002). Time courses of inhibitory synaptic processes have been shown to be highly variable and to lie in a range between lengths of the order of 20 ms (Thomson and Deuchars, 1997) and 500 ms (Otis et al., 1993). The time course of the slow IPSP used here is of the order of 300 ms (see Figure 4.1) and is thus within this physiologically plausible range. Furthermore, both of our IPSP time scale parameters reside within a physiologically plausible range suggested for time scale parameters of the Jansen model in a recent study (Spiegler et al., 2010).

We maintain the original internal connectivity ratios used to calculate $C1$ through

Parameter	Description	Value
A	Average excitatory gain	3.25mV
B	Average fast inhibitory gain	44mV
B_s	Average slow inhibitory gain	8.8mV
a	Average excitatory time constant	$100s^{-1}$
b_f	Average fast inhibitory time constant	100s^{-1}
b_s	Average slow inhibitory time constant	20s^{-1}
C, C_1, C_2	Connectivity constants	C is varied, $C_1 = C, C_2 = 0.8C$
C_3, C_4		$C_3 = C_4 = 0.25C$
I	External input to pyramidal neurons	I is varied
R	Matrix of connectivity constants	R is varied though is homogeneous.
v_0	Parameters of the sigmoid function	$v_0 = 6\text{mV}$
e_0, r		$e_0 = 2.5s^{-1}, r = 0.56\text{mV}^{-1}$

Table 4.1: Parameter values used for all output shown in this chapter. The fast and slow inhibitory gain parameters were derived by fixing the respective time scales and then deriving the gain from the ratio B/b, as suggested by David and Friston (2003).

$C4$. The total connectivity, given by C and the input parameter I are varied throughout the paper, though within ranges of previous publications (e.g. Jansen and Rit 1995; Wendling et al. 2002; Labyt et al. 2006). Parameters of the sigmoid function are the same as those used in previous incarnations of this model (Jansen and Rit, 1995). Figure 4.1 shows the time profile of the PSPs used in the model and Table 4.1 lists parameter values used in this study.
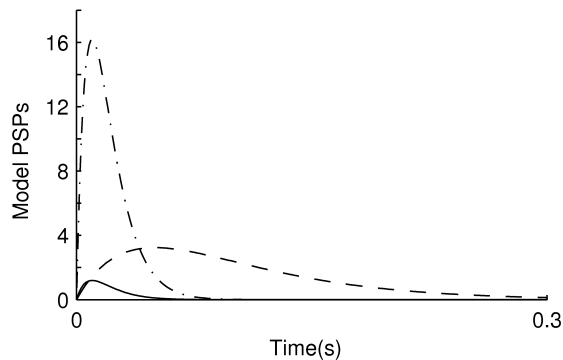
Figure 4.1: Time course of the three PSPs used in the model of section 4.3.1 with $R=0$: EPSP (solid line), fast IPSP (dot-dashed line) and slow IPSP (dashed line).

4.3.3 Analysis

Solutions of the model were explored by plotting bifurcation diagrams of time series maxima and minima over changes in parameters I, C, b_f and R. I represents input into the system and has been explored in previous bifurcation analyses (Grimbert and Faugeras, 2006; Spiegler et al., 2010), C and R represent connectivity within and

between cortical masses (Jansen and Rit, 1995), respectively, and are thus of interest in relation to ictogenesis. The time scale of fast inhibition, here represented by b_f, has been shown to be variable in experimental studies (Thomson and Deuchars, 1997). For each of these bifurcation diagrams, the presence of different solutions was determined by evaluating the model over increasing and decreasing values of one of these parameters, with all other parameters fixed. Relevant solutions identified by this procedure were allocated distinct marker types, as shown in Figure 4.3. In systems of multiple compartments, maxima and minima plots were given for one compartment only, though we note in each case qualitatively similar diagrams were obtained for the remaining compartments. In this case, we also calculated the distribution of pair-wise phase differences between compartments over a 2 second window using the Hilbert transform. The mean phase difference was plotted over the range of bifurcation parameter, with solution type extracted by inspection. Thus, in all bifurcation plots, regions of bistability were uncovered by forward and backward parameter scans, with markers allocated on plots by visual inspection of the time series of each solution.

In the spatially extended, heterogeneous models, the amplitude of the time series provided a good distinction between seizure (turbulent) and non-seizure (laminar) phases (see Figures 4.9 (b) and 4.10 (a)). It was observed that seizure periods predominantly carried amplitudes greater than 10, whereas non-seizure periods were of a much lower amplitude. Since each of these simulations was at least 1000 seconds in length, it was decided that phase lengths would be determined at a resolution of 1 second. The lengths of laminar and turbulent phases were therefore characterised by whether the maximum amplitude was greater than 10 in non-overlapping windows of 1 second length.

4.4 Results

The results section is divided into three parts, representing an investigation of model dynamics at three different spatial scales. Section 4.4.1 deals with a model of a single compartment, section 4.4.2 considers two coupled compartments, and finally, section 4.4.3 explores the dynamics of a model of a small cortical region composed of twenty five connected compartments. In Figure 4.2 we provide a peri-ictal recording of frontal scalp electrode EEG during absence seizure in order to demonstrate several important clinical features of these events and also to facilitate comparisons with features of the model transitions described. In particular we note the apparently spontaneous transition from low amplitude oscillatory background dynamics into high amplitude SWD activity and back again.
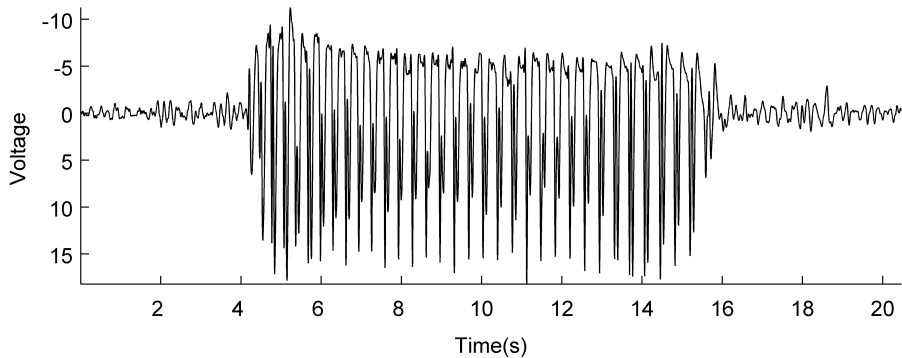
Figure 4.2: 20 second extract of a clinical absence seizure recorded from a frontal electrode. Negativity is plotted upwards by convention.

4.4.1 One compartment

The dynamics of the one compartment model were explored numerically by evaluating model output over a range of a selection of system parameters. The effect of changes in I, C and b_f are shown in the bifurcation diagrams of Figure 4.3. Figure 4.3 (a), (b) and (c) show model dynamics over changes in I for C=190, 220 and 240 respectively. It can be seen that different system behaviours emerge for different combinations of I and C. In particular, the system is capable of displaying fixed point (thin lines, single maxima, "Fp", Figure 4.3), sinusoidal limit cycle oscillations (henceforth referred to as "background" oscillations, marked as "Bckg", open circles Figure 4.3), SWD (marked as "SWD", stars in Figure 4.3), poly-SWD (marked as "pSWD", open squares in Figure 4.3) and "other oscillations" (marked as "O1", "O2" and "O3", grey lines, Figure 4.3). Exemplary time series for each of these solutions are given in Figure 4.3 (f), which also serves as a legend for this and subsequent bifurcation diagrams (Figure 4.6 and Figure 4.8). Maxima and minima of the SWD solution are identical in the forward and backward scan. Note that there are two minima and two maxima per spike wave complex.

For small values of C, solutions are either fixed point or background oscillations (Figure 4.3 (a)). There is a region of bistability between these two solutions for small I at C=190 (Figure 4.3 (a), "BS1"). The SWD solution emerges for larger C (Figure 4.3 (b), "SWD") and widens over I as C increases (Figure 4.3 (b), (c)). The amplitude of the background oscillations is consistently smaller than that of the SWD. There is also the emergence of poly-SWD behaviour for large I and C (Figure 4.3 (b), "BS3" and Figure 4.3 (c), "pSWD").

With I fixed at 135 s^{-1}, dynamics over changing C are shown in Figure 4.3 (d). As C increases the system moves from fixed point to background oscillations and then into SWD for large C. With C fixed at 190, dynamics over changing b_f are shown in Figure 4.3 (e). It can be seen that low values of b_f result in a large amplitude slow oscillation (Figure 4.3 (e), "O3"), whereas intermediate values produce SWD dynamics. As b_f nears the default parameter value of 100 s^{-1} the

system passes through a region of bistability between SWD and background oscil-lations (Figure 4.3 (e), "BS8"). Though several other small regions of bistability were encountered (Figure 4.3 (b) "BS2", Figure 4.3 (c), "BS4" and "BS5", Figure 4.3 (c), "BS6" and "BS7"), the default parameter values used throughout this study placed the one compartment system into a monostable regime, with respect to the parameters investigated. These default parameter values are indicated by vertical lines in Figure 4.3.

Figure 4.4 shows details of two of the oscillatory solutions in the model, namely the SWD and the background oscillation, which are the focus of this study. The SWD solution consists of rhythmic "on/off" firing of neurons in the mass (Figure 4.4 (e)) as is commonly observed in animal models of SWD. The SWD waveform carries contributions from all three underlying PSPs, with increased EPSP and firing during the positive (downwards) deflection and quiescence of firing during the "wave" (Figure 4.4 (c), (e)). The background solution also has rhythmic firing at a faster frequency (approximately 15Hz, Figure 4.4 (f)), though firing is not "on/off" as it reaches neither the maximum nor minimum firing capability. The Fourier spectrum of the SWD (Figure 4.4 (g)) shows a dominant peak at 2.5 Hz and a number of harmonics due to the nonlinear waveform. The Fourier spectrum of the background oscillations (Figure 4.4 (h)) has its main peak at 15 Hz.

There exist several modes of transition into SWD dynamics within this model. In Figure 4.5, we demonstrate two possible such transitions, namely i) a ramping of parameter C for fixed I and ii) a perturbation of the input parameter I. Figure 4.5 (a) shows a model time series under the ramp in parameter C, which is displayed in Figure 4.5 (b). In the "pre-seizure" state, the system oscillates at the background frequency. As C starts to increase the amplitude of the oscillation increases and at a threshold level of C the spike-wave oscillation is activated. When the control parameter crosses the critical point the dynamics return to the original background oscillation. The bistability (Figure 4.5 (d) "BS7") seen for changing C means that the threshold level on the way up and the critical point on the way down are not equivalent.

To demonstrate transition ii), with the system in the background oscillation state (e.g. C=190, I=135 s^{-1}), a finite pulse of short duration (see section 4.4.2) was applied. Depending on the phase at which this pulse was delivered, the system could respond with a transient single spike-wave oscillation before returning to the background oscillation. An example of this behaviour is shown in Figure 4.5 (c), with stimulus time indicated by an arrow.
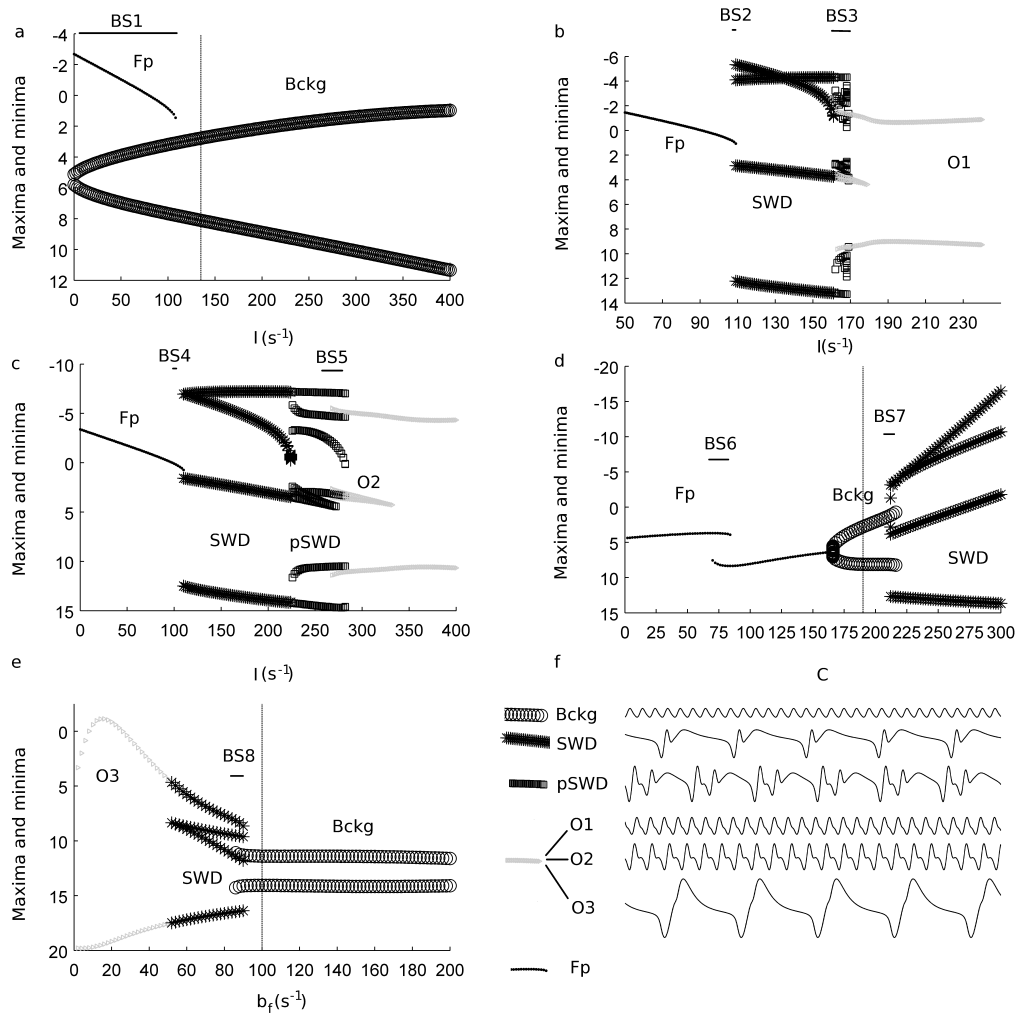
Figure 4.3: Bifurcation diagrams showing model dynamics of a single compartment (maxima and minima) over changes in I, C and b_f. (a), (b) and (c) show dynamics for changing I at C=190, 220 and 240, respectively. (d) shows dynamics for changing C with I fixed at 135 s^{-1}. (e) shows dynamics for changing b_f with I=135 s^{-1} and C=190. (f) shows 6 solutions along with the marker style used to represent them. For clarity, background (Bckg), SWD (SWD), poly SWD (pSWD) and other (O1, O2 and O3) solutions are also indicated by text labels on each figure, as are regions of bistability (BS1 to BS7). The location of parameter values used in later parts of the study are indicated by vertical lines.

4.4.2 Two compartments

To investigate the effect of spatial interactions in this model, the dynamics of a system of two coupled compartments was explored (Figure 4.6). Here, C was fixed at 190, which in the one compartment model resulted in background oscillations or a fixed point (see Figure 4.3 (a)). In this regime, the effect of the input parameter, I, was explored for different coupling strengths, with bifurcation diagrams of time series minima over changing I shown for two of the investigated values, R= 25 and R=50 in Figure 4.6 (a) and (b), respectively.

In the two compartment model we observed each of the dynamics observed in the
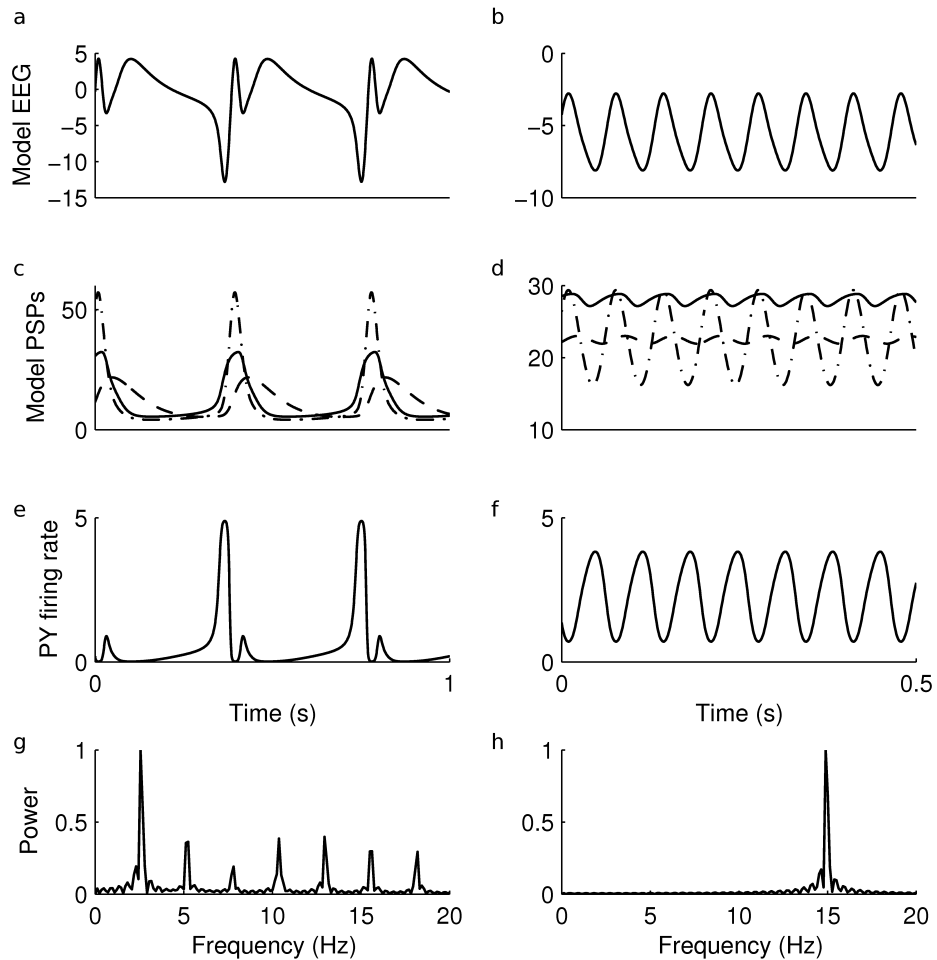
Figure 4.4: Properties of two of the oscillatory model solutions in the one compart-ment model. The left column (a, c, e, g) represents the SWD solution (C=220, I=135 s^{-1}) whereas the right column (b, d, f, h) represents the background oscil-lation (C=190, I=135 s^{-1}). (a) and (b) show model time series (1 second and 0.5 seconds, respectively), (c) and (d) show internal PSPs, (coded as in Figure 4.1), (e) and (f) show firing rate of principal neurons (minimum is 0 and maximum is 5) and (g) and (h) show normalised power spectra.

single compartment model. In addition to the qualitative differences in waveforms observed with changing parameter values, which can be represented by standard bifurcation plots of time series extrema (of one compartment only, Figure 4.6 (a) and (b)), qualitative differences also emerged in terms of synchrony between the two compartments. This was manifest by differences in both amplitude and phase. In order to represent these effects, plots of phase difference between the two compart-ments are shown in Figure 4.6 (c) and (d) (see section 4.3.3).

At a coupling value of R=25 (Figure 4.6 (a)), a region of bistability between background and SWD oscillations emerges (Figure 4.6, (a) "BS9"). We note that since the uncoupled individual compartments are set into the background oscillation regime (see Figure 4.3, vertical lines), this new behaviour is entirely the result of
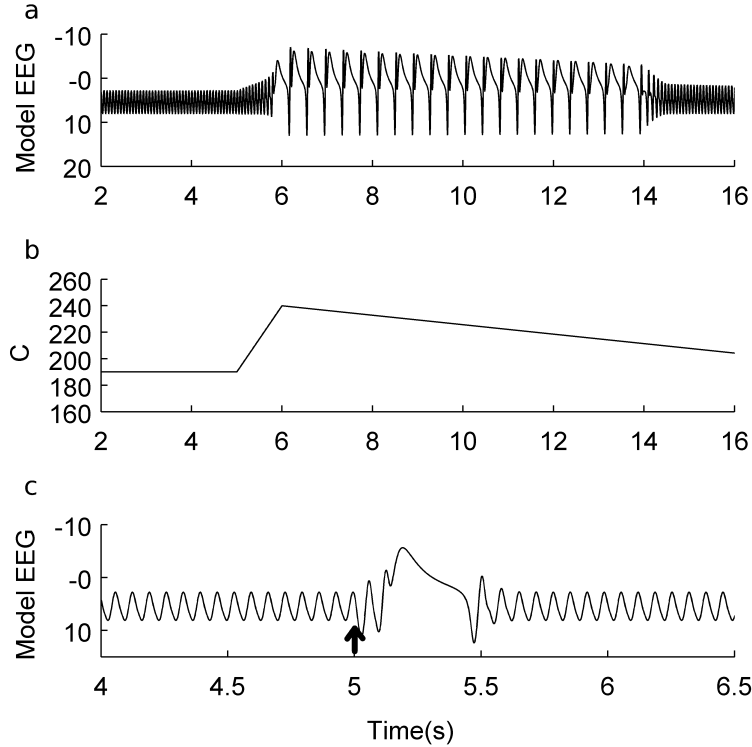
Figure 4.5: Transitions from background ($C=190$, $I=135$ s^{-1}) to SWD in the one compartment model. (a) shows model time series output as C changes according to the profile in (b). (c) shows the emergence of a SWD oscillation after perturbation from the background state with a finite pulse (strength $I=300$ s^{-1}, duration 0.15 seconds, onset at 5 seconds).

spatial coupling. In addition, the SWD solution is always homogeneous in the two compartments (Figure 4.6 (c), zero phase difference for SWD solution in region "BS9"), whereas the background solution in this region is always heterogeneous (Figure 4.6 (c), open circles). In this case (as well as in the qualitatively similar solution Figure 4.6 (d)) there exists a second solution with waveforms exchanged between compartments due to the symmetry of the model. We note that the power spectrum of the mean field of the SWD solution and the background solution are comparable to the one compartment case (Figure 4.4). For higher values of I, less sinusoidal "other" oscillations emerge, initially out of phase and with a periodic amplitude modulation, then settling to higher amplitude, in-phase solutions for larger I.

At $R=50$, SWD and pSWD solutions are identical in both compartments (Figure 4.6 (b) and (d)). A region of bistability exists for intermediate I between identical pSWD and out of phase "other" oscillations (Figure 4.6 (b), "BS10"). The insets of Figure 4.6 (c) and (d) indicate the nature of two of the out of phase solutions.

The bistable region between low amplitude, heterogeneous background oscillations and high amplitude, homogeneous SWD found for $R=25$ represents a good

model to study perturbation-induced transitions. The nature of such a transition in the model was explored by means of a stimulus to the input (I) of the model in its background state (Figure 4.7), with C=190 and initially I=135 s^{-1}.

The nature of model evolution post stimulus depended upon the strength, timing and duration of stimulus, and could either result in a return to background (sometimes accompanied by a switch in amplitudes (high vs. low) between the two compartments, results not shown) or transient or permanent SWD. In order to investigate these possibilities, the stimulus duration and amplitude were fixed (duration = 0.1s, amplitude = 300), and the effects of stimulus timing were explored. Results for two different stimulus times are given in Figure 4.7. The times relative to phase of underlying activity are shown by vertical bars in Figure 4.7 (a).

In the case that the model eventually returned to the background state, this invariably evolved via a transient of SWD activity. The length of this transient event, and also the degree to which the two compartments were synchronised during the transient period was found to be variable and dependent upon the state of the system at time of stimulus. An example of such a transient, resulting in a two second "seizure" is shown in Figure 4.7 (b). The underlying model PSPs for the onset and offset of SWD activity in this transient are shown in Figure 4.7 (c) and (d). It can be seen that the stimulus provides an increase in magnitude of all internal PSPs and results in an increased contribution of the slow IPSP, relative to the fast IPSP, thus starting the cycle of slow IPSP activation (dashed line) and subsequent system rebound. The offset, or transition from SWD to background activity stems from a rebound of activity before the end of the slow IPSP (Figure 4.7 (d)). In this case, immediate post-SWD compartments are in anti-phase and settle back to the heterogeneous background state. The stimulus could also provide immediate transition into permanent SWD (Figure 4.7 (e)).

4.4.3 Twenty-five compartments

The relevance of these results to larger cortical regions was explored by investigating a model consisting of twenty-five compartments with homogeneous (all-to-all) coupling (see section 4.3.1). The choice of twenty-five compartments enables the exploration of a system with increased complexity, whilst maintaining computationally tractable analysis time. An initial exploration of systems varying in size from three compartments to hundreds of compartments have demonstrated the results of this chapter to be conserved across vastly different system sizes. Here, we fixed C=190 and I=135 s^{-1}, and explored the dynamics of the system under changing R. Maxima and minima are plotted for one of the twenty-five compartments in the bifurcation diagram of Figure 4.8 (a). For low R, the system displayed out of phase background oscillations, which developed a quasiperiodic (amplitude modulated) dynamics with increasing R (Figure 4.8 (a), "Bckg" and "pBckg"). We stress that
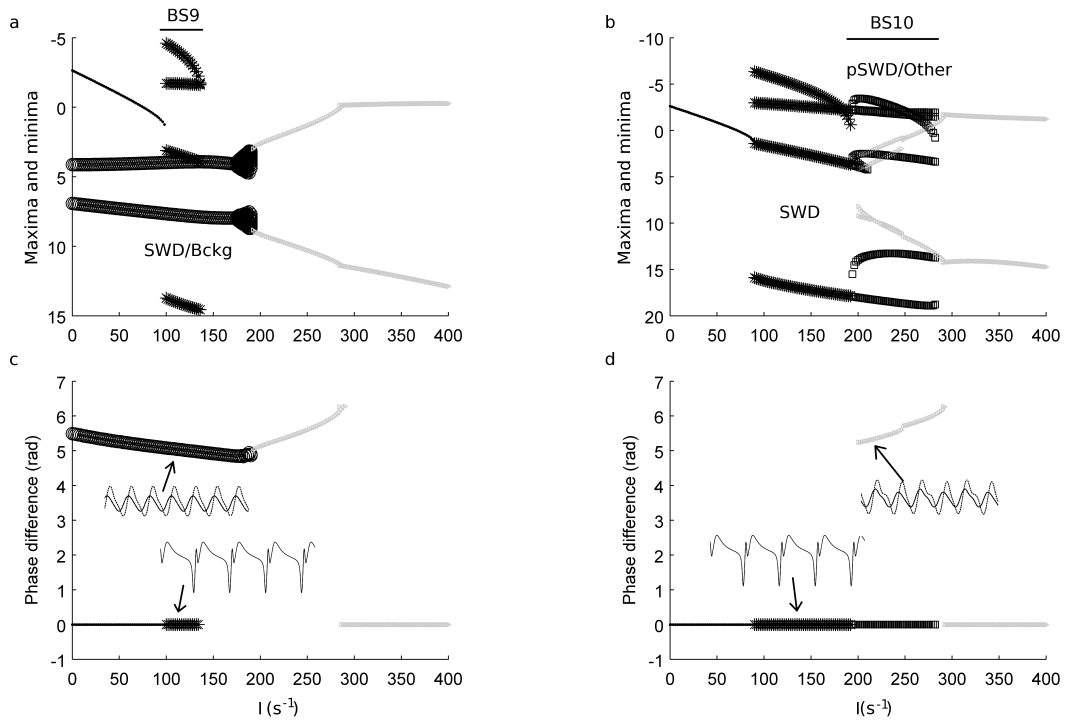
Figure 4.6: Bifurcation diagrams showing model dynamics in a system of two coupled compartments over increasing I for different values of R. C is fixed at 190. (a) represents dynamics at $R=25$, whereas (b) represents $R=50$. Maxima and minima are plotted using the same markers as in Figure 4.3, and are plotted for one compartment only. Bistable regions of interest are marked BS9 and BS10. (c) and (d) represent phase differences between the two compartments over the same ranges of I used in (a) and (b) (see section 4.3.3). Example time series for the out of phase solutions as well as the in phase SWD are shown in the insets of (c) and (d) at parameter locations indicated by arrows.

although this region with periodic amplitude modulation may look like a noise artefact, it is actually representative of certain periods during the time course in which the amplitude in all compartments undergoes a smooth increase and decrease. For higher R, the model produced a region of bistability (Figure 4.8 (a), "BS11"), again between in phase SWD and out of phase background oscillations (phase-locked or quasi-periodic). For values $R > 40$ the synchronised spike-wave is the only stable solution. The phase relationships for each of these solutions are represented in Figure 4.8 (b) as the mean of the distribution of pair-wise phase differences (see section 4.3.3). We note that in this and in the two compartment case, a small random error term was added to the initial conditions of each compartment prior to simulation in order that the compartments were not simply starting from identical initial conditions.

With reference to the results of Figure 4.7 in the two compartment case, we note that in the twenty-five compartment model in the region of bistability "BS11" in Figure 4.8 a pulse perturbation to the background oscillation most often elicited only a single SWD. However, more complex perturbations, for example a train of
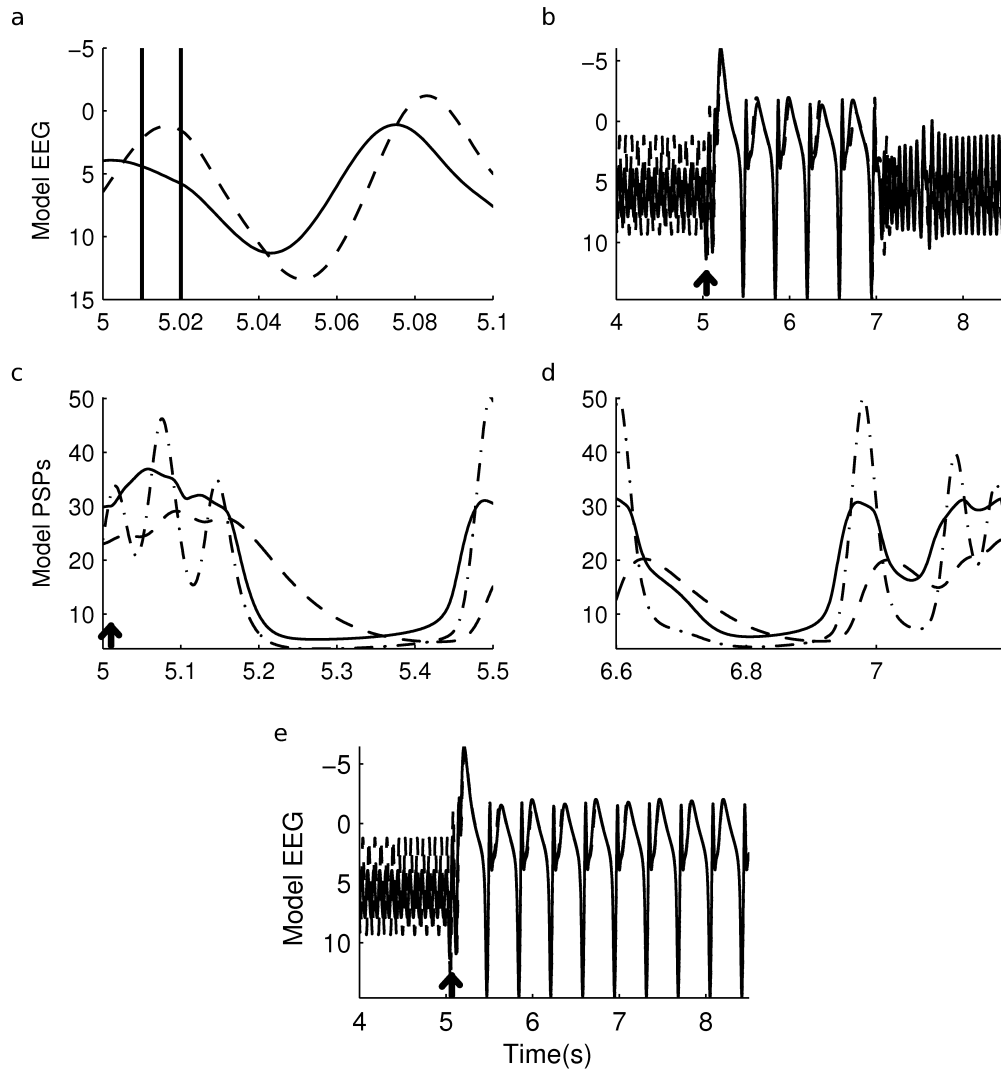
Figure 4.7: Effect of transient stimulus (strength $I=300$, duration 0.1 seconds) to the background state ($C=190$, $I=135$ s^{-1}, $R=25$) of the two compartment model. (a) shows a close up of the two compartments with stimulus times indicated by vertical lines. (b) shows model evolution for stimulus 1, both compartments are plotted, one solid and one dashed. (c) and (d) show close ups of underlying PSPs at onset of stimulus and offset of the transient SWD. PSPs are coded as in Figure 4.1, and are plotted for compartment one only for clarity. (e) shows model evolution for stimulus 2. Stimulus times are indicated by arrows.

two consecutive pulses, could lead to longer transient SWD trains or permanent SWD.

It is expected that spatially extended regions of cortex will not be homogeneous either in terms of connectivity or intrinsic dynamics. In order to investigate the effect of heterogeneity in our local cortical model, a random value drawn from a normal distribution was added to the time scale parameter of the fast IPSP. This attempts to reflect the array of fast inhibitory time scales observed in neocortex (Thomson

and Deuchars, 1997). The dynamics of the resulting system of non-identical compartments is explored in Figures 4.9 and 10. We found that the system could either display stable background oscillations, stable SWD oscillations or intermittent SWD trains of varying lengths and frequency of occurrence. Intermittency is an important type of dynamics in deterministic nonlinear models (see e.g. Berge et al. (1987) for an accessible introduction based on low-dimensional discrete dynamical systems). Intermittency is defined as the spontaneous switching between a (quasi-) regular (or laminar) phase of dynamics (in our case the background oscillations) and irregular outbursts of a second type of dynamics (in our case SWD). Different types of intermittency are classified according to the local instability of a periodic orbit using Floquet multipliers (Berge et al., 1987). This means that the SWD spike trains occur at irregular intervals and with irregular duration due to the intrinsic model dynamics and do not require parameter changes or additional noise terms in the model. Though we focus here on deterministic dynamics, the effect of noise on the parameter I was tested (results not shown). Noise with standard deviation 25% of I left the qualitative picture unchanged in that intermittent transitions with similar characteristics to the deterministic case were observed. When the standard deviation was increased to 50% of I, transitions became less distinguishable in terms of the difference in amplitude between non-seizure and seizure periods.

In an initial investigation of long simulations (200 seconds) of this heterogeneous system we noted that the mean value of b_f was smaller on occasions leading to the intermittent solution, and that in particular, values $b_f < 90$ s^{-1} in a number of compartments conferred either permanent SWD or intermittent dynamics. To clarify this point we made 50 long simulations, each of 10,000 seconds duration and each with a random normal distribution of b_f parameters, centred at b_f=100 s^{-1} and with standard deviation $b_f/10$=10. We categorised each of these simulations as either permanent SWD (Figure 4.9 (a), black regions), permanent Bckg (Figure 4.9 (a), white regions) or intermittent seizures (Figure 4.9 (a), grey regions) (see section 4.3.3). Figure 4.9 (a) shows the distribution of number of compartments with $b_f < 90$ s^{-1} for each of the aforementioned categories. It is clear that there is a systematic increase in propensity for SWD activity when a greater number of compartments have $b_f < 90$ s^{-1}. Note that in a single compartment, values less than 90 s^{-1} for b_f lead to SWD rather than background activity (see Figure 4.3 (e)).

To study the nature of the intermittent seizure activity, we present in Figure 4.9 (b) 5000 seconds of one of the intermittent solutions. This solution corresponds to a single point in parameter space. The horizontal lines provide a guide to the amplitude cut off used to distinguish SWD from background. In this example, a long simulation producing in excess of 1000 seizures provided a mean seizure duration of 8 seconds and a mean inter-seizure duration of 74 seconds. Following the analysis of intermittency in EEG from rat models of absence seizures (Hramov et al.,

2006; Velazquez et al., 1999), we analysed the type of intermittency by examining the distribution of lengths of the laminar phase (Figure 4.9 (c)) and by plotting a second return map of model amplitude for the laminar phase (Figure 4.9 (d)). Figure 4.9 (c) shows the distribution of laminar lengths on a log-log scale, overlaid on which is the gradient -1.5 expected for the case of parametrically driven one-dimensional maps with on-off intermittency (Heagy et al., 1994). Figure 4.9 (c) therefore demonstrates that this specific instance of our model is not consistent with power law scaling. Power law scaling is only expected close to the onset of intermittent behaviour (Chate and Manneville, 1987). In addition, the study of Hramov et al. (2006) demonstrated deviations from the power law under certain experimental conditions. A more complete understanding of the intermittency in our model and the relevance of this to experimental findings can therefore only be found with a full characterisation of the distributions with respect to its parameter space. The second return map of the laminar phases shows a noisy distribution of maxima (Figure 4.9 (d)). This is in disagreement with any of the types of intermittency that follow local bifurcations (e.g. type III intermittency) and in agreement with intermittencies associated with a global bifurcation.

One of the seizures from an intermittent solution is explored further in Figure 4.10. Figure 4.10 (a), shows the mean field model EEG during the seizure period, calculated as the average output of all 25 compartments. It can be seen that this mode of transition from background oscillation to synchronous SWD is comparable to the real seizure event shown in Figure 4.2 in terms of the change in amplitude and also the spontaneous onset and offset of SWD.

Overlaid on Figure 4.10 (a) are a succession of grids indicating the involvement of SWD in each of the twenty-five compartments during six five-second windows. The grids are colour coded to indicate the presence of SWD at some point during the window in each compartment, with grey indicating that a SWD oscillation was present. This was achieved by comparing the average time series maxima in this epoch against the mean from a known "seizure-free" period. Each grid represents the five second window at which it is located between the tick marks on the horizontal axis. It can be seen that in the pre-ictal and post-ictal periods, a small number of compartments are involved in intermittent SWD and that this behaviour is generalised over the whole local system during seizure. We note that the grey shading does not indicate that the compartment produced persistent SWD in this period, rather it indicates the presence of at least one SWD. Figure 4.10 (b),(c) and (d) show close ups of model time series at seizure onset, middle of seizure and seizure offset, respectively. Before seizure onset, most of the compartments oscillate without SWD dynamics, though the waveform of oscillations is heterogeneous due to the variance in time scale parameter. Occasional SWD also appear in some time series. During seizure, however, most compartments are clustered into SWD activity. The

heterogeneity in time scales can still be observed in the slight differences between SWD waveforms, though the activity remains predominantly phase locked. At the end of the seizure, this synchronous activity breaks apart as more compartments revert to background oscillations.

Figure 4.10 (e) shows a close up of the mean field model activity during the seizure, in which it can be seen that the underlying heterogeneity causes a fragmentation of the "clean" SWD waveform. For comparison, a segment of EEG recording during a typical absence seizure is shown in Figure 4.10 (g). Though the mean field model captures well the fragmentation of the wave observed in the real recording, the spike part of the SWD in the model is truncated. However, if an alternative conversion of model output to EEG is used (see Chapter 5), in which the internal model variables carry adjusted weights, the dynamics of the real EEG can be matched more closely. This is demonstrated by the model output of Figure 4.10 (f) in which the amplitude of spike relative to wave and the waveform in general closely resembles the recorded time series. In this case, certain deformations of the "classical" waveform, such as the introduction of small spikes into the wave, are captured by the model.

Interestingly, the power spectrum of the "pre-seizure" model mean field has a region of dominant power between 9 and 13 Hz. The power spectrum reflects the desynchronised irregular background dynamics. Due to the ergodic properties of the deterministic dynamical system, each of the compartments would have a similar power spectrum if evaluated over a very long time. However, on short time scales, the power spectrum of an individual compartment is typically more peaked than the spectrum of the mean field signal. This is in contrast to the background solution of the one compartment case which has a single peak at 15Hz (Figure 4.4). In the SWD region, the power spectrum peak has increased to approximately 3.2Hz and associated harmonics. However, due to the variability in waveform in the heterogeneous system, peaks are slightly broadened.

4.5   Discussion

We have shown that a cortical neural mass model containing two explicitly modelled time scales of inhibition can produce slow SWD as well as sinusoidal background oscillations, thus providing the means for a parameter driven transition to seizure. Exploration of dynamics in coupled models revealed that spatial extensions could in addition confer spontaneous transitions from irregular cortical background to synchronised spike-wave dynamics.

The single compartment model was capable of producing low amplitude oscillatory and high amplitude SWD or poly-SWD dynamics. The SWD oscillations were
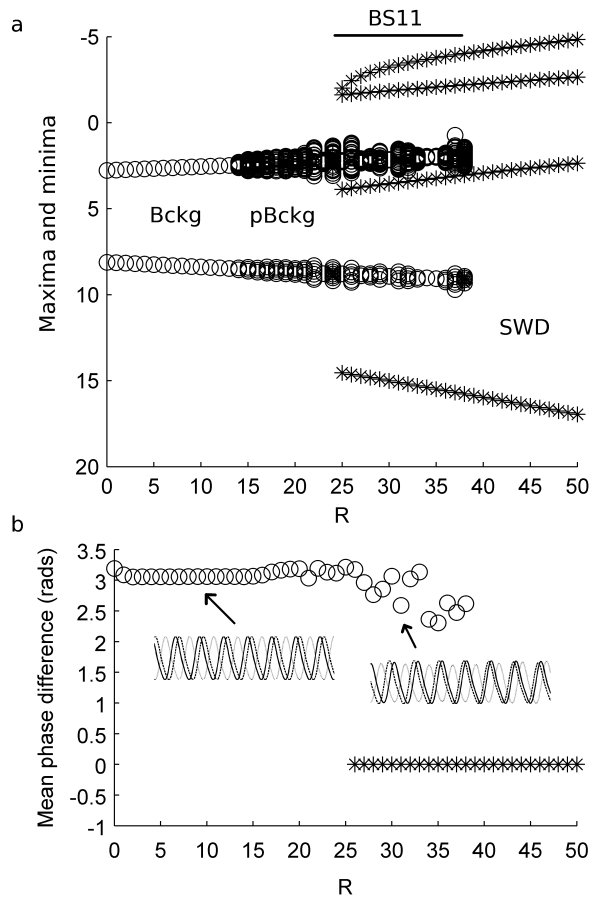
Figure 4.8: Bifurcation diagram over coupling strength for the homogeneous 25 compartment model (C=190, I=135 s^{-1}). In (a), maxima and minima are plotted for one compartment only, for clarity. Symbols are as in previous figures. "pBckg" indicates the start of a solution in which the background oscillation undergoes periodic amplitude modulation and leads to multiple circular markers per value of R. A bistable region is marked BS11. (b) shows the average pair-wise phase difference between all 25 compartments over changing R. Different symbols indicate different solutions as in Figure 4.3 (open circles are background, stars are SWD). Exemplary background solutions are given as insets in (b) at parameter locations indicated by arrows.

accompanied in the model by rhythmic "on/off" firing as is ubiquitously observed in recordings from animal models of SWD (Gloor et al., 1977; Marescaux and Vergnes, 1995; Steriade and Contreras, 1998; Coenen and Van Luijtelaar, 2003). This firing pattern was mediated by the increased relative contribution of the slow IPSP, whereas in the background state, a faster frequency of oscillation was present. We note that the frequency of this background oscillation was of the same order of magnitude as the spike of the SWD, as observed, for example, in the frequency of the fast runs that lead to SWD in a feline model of SWD (Steriade et al., 1998a).

A transition between background oscillations and SWD dynamics could be observed with an increase in C for fixed input (Figure 4.5). This parameter encompasses the magnitude of connectivity within a neural mass (Jansen and Rit, 1995) and increasing its value results in two effects on system dynamics. Firstly, activated
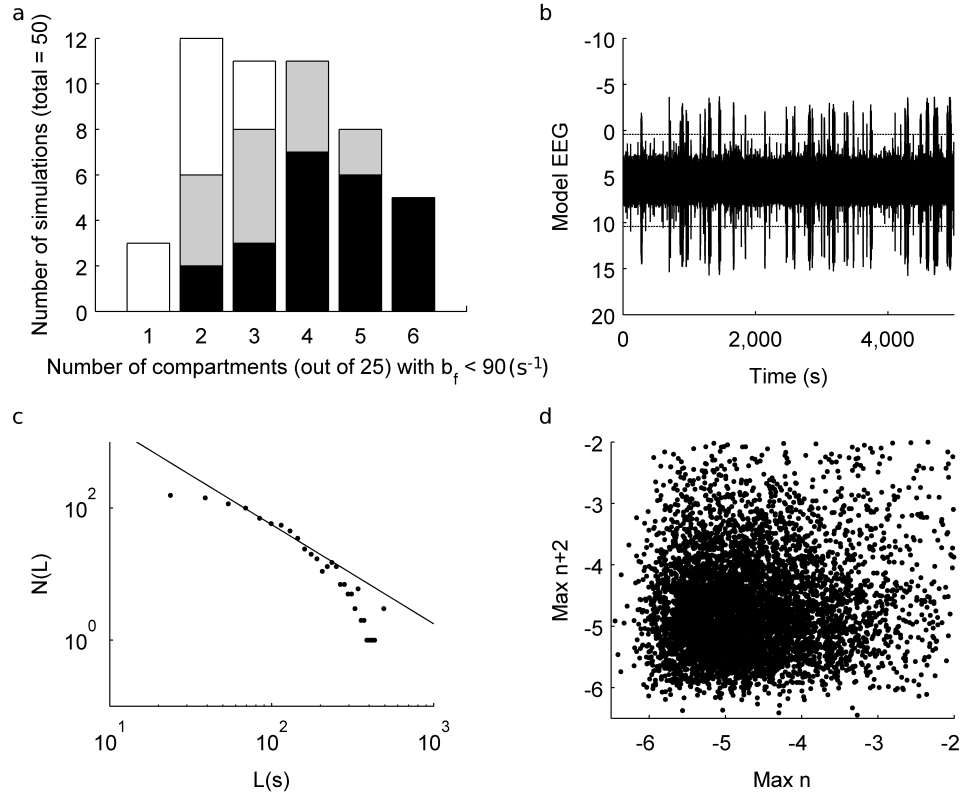
Figure 4.9: Statistics relating to model intermittency. 50 long runs of 10,000 seconds length were simulated, each with a randomly drawn spatial distribution of b_f. Other parameters were homogeneous (C=190, I=135 s^{-1}, R=45). Each of the 50 simulations were classified as either "no seizure" ((a), white regions), "intermittent seizure" ((a), grey regions) or "always seizure" ((a), black seizures). (a) displays the relationship between the number of compartments allocated a value of b_f less than 90 s^{-1} and the number of solutions in each category. (b) shows a 5,000 second extract from one of the intermittent solutions. Horizontal lines are drawn at plus and minus 5 around the mean as a guide to the amplitude cut-off for seizure identification (see section 4.3.3). (c) shows the distribution of laminar phase lengths for an extended time series (containing more than 1200 seizures) of the solution in (b), along with a line showing a slope of -1.5 for comparison. (d) shows a second return map for maxima of the laminar phases of the solution plotted in (b).

excitatory and inhibitory interneurons move position in the sigmoid function towards higher voltages and therefore are more excitable in the sense that their firing rate is higher in the linear part of the sigmoid activation function, or closer to activation in the non-firing part of this curve. Secondly, the firing rate of these neurons is scaled to provide an increased input into the PSPs of the principal neurons. Indeed, increasing C with constant input led to an increase in magnitude of oscillations in internal PSPs (data not shown). In this sense, an increase in C encompasses a notion of enhanced local excitability, which has been postulated during seizure states in animal models (Steriade et al., 1998a; Polack et al., 2007). Alternatively,
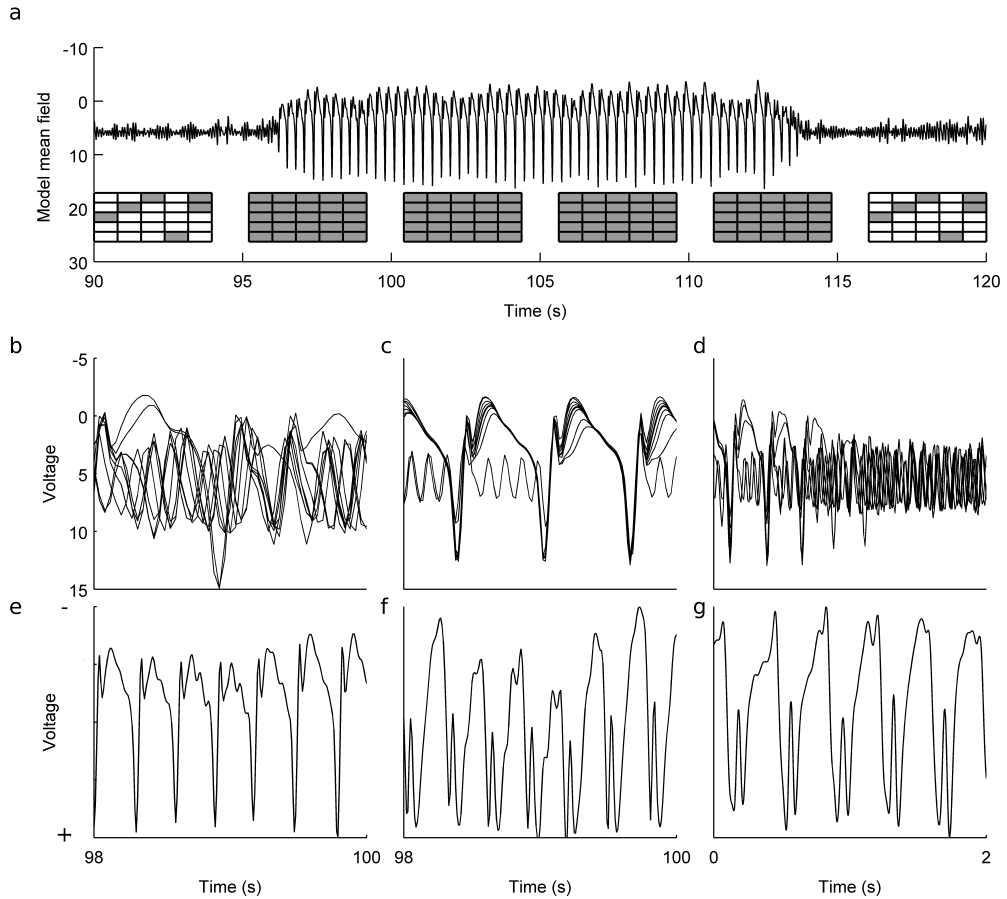
Figure 4.10: Intermittent SWD in a heterogeneous model of 25 compartments (C=190, I=135 s^{-1}, R=50). (a) shows an example of an intermittent model SWD event, spontaneously arising from background. The insets of (a) are grid layouts of the 25 compartments for 6 five-second windows through the time series, at the time locations indicated by position of the grid on the horizontal axis. Grey indicates the presence of SWD during the window, whereas white indicates no SWD, based on a comparison of amplitude with the average of a known background state. For example, the first grid of 25 squares represents the state of all 25 compartments between t=90 and t=95 seconds. (b), (c) and (d) show two seconds of underlying time series for seizure onset, seizure, and seizure offset respectively. Not all 25 time series are plotted here for clarity. (e) shows a close up of the model output during seizure. (f) shows the same model dynamics as (e) under an alternative conversion to EEG output (see text). (g) shows a clinical EEG recording from a frontal electrode during absence seizure.

individual spike wave responses could be induced transiently by means of a short stimulus (Figure 4.5 (c)). This was further explored in a spatially extended version of the single-compartment model.

We demonstrated that a spatial extension to this model confers the system with additional dynamics (Figure 4.6), including the existence of a region of bistability between background oscillations and SWD. In addition to differences in waveform and frequency between the two solutions in this parameter region, there was also

a difference in the phase relationship between the two compartments of the model, namely that background oscillations were out of phase whereas SWD were in phase. This is equivalent to the dynamics of brain activity during absence seizures in animal model studies, in which the seizure state is accompanied by time locked firing of cortical neurons relative to more diffuse temporal relationships during background activity (Steriade and Amzica, 1994; Neckelmann et al., 1998). The large amplitude observed on scalp EEG during SWD seizures is also indicative of a significantly increased degree in time synchrony of underlying neuronal activity compared to a background state.

The existence of a region of bistability between these two states indicates a capability of the system to undergo spontaneous transitions into and out of seizures. This property could be important, for example, in explaining the spontaneous transition from background EEG into 3/s SWD activity as seen in absence seizures (Lopes da Silva et al., 2003a). Indeed, a previous model of the thalamocortical network was demonstrated to be capable of noise-induced transitions in a region of bistability between a fixed point and limit cycle with relevant power spectra (Suffczynski et al., 2004). In contrast, a different thalamocortical model demonstrated a transition from background to SWD that was mediated by smooth changes in model output with the dynamic modulation of a relevant model parameter (Breakspear et al., 2006). In terms of system dynamics, the 2 compartment model presented here makes notable improvements on these previous studies by reconciling i) an oscillatory background state, ii) a relevant difference between the phase relationship of background and seizure oscillations and iii) bistability between background and SWD oscillations. We therefore present important new tools in the investigation of SWD generating mechanisms from the non-linear dynamics perspective. A noise driven oscillatory background state has been assumed in a large number of previous studies (see e.g. Jansen and Rit 1995; David and Friston 2003; Wendling et al. 2002), whereas a previous mathematical model of absence seizures assumed the background to be a noise driven steady state in order to account for the irregularity of background EEG (Breakspear et al., 2006). While our two compartment model is more regular than clinical background EEG, we address this point by suggesting that the recorded EEG signal is in fact a mean over a larger number of coupled compartments. For example, the disorganised or complex oscillations in the mean field of the twenty-five compartment model provides an alternative explanation for observations likening background EEG to filtered noise.

Cortical stimulation has been shown to elicit seizure activity in the feline model of SWD seizures (Steriade et al., 1998a). We investigated this mode of transition to SWD in the model by applying a short time dependent rise in the input parameter, I. It was shown that such stimuli could lead either to prolonged (permanent) SWD dynamics or a transient period of SWD which decayed to the background state

(Figure 4.7). The fate of the system subsequent to stimulus depended upon, amongst other factors, the state of the system at time of stimulus. System evolution post-stimulus differed in terms of length of seizure activity and degree of homogeneity in output between the two compartments, resulting in fragmentation of the SWD. Such variability is often observed on human EEG recorded during absence seizures (Sadleir et al. 2006 and Figure 4.10 (g)).

In the study of Steriade et al. (1998a), the authors hypothesised that stimulating fast bursting neurons would be particularly effective in generating spatially extended pathological oscillations, presumably via synaptic connectivity, just as in our model the two compartments interact via excitatory connectivity to synchronise in SWD. However, we note that in our model, onset of seizure activity was predominantly instant, whereas in the feline model repeated stimulus was required for a time delayed transition to seizure. These differences can probably be explained by our simplistic model of local interactions which does not incorporate the extensive and complex activity of the brain *in vivo*.

An extended area of cortex was modelled by a network of twenty-five reciprocally connected compartments. We observed that this configuration with heterogeneous fast inhibitory time scales could display intermittent seizure activity in the mean field. We stress that no time dependent noise term was applied to the model in order to mediate these transitions, which therefore provide a means of SWD onset and offset not previously reported in modelling studies of SWD to our knowledge.

The simulation depicted in Figure 4.9 (b) over a longer duration possessed mean seizure and non-seizure lengths of 8 and 74 seconds, respectively, both of which values are in line with analysis of recordings from the WAG/Rij rat model of absence seizures (Akman et al., 2010; Hramov et al., 2006). Previous studies have attempted to classify the nature of intermittency in both human epilepsy and animal model EEG. Velazquez et al. (1999) described type III (low dimensional) intermittency both in fast spiking recordings from human partial epilepsy and in SWD during temporal lobe epilepsy (Velazquez et al., 2003). EEG of rats with genetic absence epilepsy, on the other hand, have been reported to be of the on-off type (Hramov et al., 2006). This latter characterisation was made by comparison to a power law distribution with exponent -1.5. However, alternative analyses of ictal and inter-ictal phase duration have hypothesised exponential or gamma distributions (Suffczynski et al., 2004, 2006a). The results of our phase length and second return map in a specific case (Figure 4.9 (c), (d)) do not support a straight-forward categorisation of the behaviour of the single instance of our model shown. This is to be expected given that the power law holds strictly near the onset of intermittency (Chate and Manneville, 1987). Also the predictions of statistics regarding types of intermittency were derived using low dimensional space independent models (Heagy et al., 1994) or infinite dimensional partial differential equations (Chate and Manneville, 1987).

In principle, the behaviour of our coupled model with its 200 variables may allow for different types of intermittent solutions which have not yet been characterised mathematically. A detailed characterisation of the bifurcation scenarios leading to the observed intermittency will provide further insight into the different types of distributions to be expected in experimental models.

Previous mathematical models displaying intermittent behaviour have been of an abstract nature (Ohayon et al., 2004). In contrast to the idea that intermittency is only found in abstract constructs (Kalitzin et al., 2010), we find that this type of dynamics can emerge when explicit spatial interactions and heterogeneities are considered in a physiologically motivated model. Thus our current model provides the means to investigate further the nature of such transitions to epileptic activity, for example in relation to stimulus feedback control (Kalitzin et al., 2010).

In addition to intermittency in model behaviour, the mean field displayed fragmentation of the SWD waveform as commonly observed in SWD of human absence seizures (Sadleir et al., 2006). We therefore propose that such fragmented SWD, or the appearance of additional "spikes" could be mediated by spatial variation in underlying pathological rhythmic activity. Interestingly, the frequency of the background model mean field consisted of peaks in the alpha range of the power spectrum as is often observed in clinical EEG. This is in contrast to the one compartment case, which possessed a single peak at 15Hz. We postulate that this more relevant frequency of background activity is due both to the heterogeneity in time scale parameters and the effect of averaging local heterogeneous compartment behaviour to form the mean field EEG.

The background state in this heterogeneous model included intermittent or permanent pathological oscillations in a subset of model compartments. Thus, the mode of seizure onset at the macroscopic level related to the spreading of SWD rhythms from a small number of compartments to the whole system. This is in line with recent findings from animal model studies that suggest a cortical focus for the initiation of generalised seizures (Meeren et al., 2002; Polack et al., 2007). Polack et al. (2007) reported that epileptic foci were capable of producing pathological oscillations that did not become generalised seizures, which relates directly to our finding of clusters of SWD activity outside of the seizure period. However, we note that in the findings of Polack et al. (2007) such "background" pathological oscillations were not equivalent to those during the seizure periods.

Regional changes are found both structurally (Woermann et al., 1999) and functionally (Holmes et al., 2010) in human generalised epilepsy. In addition, intracranial recordings from human epileptic and control subjects suggest that in focal epilepsy, pathological activity or "microseizures" do exist at small spatial scales (Stead et al., 2010). This finding implies that epileptic rhythms could be an intrinsic part of healthy cortical circuits, and that icto- and epilepto-genesis are related to

the ability of these pathological rhythms to spread in the cortex. Spatially extended models like the one presented here will provide the means to investigate this spread and therefore will be important in future studies of ictogenesis in both generalised and focal seizures.

Numerical integration of spatially extended dynamic models requires a compartmentalisation of the system at a chosen spatial scale. The original model of Jansen and Rit (Jansen and Rit, 1995) was formulated at the level of a cortical column (Mountcastle, 1997) incorporating local inhibitory and excitatory feedback mechanisms. It has become clear that this assumption of a well defined columnar modularity is an over simplification of the complex horizontal and laminar connectivity within different regions of the cortex (da Costa and Martin, 2010; Douglas and Martin, 2007). At the other extreme, spatially continuous approaches cannot so easily account for the observed spatially restricted activity of local neuronal subsystems. However, spatial extensions in the Jansen approach (David and Friston, 2003; Sotero et al., 2007; Babajani-Feremi and Soltanian-Zadeh, 2010; Ursino et al., 2010) allow one to model connectivity at a hierarchy of scales. Thus, if the notion of space in these models is made more abstract, so that we consider modelled compartments to represent "canonical microcircuits" (da Costa and Martin, 2010), in the spirit of the extended model of David and Friston (2003), the effect of connectivity between heterogeneous local networks incorporating known feedback networks can be investigated. Such an approach is particularly relevant in the study of epilepsy where spatially isolated rhythm generation is an important observed phenomenon (Stead et al., 2010).

Our model incorporates excitatory and inhibitory feedback with two inhibitory time scales. The parameters of the excitatory PSP were preserved from the original model (Jansen and Rit, 1995). A wide variety of synaptic inhibitory mechanisms have been recorded in animal cortex preparations (for example Thomson and Deuchars 1997; Otis et al. 1993), some of which have been incorporated in previous models of focal epileptic dynamics (Wendling et al., 2002; Labyt et al., 2006). Since there is no consensus regarding the exact origin of the hyperpolarising wave during SWD, we fixed an arbitrary slow IPSP which, combined with the fast IPSP resulted in SWD in the region of 3/s. We therefore suggest that this longer IPSP could represent an average of fast and slow IPSPs from a variety of different inhibitory interneurons. However, there is much evidence that this rhythmic hyperpolarisation is not mediated by IPSPs, but could instead be attributable to a change in neuronal input resistance, perhaps mediated by potassium ion concentrations (Bazhenov et al., 2008). Though the model presented here is based on synaptic interactions, the principle of delayed, non-linear activation of a slow inhibitory process could provide an abstract model for non-synaptic mediated inhibition (Llinás, 1988). Furthermore, since little is known about the cellular correlates of SWD in humans, one cannot rule

out the presence of a long synaptic inhibitory process. We suggest that in order to uncover further the effects of interactions between different time scales of inhibitory and excitatory processes, future neural mass modelling work should explicitly account for a wide range of inhibitory time scales (Labyt et al., 2006), representative of synaptic and non-synaptic processes. We also note that the principal aim of the current study was to investigate the importance of spatial coupling between neural masses capable of rhythmic "on/off" firing, rather than to uncover the exact physiological mechanisms mediating this behaviour.

Our spatial extension considered only excitatory coupling between pyramidal neurons, and therefore does not account for spatially extended synapses onto inhibitory or excitatory interneurons. In previous models, these connections, as well as interactions between different inhibitory populations, have been shown to affect dynamics within the Jansen framework (e.g. Ursino et al. 2010). The values of the connectivity parameter, R, used in this study are difficult to relate exactly to physical coupling, though they embody a notion of number of synaptic connections between pyramidal neurons (Jansen and Rit, 1995). We note that these values of R are within bounds used in the study of Ursino et al. (2010).

In this study we have considered only cortical mechanisms for the onset of pathological activity. However, subcortical structures are thought to play an ictogenic role in some epilepsies. Despite reports of cortical initiation of absence seizures (Meeren et al., 2002; Polack et al., 2007, 2009), for example, it is accepted that thalamic mechanisms are necessary for the development of SWD in certain animal models (Meeren et al., 2009). In fact, absence seizures are understood to be a disorder of thalamocortical network interactions (Blumenfeld, 2005). A limitation of the current model in explaining absence seizure ictogenesis in particular is the exclusion of a thalamic component interacting with the cortex, as is presented in the models of Suffczynski et al. (2004) and Breakspear et al. (2006). A natural extension to the current model is therefore the addition of a thalamic component, as provided in a recent study of whole brain dynamics within the neural mass model framework (Sotero et al., 2007). An extension of the model into a larger cortical domain would also provide further insight into the role of hierarchies of cortical connectivity in ictogenesis. Such large scale neural mass models have previously been reported (Sotero et al., 2007; Babajani-Feremi and Soltanian-Zadeh, 2010), as has the importance of forward models in comparing simulations to empirical EEG data (Cosandier-Rimélé et al., 2008). A large-scale extension of the model presented here, combined with a forward model to EEG, may provide insight into the nature of cortical dynamics underlying heterogeneous SWD recordings of human absence seizures (Weir, 1965; Cohn and Leader, 1967; Lemieux and Blume, 1986; Rodin and Ancheta, 1987; McKeown et al., 1999).

4.6   Summary

To summarise, we have demonstrated that important dynamic features of epileptic EEG may emerge from a mathematical model with explicit spatial interactions. In particular, the spatial extension can lead to intermittent seizure periods when parameter distributions are heterogeneous. In recreating relevant aspects of background and SWD dynamics reported in humans and animal models, we thus provide a framework with which to better understand ictogenesis in terms of spatio-temporal cortical mechanisms.

Chapter 5

Considerations on the mass modelling of multi-modal waveforms

5.1 Abstract

Neural mass models are used extensively in order to investigate the mechanisms of epileptiform rhythms. In many cases, these rhythms manifest as complex, multi-modal waveforms, which may bear a non-trivial relationship to the underlying activity of an assumed population of neurons. In particular in the case of SWD there is an apparent conflict between the multi-phasic EEG waveform and the mono-phasic burst pattern of neuronal firing observed in cortical neurons in animal models.

Since the traditional conversion of mass model activity to EEG is via a constant of proportionality applied to the activity of principal neurons, or their net depolarisation, modelled EEG SWD are necessarily underpinned by a bi-modal firing pattern. A more compatible approach would be to consider a uni-modal activity pattern of firing during the spike and quiescence during the wave. Clearly this is incompatible with a multi-modal EEG waveform under the traditional conversion of mass model variables to EEG. Therefore, in the case of SWD, a more elaborate consideration of the cortical contributions to EEG is required.

Here we propose an alternative approach in neural mass modelling assuming four distinct cortical populations. We refer to animal model results for a differential laminar distribution of the current sources and sinks to generate SWD. Based on a simple conversion of model variables to EEG output we then show that this output can recreate a variety of clinically observed SWD morphologies from a physiologically plausible, uni-modal firing activity. We therefore argue that more detailed modelling of cortical structure will be an essential part in furthering our understanding of macroscopic epileptic dynamics resulting from specific interactions between neuronal populations.

5.2 Introduction

Neuronal firing during SWD in animal models

As described in Chapter 4, investigations into the cellular correlates of surface SWD have been undertaken in animal models. Although these models fulfil criteria for experimental absence seizures (Snead, 1995), they provide very different EEG morphologies during seizures, none of which specifically match those observed in typical absence epilepsy. However, cellular activity in each of these models during SWD are commonly described as organised into firing during the spike and quiescence during the wave (see for example Steriade et al. 1998a for feline recordings, Pinault et al. 1998 for GAERS and Inoue et al. 1993 for WAG/Rij). In general, action potentials (single spikes, clusters or bursts) fire at the peak of a large depolarisation which is rhythmically interrupted by a hyperpolarising wave. Although in the feline models model faster hyperpolarisations can be seen to coincide with spike patterns, for example in poly-spike wave trains, and firing at the peak of the depolarisation can be clustered into two bursts (Steriade et al., 1998a), it has not been shown that a clear bi-modal depolarisation or firing pattern is concomitant with surface SWD spikes in general. Such analysis in the WAG/Rij rat model rather points to a uni-modal firing on average during the spike (Inoue et al., 1993). In fact, a uni-modally distributed firing pattern has been specifically incorporated in the derivation of EEG in a model recreating SWD patterns in the rat model (Sargsyan et al., 2007). In this case, the depth distribution of synaptic activity was shown to be important in recreating relevant EEG waveforms. In addition, models of network interactions underlying SWD at the neuronal level do not require or produce strictly bi-modal firing patterns (Destexhe, 1998; Traub et al., 2005).

Conversion of model variables to EEG

A review of models whose output resides at the scale of the EEG is provided in Chapter 2. As described, the frequency of activity generated by these models is in most cases the characteristic of interest and is assumed to be proportional to the "activity" of principal cells within the model. Thus, a multi-modal waveform such as the SWD is necessarily generated by an underlying multi-modal fluctuation in the activity of modelled principal cell populations. Such activity is usually converted into a firing rate by a non-linear activation function and then provides input into other neural masses in the model system.

Therefore, a model verified by its alignment with different SWD morphologies in the standard conversion of output to EEG necessarily conducts different firing patterns through its network connectivity, which in turn are not the mono-phasic patterns observed *in vitro*. In addition, under this kind of model, differences in SWD waveforms (which are ubiquitous (Weir, 1965)), would be underpinned by a model

conducting different activity through its network. However, results from animal model studies suggest that differences in surface EEG patterns are more likely to reflect changes in intracortical laminar current flow rather than underlying cellular firing patterns (Gloor et al., 1979; Giaretta et al., 1987). Thus, the conclusions drawn from modelling studies such as that of Marten et al. (2009a), in which different SWD waveforms are specifically suggested to be generated by different parameter sets of a model (and therefore different population dynamics) can be questioned. Detailed analyses of cortical activity during SWD have revealed the complex, laminar, multi-phasic and dynamic nature of cortical contributions to SWD (Kostopoulos et al., 1982; Kandel and Buzsáki, 1997). In contrast, the gross, or population level "on/off" firing of cortical neurons appears to be conserved. It is therefore clear that further considerations regarding the origin of the EEG are required for mathematical models of SWD. This requires a more detailed examination of the creation of electrical fields in the brain.

Generation of the EEG

A thorough exploration of the generation of potential fields in the brain has been provided in the work of Nunez (Nunez, 1981). Equations for the generation of electric fields on the scalp given known current sources have been provided under certain assumptions relating to, for example, the shape of the head and the conductivity of the different tissues between generators and recording equipment. However, recordings of EEG from the scalp or the ECoG do not derive from sources of known size or origin. The question of inferring these brain tissue generators of EEG recordings is known as the "inverse problem", and is a major problem without a unique solution.

Despite early ideas relating EEG generation to action potential firing of neurons, electrical activity recorded on the scalp EEG (or intracortically on the ECoG) is now known to derive predominantly from currents generated by post-synaptic potentials on pyramidal dendrites (Creutzfeldt and Houchin, 1974; Niedermeyer and Lopes da Silva, 2005; Olejniczak, 2006). Evidence for this theory is given, for example, by the observation of EEG waves during periods of neuronal silence (e.g. under anaesthesia). In this case, EEG waves are produced by sub-threshold membrane oscillations (Creutzfeldt and Houchin, 1974). In addition, the time scale of action potentials ($O(1\text{ms})$) is considered too short to contribute to deflections on the EEG, whereas the time scale of post-synaptic potentials is generally slower ($O(10\text{ms})$). A particular structural reason for the predominance of post-synaptic currents is the orientation of cortical pyramidal neurons which are aligned perpendicular to the surface of the brain. This means that currents induced in a population of pyramidal neurons are also oriented perpendicularly to the surface, in the so called "open field" configuration, and thus facilitate the formation of summed current dipoles (Niedermeyer and Lopes da Silva, 2005), or dipole layers (Nunez, 1981). This is in contrast to

other neuronal populations with radially oriented dendrites, which permit instead a "closed field" in which current dipoles cancel out and no field potential can be recorded at macroscopic distances.

Although the relationship between post-synaptic potentials on cortical pyramidal neurons and EEG waves is established, there unfortunately is not a one to one relationship between the observed surface deflection and the type, or vertical location of the PSP (Creutzfeldt and Houchin, 1974; Niedermeyer and Lopes da Silva, 2005). This in turn reflects an ambiguity in the relationship between underlying neuronal firing patterns and observed EEG waves. Thus, in modelling the neuronal mechanisms of complex, human, epileptiform EEG rhythms an additional "inverse problem" relates to inference regarding the accompanying firing patterns of principal and inter-neurons. This is a particular problem that forms the motivation for the current chapter.

In fact, the relationship between neuronal firing patterns, PSP direction (excitatory or inhibitory) and EEG waves can be shown to be state dependent. For example, the negative deflection of surface EEG spindle waves has been shown to be underpinned by a cellular depolarisation of cortical neurons (Creutzfeldt and Houchin, 1974; Niedermeyer and Lopes da Silva, 2005). However, the exact phase relationship between neuronal membrane and EEG wave is diffuse, implying the existence of spatio-temporal delays between the depolarising influences, which are thought to be summed EPSPs. The relationship between neuronal activity and waveform here is compounded by the observation that many of the depolarisations are sub-threshold, thus implying that IPSPs do not contribute to the surface waveform, as presumably cortical inhibitory circuits are not activated. In the case of spike-wave discharges (SWD), however, it has been shown that the surface negative EEG wave corresponds to a hyperpolarised state of cortical neurons (Steriade et al., 1998a), though it is unclear whether this is likely to be mediated by IPSPs (Bazhenov et al., 2008). The spike of the SWD is associated with a depolarisation of cortical neurons and subsequent bursting, such that in this case, the relationship between gross neuronal firing patterns and EEG waveform is a little clearer. However, the mechanisms leading to the generation of the multi-phasic EEG waveform of the SWD have not been made explicit.

Previous approach to the problem

Lopour and Szeri (2010) identified the problem of relating mean soma potential to EEG dynamics when employing macroscopic modelling to investigate stimulation feedback control in epilepsy. The authors pointed out that one should consider measured EEG as a function of extra-cellular currents rather than the mean soma potential. It was also highlighted that the depth of sources and sinks relative to the recording electrode would affect their contribution to surface EEG deflections.

Their solution to this problem was to form a linear sum of afferent activity to the excitatory neuronal population, weighted in direction to the presumed contribution to surface deflection. This was then filtered with the synaptic operator to provide an approximation to trans-membrane potential and compared to the resting membrane potential to determine the direction of current flow.

Aims of the current chapter

The neural mass model described in Chapter 2 (Jansen and Rit, 1995) specifically incorporates time courses of inhibitory and excitatory PSPs on pyramidal neurons. This provides the opportunity to examine how these dynamics might combine to provide multi-modal waveforms. We aim to take an abstract approach to this problem in the first instance by assigning a sign to these dynamics based upon their putative contribution to the surface EEG. In particular, we aim to address the question of how multi-modal waveforms can be produced by an underlying uni-modal "on/off" dynamic in neural masses.

5.3   Model

The model employed in the current chapter is the same as that in Chapter 4. We recreate the equations here so that the conversion operations on its variables is more readily accessible within the current chapter.

The model equations are:

$$
\begin{aligned}
\dot{y_0}(t) &= y_4(t) \\
\dot{y_4}(t) &= AaS[y_1(t) - 0.5y_2(t) - 0.5y_3(t)] \\
&\quad - 2ay_4(t) - a^2 y_0(t) \\
\dot{y_1}(t) &= y_5(t) \\
\dot{y_5}(t) &= Aa\{I + C_2 S[C_1 y_0(t)]\} - 2ay_5(t) - a^2 y_1(t) \\
\dot{y_2}(t) &= y_6(t) \\
\dot{y_6}(t) &= Bb\{C_4 S[C_3 y_0(t)]\} - 2by_6(t) - b^2 y_2(t) \\
\dot{y_3}(t) &= y_7(t) \\
\dot{y_7}(t) &= B_s b_s\{C_4 S[C_3 y_0(t)]\} - 2b_s y_7(t) - b_s^2 y_3(t)
\end{aligned}
\tag{5.1}
$$

Parameter	Description	Value
A	Average excitatory gain	3.25mV
B	Average standard inhibitory gain	22mV
B_s	Average slow inhibitory gain	8.8mV
a	Average excitatory time constant	$100s^{-1}$
b	Average standard inhibitory time constant	$50s^{-1}$
b_s	Average slow inhibitory time constant	$20s^{-1}$
C, C_1, C_2	Connectivity constants	$C = 300, C_1 = C, C_2 = 0.8C$
C_3, C_4		$C3 = C4 = 0.25C$
I	External input to pyramidal neurons	$I = 200$
v_0	Parameters of the sigmoid function	$v_0 = 6mV$
e_0, r		$e_0 = 2.5s^{-1}, r = 0.56mV^{-1}$

Table 5.1: Parameter values used for all output shown in this chapter. Note parameter values are identical to the standard values used in Jansen and Rit (1995), except for those of the slow inhibitory process. These parameters were derived by fixing the time scale and then deriving the gain from the ratio B/b, as suggested by David and Friston (2003).

5.4   Calculation of EEG output

As described in Chapter 2, the output of this model is traditionally assumed to be directly proportional to the net depolarisation of principal neurons (see e.g. David et al. 2005) which in our model is given by the term $y_1(t) - 0.5y_2(t) - 0.5y_3(t)$. To formulate a more relevant transformation to EEG output in the case of SWD, we refer directly to the study of Kandel and Buzsáki (1997). The authors examined the laminar distribution of cortical sources and sinks during SWD in a rat model of absence epilepsy. In particular they noted the presence of 3 dominant time-varying dipoles that contributed to the surface signal. Dipole 1 was an early positive deflection mediated by a deep sink in layer 6, dipole 2 was a layer 4 sink corresponding to a surface negative deflection and dipole 3 was a delayed surface negative component. Strong sources were also observed in layers 2 and 3 and were adjudged to contain an active, inhibition mediated component. We focus here upon the first two dipoles and the superficial sources. Though the origin of these sources and sinks is not exactly known, the authors suggested that they derived predominantly from the intra-cortical circuitry.

The Jansen model is based upon the feedforward and feedback mechanisms inherent in cortical column or canonical circuit architecture, namely i) principal (pyramidal) neurons; ii) positive feedback (stellate) cells and iii) negative feedback (inhibitory interneurons) cells (Jansen and Rit, 1995; Douglas and Martin, 2007). We note that the depth locations of these model populations have previously been considered in a hierarchical model of evoked potentials (David et al., 2005). In that study model pyramidal neurons occupied agranular layers and model stellate cells

were positioned in layer 4. Similar considerations were also made in Lopour and Sz-eri (2010) in which the authors specifically weighted the afferent activity according to its signed contribution to surface recording deflections.

In order to model the contribution to the EEG of the cortical sources and sinks referred to in Kandel and Buzsáki (1997), we must make assumptions regarding their electro-physiological origin (for a review of absence siezures see Pinault and O'Brien (2005)). If they are to contribute to the surface EEG, it is likely that they are derived from PSPs on pyramidal neurons (Schaul, 1998; Olejniczak, 2006). Three such PSPs are already represented in the model equations, namely the excitatory (E)PSP (y_1) and the two inhibitory (I)PSPs (y_2 and y_3). If we assume that the sink in layer 4 is derived from EPSP activity on principal neurons (mediated by positive feedback from stellate cells in this layer), we can model the strength of this sink by some function of y_1. Similarly, if we assume that the layer 2/3 sources are derived from IPSPs on principal neurons (mediated by negative feedback from inhibitory interneurons in those layers) the strength of these sources can be modelled by functions of of y_2 and y_3. We assume that the sink in layer 6 is mediated by the excitation of layer 6 pyramidal neurons via EPSPs in layer 6 from other pyramidal cells (in the same layer or from layer 2/3) (Binzegger et al., 2004; Douglas and Martin, 2007). An approximation to the EPSP induced by pyramidal neurons in the model is the excitatory impulse response used to activate interneurons via activity of pyramidal cells, i.e. y_0.

In lieu of a detailed, mechanistic derivation, we initially seek a simple functional form relating model variables to the strength of these sinks and sources. The simplest such transformation is a linear combination of model variables. Although it is not known how these sinks and sources contribute to the surface EEG, we refer directly to the observations of Kandel and Buzsáki (1997) which suggest that the layer 6 sink is responsible for a positive surface deflection, whereas the layer 4 sink corresponds to a surface negative deflection. We assume that the active superficial sources also contribute to surface positivity. This allows the sign of contribution to the surface EEG to be designated, similarly to the study of Lopour and Szeri (2010). However, in the current study we neglect the conversion of trans-membrane potential to current source magnitude in the first instance.

In summary, EEG output can be modelled as a linear combination of the 4 model variables, with their laminar position fixed. We use the results of Kandel and Buzsáki (1997) to directly infer the sign of their contribution to the surface signal. The layer 6 sink (y_0) corresponds to a surface positive deflection and is therefore positively weighted, as are the superficial sources (y_2 and y_3, placed in layers 2 and 3, respectively). The layer 4 sink (y_1) corresponds to a surface negative deflection and is therefore negatively weighted. Thus we find the following equation for EEG output:

$$Y = w_0 y_0 - w_1 y_1 + w_2 y_2 + w_3 y_3 \qquad (5.2)$$

We note that since the magnitude of the model variables are asymmetric, the terms $w_i y_i$ give the relative strength of contributions, rather than the weights (w_i) themselves.

5.5   Examples

In Figure 5.1 we demonstrate previous observations regarding neuronal firing patterns during experimental SWD seizures. Figure 5.1 (a) shows the widely reported alternating depolarisations and hyperpolarisations with action potential bursting at the peak of the depolarisation. Figure 5.1 (b) demonstrates that these depolarisations can be interrupted by faster rhythmic hyperpolarisations, which could contribute to spiking patterns on the depth EEG. On the other hand, Figures 5.1 (c) and (d) show unimodal averaged firing of neurons in cortex and thalamus recorded during experimental seizures in WAG/Rij rats and the feline models, respectively.

Figure 5.2 (a) shows the assumed firing pattern in a widely studied thalamocortical mass model of SWD activity (Robinson et al., 2002; Breakspear et al., 2006; Marten et al., 2009a). The output of the variable taken to represent EEG clearly propagates a bi-modal firing pattern through the model thalamocortical network. In contrast, we show in Figure 5.2 (b) the output of the cortical neural mass model employed in this study, which can display a uni-modal firing pattern. The top picture in Figure 5.2 (b) demonstrates that this uni-modal firing pattern is not converted into a SWD EEG waveform under the assumption that the EEG is proportional to a net depolarisation on pyramidal neurons.

We explored the effect of varying the strengths of contributions from modelled sources and sinks by varying the weight parameters described in section 5.4. In Figures 5.3 and 5.4 we present a comparison of model output to real EEG recordings from frontal electrodes during absence seizures. Each component of Figures 5.3 and 5.4 displays real EEG recording (top), model output (middle) and laminar representation of inferred underlying contributions (bottom). This latter figure colour codes sinks in blue and sources in red with intensity of colour proportional to strength of sink or source, normalised to the maximum strengths observed in Figure 5.4 (d) and 5.4 (f) (c.f. figures in Kandel and Buzsáki (1997)). Overlaid on these images are the time courses of the underlying model variable at each location, with positivity up, and deflection dependent upon whether the variable represents source (upwards) or sink (downwards). Model and real EEG are displayed with negativity up in order to draw comparison with the results of a published study of SWD waveforms (Weir, 1965), which we also refer to for its descriptive terminology. We stress that in each of these figures the underlying pattern of mass activity is identical and "on/off", as
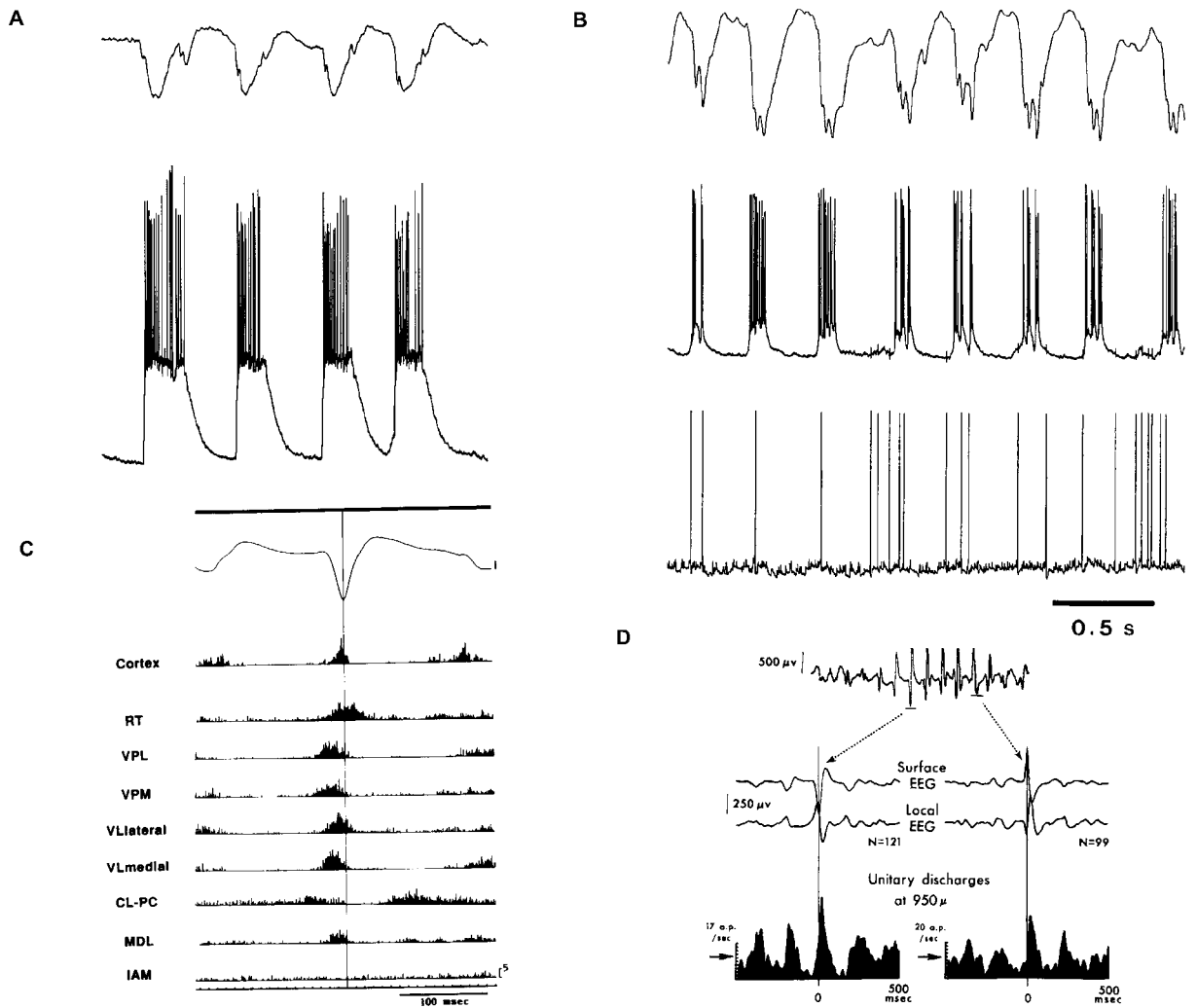
Figure 5.1: A collection of results relating to neuronal firing during experimental seizures. (a) and (b) represent intra-cellular recordings from spontaneously occurring and cortically initiated seizures in a feline model, respectively. (a) shows top: depth EEG from area 5 and bottom: intracellular recording from area 5. (b) shows top: field recording from area 4, middle: intracellular recording from area 4 and bottom: intracellular recording from ventral lateral thalamus. (c) shows spike averaged unit firing in cortical and thalamic regions of WAG/Rij rats during SWD. (d) shows wave triggered unit firing recorded in a feline model. (a) and (b) are adapted from Steriade et al. (1998a), (c) from Inoue et al. (1993) and (d) from Kostopoulos et al. (1981).

seen in Figure 5.2 (b).

Figures 5.3 and 5.4 demonstrate four different morphologies commonly seen in EEG recordings from absence seizures and attainable from identical model dynamics. Figure 5.3 (a) shows a rounded initial wave segment followed by a sharp "positive transient". The spike ("spike 2" of Weir (1965)) begins on the down slope of the wave and hence the second positive component of the spike is more prominent than the first (compare Figure 4, 2, occipital lead in Weir (1965)). We note that this waveform is brought about by the inclusion of a strong sink in layer 6 as well as a
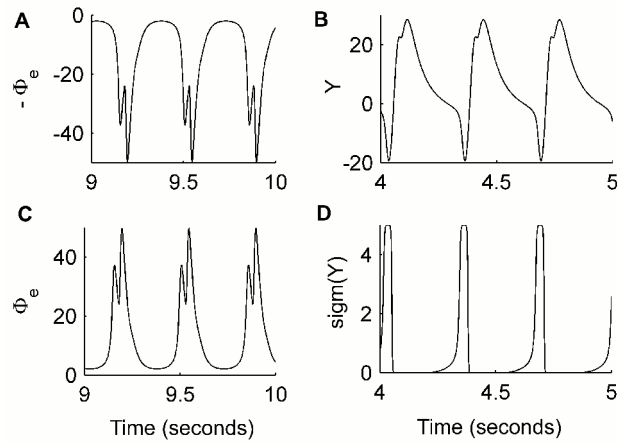
Figure 5.2: Model EEG and underlying activity in (a) the model of SWD activity of Marten et al. (2009a) and (b) an extended version of the cortical model proposed by Jansen and Rit (1995) with rhythmic "on/off" firing. In each case the top panel shows model EEG output and the bottom panel shows the time course of the variable output as it is connected to other masses in the network.
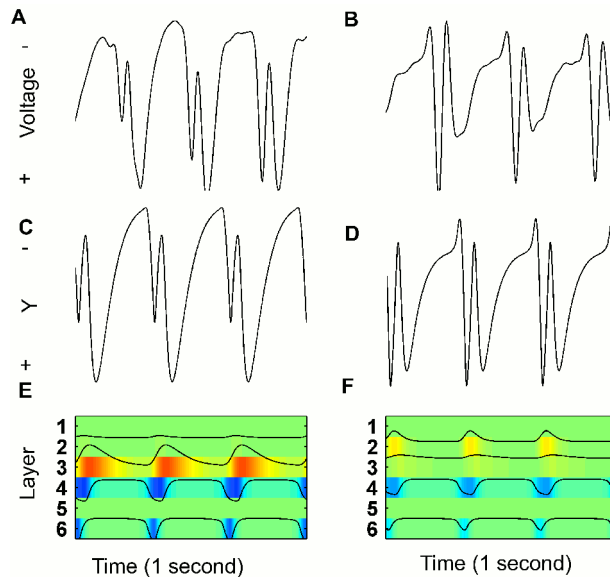
Figure 5.3: Comparison of model output with clinically recorded EEG. (a) and (b) represent 1 second of real recordings from frontal electrodes of two different patients (Hjorth reference). (c) and (d) show 1 second of model EEG. (e) and (f) show corresponding laminar activity in the model.

strong source in layer 3, corresponding to the slow inhibitory time scale. There is little contribution from the fast inhibitory process here. Figure 5.3 (b) shows the appearance of a small "spike 1" (Weir, 1965), followed by a more pronounced "spike 2" than that observed in Figure 5.3 (a) (compare Figure 4, 2, temporal lead in Weir (1965)). The underlying strength of both sinks and the slow source are lower here than in Figure 5.3 (e) although the fast source in layer 2 has increased contribution. Figure 5.4 (a) shows a small spike at the bottom of the positive transient and a more pronounced "wave" (compare Figure 6 trace 1 or 2 in Weir (1965)). In this case,
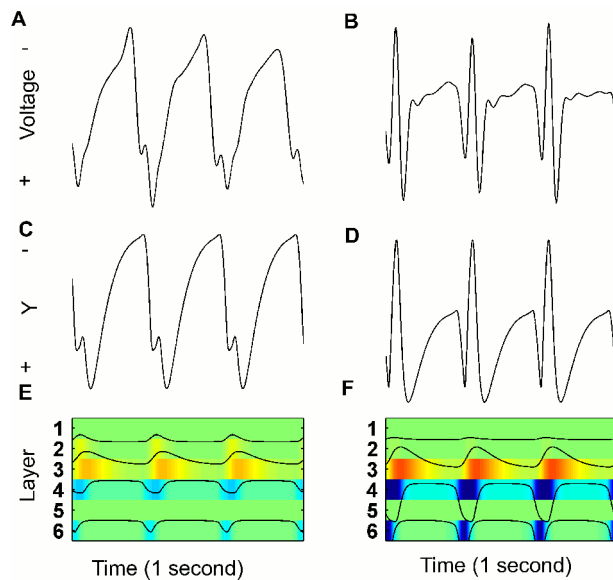
Figure 5.4: Comparison of model output with clinically recorded EEG. (a) and (b) represent 1 second of real recordings from frontal electrodes of two different patients (Hjorth reference). (c) and (d) show 1 second of model EEG. (e) and (f) show corresponding laminar activity in the model.

all 4 model PSPs provide similar contributions. The strength of these contributions compare to those of Figure 5.3 (f), although the strength of the slow source in layer 3 has increased. Figure 5.4 (b) shows a pronounced "spike 2" of amplitude greater than that of the wave. This output arose from very strong contributions from all variables except that representing the fast inhibitory time scale.

5.6 Discussion

In this study we presented a new method for calculating the EEG output of a neural mass model. We showed that by relating model variables to the putative activity of depth distributed sources and sinks a variety of relevant SWD waveforms can be realised in a model of underlying uni-modal firing. Thus we suggest that future modelling studies of epileptiform activity could benefit from a detailed consideration of the vertical distribution of cortical activity.

The morphology of SWD were extensively discussed by Weir (1965) and shown to be highly variable. Weir (1965) also suggested that SWD morphology can be explained in terms of the relative contribution of 4 components, namely spikes 1 and 2, a positive transient and the wave. In Figures 5.3 and 5.4 we demonstrated that, under the assumptions of the model, this variability in SWD can be modelled by depth weighted activity. It is therefore suggested that modelling of realistic epileptic waveforms can be achieved with a simple transformation of model variables to EEG output within the Jansen framework (Jansen et al., 1993; Jansen and Rit, 1995), so long as depth distributions of activity are accounted for. We note that

the study of Kandel and Buzsáki (1997) provided the means with which to locate relevant sources and sinks within the cortex during SWD. Such electrophysiological investigations combined with mass modelling of underlying activity may therefore provide additional insight into the mechanisms of epileptiform activity.

In addition, future benefits may be found by adding a forward model to the generation of the EEG to account for the measurement of activity at different locations on the scalp. Cosandier-Rimélé et al. (Cosandier-Rimélé et al., 2007; Cosandier-Rimélé et al., 2008; Cosandier-Rimélé et al., 2010) provided such an approach in the context of epilepsy. In this case it was assumed that the time varying dynamics of the current dipole induced by afferent synaptic activity on principal neurons could be related to mass model variables. The authors considered the dynamics of current dipoles in a triangular mesh approximation to the cortical geometry derived from MRI, with each triangle representing $1mm$ of cortical area. The intensity of the dipole was assumed to be weighted by the output of the neural mass model, thus no consideration was given to the laminar arrangement of afferent activity in generating the signal.

The new assumptions presented here regarding the transformation of model variables to EEG represent the simplest means with which to account for a laminar organisation of model activity. Model variables appropriately relating to observed sources and sinks were identified and then weighted in order to produce the EEG output. This provides a first attempt at incorporating depth location factors relating to the production of EEG directly into a single neural mass model, though we note that similar considerations have been made regarding the connection of multiple neural masses in the generation of realistic evoked responses (David et al., 2005). The array of model waveforms closely matching clinical EEG demonstrate that such an approach is relevant. Strictly one should aim to calculate the magnitude of current sources and sinks in the vertical direction for a population of neurons. In the Hodgkin-Huxley formalism, one can consider the capacitive currents across the membrane as proportional to the time derivative of the membrane voltage. In the model of Jansen and Rit (1995) one can therefore consider the first derivative of the PSP variables (i.e. y_5,y_6 and y_7 in the formula above) to be representative of currents (Moran et al., 2007) and construct the measured field potential accordingly. Incidentally, it was found that linear combinations of these variables can also give rise to relevant SWD morphologies (data not shown).

The current study invites a more detailed derivation of methodological approaches that can account for laminar activity using neural mass model variables. Such advances will provide valuable tools for the investigation of epileptiform activity in humans via the mechanistic modelling of epileptic dynamics. In particular, models at the neural mass scale will be vital in understanding epileptiform activity at the level of large cortical regions, an undertaking that is recently being pursued

(Cosandier-Rimélé et al., 2008). For example, the relative depth of PSP activity in the cortex, which is known to attenuate contributions to cortical EEG (Niedermeyer and Lopes da Silva, 2005; Avitan et al., 2009), has been considered in the derivation of a recent forward model of EEG activity (Avitan et al., 2009). Sargsyan et al. (2007) also considered depth dependent contributions of activity to local field potentials, whereas Destexhe (1998) used an integration of postsynaptic currents in one dimension. In contrast, our approach explicitly relates model variables to experimentally localised current source distributions (Kandel and Buzsáki, 1997).

The consideration of underlying firing patterns is vital in modelling epileptic rhythms arising from connected brain networks. Previous macroscopic modelling studies have considered small local cortical networks (Wendling et al., 2002), thalamocortical networks (Breakspear et al., 2006; Marten et al., 2009a) or models with more expansive connections (Labyt et al., 2006). In each case conclusions and inference are based upon a comparison of aspects of model output with clinical or animal model data. We argue here that the modelled networks supporting the production of pathological rhythms should incorporate some consideration of the underlying dynamics of neuronal activity. That is, more emphasis should be placed on the relevance of the interactions at the level of information transfer in the circuits, i.e. the neuronal firing of action potentials. This is imperative when conclusions are to be drawn from the dynamics of a system built to model synaptic connectivity. These considerations will prove vital as macroscopic models are expanded to incorporate larger network connectivities, an undertaking which will be necessary in order to understand generalised epilepsies at a level corresponding to clinically relevant activity, i.e. distributed regions of cortical and thalamic structures (Moeller et al., 2008; Westmijse et al., 2009).

We note that our results also carry implications for the practice of measuring functional connectivity or correlation structures within EEG time series. Measures of connectivity that rely on the co-morphology of waveforms, such as linear and non-linear regressive measures, may be unable to reveal that the activity underlying the waveforms of model output in Figures 5.2 (b), 5.3 and 5.4 is identical. On the other hand, our approach emphasises that two identical EEG waveforms will appear as such not solely due to a strong connection between the underlying activity, but also due to the local distribution of sources, or equivalently the local cellular architecture. Future investigations of connected models within the present framework will explore the extent to which connectivity vs. local architecture contribute to observations of functional cortical connectivity.

5.7 Summary

In summary, the problem of modelling multi-modal waveforms such as the SWD using average soma membrane potential in neural mass models was discussed. In particular, it was proposed that the depth profile of current sources and sinks, along with the firing patterns of neural populations, should ultimately be taken into account. A simplified solution was proposed in which current sources and sinks were identified in the literature and their concordance with EEG deflections logged. When this information was used to provide a weighting for model variables, various relevant SWD morphologies could be accounted for by the same dynamical model, which incorporated an "on/off" firing pattern as seen in animal models of SWD.

Chapter 6

Analysis tools for the comparison of spatio-temporal patterns

6.1 Abstract

Ultimately, inference made in modelling studies of macroscopically derived EEG rhythms will rely on the quantitative comparison of spatio-temporal patterns, for example to compare model data with clinical data. Here we investigate the application and development of methods with which to make these comparisons. The focus is on properties of the channel interrelations which capture multi-variate characteristics of the data. Specifically we extend previous work which utilises the eigenvectors of the correlation matrix to represent interrelations of spatio-temporal patterns. These methods yield a vectorisation of the interrelation structure which can therefore facilitate comparisons via vector distance measures (Euclidean distance or Hamming distance).

These comparison methods are applied to seizures of patients with absence epilepsy in order to test for the conservation of spatio-temporal patterns in seizures of the same patient. Each method reveals that indeed the distance between seizure patterns is smaller when seizures of the same patients are compared.

6.2 Introduction

Spatiotemporal patterns in scalp EEG of absence seizures

Scalp EEG typically consist of electric potential recordings from multiple electrodes (for example according to the standardised 10-20 system) and thus yield a multivariate time series that represent spatio-temporal patterns of electrical activity in the brain. Segments of these time series that contain epileptic activity reflect pathophysiological brain activity and are therefore often examined in order to reveal clinically relevant univariate properties or voltage distributions. In univariate

time series analysis of epileptic EEG, important features of the data are frequency, amplitude and waveform. This can be appreciated given predominant descriptions and analyses, such as the segmentation of EEG into frequency bands (delta, theta, beta, gamma etc.), the description of high amplitude SWD and the low amplitude, high frequency onset of focal seizures, for example.

Existing methods for visualising the spatially extended patterns of activity include detailed topographic voltage and contour maps (Lemieux and Blume, 1986; Rodin and Ancheta, 1987; Yoshinaga et al., 1996) derived from univariate properties, and more sophisticated transformations such as source analysis (Rodin et al., 1994) and independent component analysis (McKeown et al., 1999), which utilise spatially extended information.

The visual analysis of generalised seizures using the above methods have highlighted several important features, and also the non-trivial and variable nature of scalp EEG during seizure. Using a dense scalp electrode grid covering central and anterior positions, Lemieux and Blume (1986) described the spatiotemporal evolution of the spike and wave components of SWD. The authors reported a spatially stationary pattern for the negative wave as opposed to a dynamic evolution of the spike. A lateral origin for spikes was reported with subsequent evolution to the midline or contralateral evolution. Interestingly the authors reported that the spike component was often bilaterally asynchronous, in contrast to the definition employed for absence seizures as bilaterally synchronous. Symmetry was higher in the wave component. The spatial distribution of all components was localised on the scalp predominantly to anterior positions, using both visual analysis and a variety of methods to quantify position. The importance of frontal regions in SWD was affirmed by Rodin and Ancheta (1987) as the location for maximum positivity and negativity. These authors also reported complex spatio-temporal dynamic evolution, which could vary within seizures and also between different seizures.

In addition to these results, several other studies have reported a focal onset in human absence seizures. Westmijse et al. (2009), for example, reported onset in frontal or central regions in a MEG study. A dense array EEG study also reported frontal onset to absence seizures Holmes et al. (2004), with frontal maximum of activity over frontal regions.

Quantifying EEG rhythms

The visualisation and description of spatio-temporal patterns during seizure represents a qualitative analysis. Based on the above methods, and also the qualitative comparison of pair-wise interrelation measures (see e.g. Amor et al. (2005); Garcia Dominguez et al. (2005); Aarabi et al. (2008); Ponten et al. (2009)), it has been consistently reported that there is larger inter-patient than intra-patient variability

in the spatio-temporal EEG during absence seizures. Unfortunately, no quantification of such comparisons has been given. In general, the quantification and quantitative comparison of spatio-temporal dynamics is an important unsolved question in non-linear dynamics (Hutt and Neff, 2001).

It is assumed that a quantification of spatial patterns will require the extraction of some features. Hutt and Neff (2001), for example, in analysing excitable media, utilised the characteristics of nearest neighbour similarity. In spatially extended neurological time series, the relationship between constituent time series is also an important characteristic (see e.g. Cohn and Leader (1967) for an early example of interrelations in time series of SWD). A variety of bivariate measures can be employed to quantify the statistical similarity between pairs of EEG channels and a number of these measures have been evaluated for absence EEG (Amor et al., 2005; Garcia Dominguez et al., 2005; Aarabi et al., 2008; Ponten et al., 2009).

Measuring the interrelation between neurologically derived time series is of major interest in neuroscience, and is referred to as estimating *functional connectivity*. A high functional connectivity implies that the time varying output at two different spatial locations is statistically similar. The use of the term *connectivity* here is perhaps unfortunate, given the importance of structural connectivity in the brain. The potential ambiguity of this description can be appreciated in the transition from background to absence seizures, wherein both the linear and non-linear functional connectivity has been shown to increase at seizure onset (Aarabi et al., 2008). Clearly spatially segregated regions of the brain do not somehow become more synaptically "connected" at the onset of seizure activity, despite the apparent increase in similarity of functional output at different spatial locations. This is also a case in which the univariate properties of the signals affects the measures of interrelation obtained. The drop in frequency, i.e. the appearance of the SWD "wave", means that in any SWD epoch two channels contain substantial segments of co-incident waveforms. A large component of these interrelations are expected to be conserved under randomisation of the multi-variate time series (*surrogate* creation), and as such the interrelations are said to have a high *random correlation* component (Müller et al., 2008).

Correlation matrix properties in multi-variate data

Recently, multivariate methods have been applied to the analysis of correlation structures in epileptic EEG (Müller et al., 2005; Baier et al., 2007; Rummel et al., 2007). These methods are based on the eigenvalues and eigenvectors of the correlation matrix C and therefore find benefit in a reduction of information from $M \times (M - 1)/2$ coefficients to M eigenvalues for the quantification of correlation structure (Müller et al., 2005).

Quantitative measures of spatio-temporal patterns based on the correlation matrix eigenvectors include the participation ratio, which is proportional to the sum of the absolute value of eigenvector components for each eigenvector. This sum describes a notion of collectivity in the contribution of channels to each eigenstate and has been shown to vary in line with changes in system correlations (Müller et al., 2005). The distribution of these elements within an eigenvector capture the extent to which each channel contributes to that eigenstate. In terms of principal component analysis, this can also be thought of as describing the relative contribution of each channel "direction" to a principal component. Müller et al. (2005) showed that in addition to the largest eigenvector (the eigenvector corresponding to the largest eigenvalue, henceforth reffered to the principal eigenvector), useful information can be gleaned from some of the smallest eigenvectors (those which correspond to the smallest eigenvalues). Since the aim of the current work is to introduce methods for comparing spatio-temporal patterns, and since the principal eigenvector captures relevant features of these, we leave the analysis of other eigenvectors to future studies.

Correlation clusters

A complementary recent focus is the identification of underlying correlation clusters in which the information contained in the eigenvector components of C is reduced to M labels in vector form. This represents an interesting and potentially highly useful transformation of the spatial structure of EEG time series. Essentially, the complete interrelation structure of the data, which is an important component of the spatially extended system (see above), is collapsed onto an M dimensional vector. It will be proposed in the current chapter that this projection offers a novel way in which to quantitatively compare spatio-temporal patterns. Essentially, the vectorisation of the data renders them amenable to quantitative comparison by vector distance measures. The feature of spatio-temporal patterns captured by this method of clustering is the optimal partitioning of channels into highly interrelated blocks (Rummel et al., 2008). This is an abstraction from the details of channel interrelations since equivalent block structures may be composed of different pair-wise interrelation distributions.

A particular advantage of the cluster identification method proposed in (Rummel et al., 2007) is that it is entirely data-driven. The importance of this advance cannot be overstated; unlike other clustering methods (see e.g. (Jain and Dubes, 1988)), the number of clusters or algorithm parameters do not have to be pre-defined. The collective morphology of activity patterns is the entire basis on which the algorithm proceeds, and it can therefore be regarded as a self-contained map from multivariate time series to cluster vectors.

This important shift of emphasis towards the creation of a simplifying map brings

with it the requirement for new tools to deal with i) variability inherent in the method; and ii) possible inconsistency in the output labels. The first is due to the estimate of number of clusters and the stochastic optimization procedure whilst the second arises because the order of the eigenvectors relating to each cluster is not conserved. This means that equivalent cluster structures may not be labelled in a way that supports a straightforward comparison of two cluster vectors, or a trivial choice of quantitative distance measure. These factors contribute to an inherent variability in the output cluster vectors. It is clear that if the aforementioned problems can be addressed this conceptual shift towards mapping time series into vectors could provide important advances in the characterisation and quantitative comparison of spatio-temporal patterns in multivariate time series.

Aims of this chapter

In this chapter we investigate the vectorisation of the correlation matrix as a means to quantify and quantitatively compare multi-variate time series (spatio-temporal patterns). The projection onto vectors allows spatio-temporal patterns to be compared by distance measures such as Euclidean distance or Hamming distance. We demonstrate the use of these methods to quantitatively compare absence seizure epochs. Three vectorisation methods are tested, namely i) the vectorised absolute correlation matrix; ii) the absolute entries of the principal eigenvector and iii) the cluster vector formed by the approach of Rummel et al. (2007). These three approaches give a successive abstraction from the detailed arrangement of the pair-wise correlation structure, as outlined in section 6.4.

6.3   EEG data

Clinical EEG data containing typical absence seizures were used in this study. These data provide a well defined ictal period in which 3 cycles per second activity is generalised on the EEG. EEG data were obtained from the Klinik für Neuropädiatrie, Universitätsklinikum Schleswig-Holstein, Kiel, Germany, and the Department of Neurology, Inselspital, Bern University Hospital, Bern, Switzerland. The data were sampled at f=256 or 250 data points per second. Data were used in the Hjorth reference and filtered with a high pass filter at 2.5Hz to reduce the influence of slow activity unrelated to the spike-wave discharges and with a low pass filter at 25Hz to eliminate high frequency artefacts. There were i=22 patients, and j=60 seizures. These were structured in terms of the number of seizures per patient as $Ns_i, \{i = 1, .., 22\}$, where Ns_i is the number of seizures recorded for patient i. The average number of seizures recorded per patient was $\overline{Ns_i}$=2.7. The average length of seizure was $\overline{ls_{ij}}$=10.5 seconds, where ls_{ij} is the duration of seizure j for patient i.

For each patient dataset, seizure periods were automatically located by increased

power in the 2-4Hz range. Specific seizure onset and offset times were located at positions encompassing all generalised spike-wave complexes.

6.4 Methods

As discussed in section 6.2, the eigenvectors of the correlation matrix contain information regarding spatio-temporal patterns in multi-variate data (Plerou et al., 2002; Müller et al., 2005; Rummel et al., 2007, 2008). The principal eigenvector provides a projection of the inter-relation structure which preserves more information than a point quantification such as the mean absolute correlation, whilst reducing the number of data from $M \times (M - 1)/2$ pair-wise interrelation measures for multi-variate data with M channels. In analogy with principal component analysis, the principal eigenvector points in the direction of largest variance in the data, and thus the *absolute* principal eigenvector captures the magnitude of contribution of each channel to this sub-space. The absolute principal eigenvector is a direction in a positive sub-space in $\mathbb{R}^M$ and thus can be compared to other vectors in this space in a simple way using the Euclidean distance. This is the first of our methods employed to quantitatively compare spatio-temporal patterns of EEG from our database.

The vectorised entries of the absolute correlation matrix provide a direction in a positive sub-space in $\mathbb{R}^{\frac{M \times (M-1)}{2}}$ and can therefore also be quantitatively compared using the Euclidean distance. Intuitively, comparing the values of the correlation matrix is sensitive to specific deviations in the order of pair-wise interrelations, whereas the eigenvector method penalises relative contributions to the direction of largest variance and is therefore less sensitive to the specific ordering of correlations. In section 6.4.2, the cluster vector method outlined maps spatio-temporal patterns to optimally interrelated blocks of channels, and is therefore even less sensitive to the specific arrangement of entries of the correlation matrix. The three comparison methods employed therefore rely on successive abstractions from the specific organisation of pair-wise interrelations.

All of the three methods employed stem from the correlation matrix, the formation of which is therefore the first step in each case. Since spatio-temporal patterns during seizure periods are the focus of this chapter, each segment of EEG containing a seizure period was extracted as a multi-variate time series block of dimension $19 \times ls_j \times f$, where ls_j is the length of seizure j, 19 is the number of channels and f is the number of data points per second. The correlation matrix, C, was then formed from the pair-wise Pearson cross-correlation coefficients between each pair of channels.

Since the analysis of eigenvectors and vectorised correlation matrices is less volatile and computationally expensive than the cluster vector method, this method was also used to analyse peri-ictal (around the seizure) and inter-ictal (between

seizures) periods. For peri-ictal analysis, a segment of data of length $ls_j \times f$ was extracted immediately preceding and immediately following the seizure. For inter-ictal analysis, a data set was formed for each patient by removing all of the ascertained seizure periods (see section 6.3 for the method to locate these periods) and concatenating the remaining data. Ns_i inter-ictal periods were then randomly sampled from this new dataset, with the length of each period set to the average length of seizures for that patient, $f \times \overline{ls_{i\cdot}}$. ($\overline{ls_{i\cdot}} = \frac{\sum_{j=1}^{Ns_i} Ls_{ij}}{Ns_i}$).

6.4.1 Eigenvector and correlation vector methods

The principal eigenvector of the correlation matrix was extracted for each epoch. In addition, the 171 entries of the absolute correlation matrix were arranged in a vector by scanning row-wise along the upper triangle of the matrix. For comparison of these vectors the Euclidean distance was employed, as defined below:

$$d_{xy} = \sqrt{\sum_{i=1}^{N_{vec}} (x_i - y_i)^2} \tag{6.1}$$

where x and y are the two vectors to be compared and N_{vec} is the length of the vector (here N_{vec} is 19 for eigenvectors and 171 for the vectorised absolute correlation matrix).

In order to test the hypothesis that spatio-temporal patterns are conserved for seizures recorded from the same patient, pair-wise Euclidean distances (d_{xy}) were calculated on two arrangements of vectors. In the first arrangement, only seizures of the same patient were compared, which resulted in a distribution of 83 distances. We call this distribution the *within patient* distribution of distances (d_w). The second set contained all 60 seizures, but compared only seizures of different patients and thus yielded $60 \times 59/2 - 83 = 1687$ distance measures. We call this distribution the *between patient* distance for all seizures (d_b). By comparing these two distributions, we can estimate the degree to which spatio-temporal patterns are conserved for EEG of the same patient. The distributions were compared by the Mann-Whitney test ("ranksum" in Matlab) for differences in medians. This analysis was also implemented for the non-seizure periods described above.

It is clear that these comparisons can be confounded by a number of factors. Firstly, it is possible that there exists an underlying preference for correlations in EEG in general, such that the differences between spatio-temporal patterns of EEG from *different* patients is more conserved than that of randomly generated spatio-temporal patterns. This could occur due to reference effects and preferred patterns due to the distribution of tissue in humans (skull thickness and conductivity, for example). The specific effects of reference could be examined by performing the analysis on data transformed to different montages, though this is beyond the

scope of the current study. Instead, we take a more general approach by examining whether the distributions d_w and d_b deviate from the random case. To this end, the distributions of absolute correlation matrix entries and absolute principal eigenvector entries over all ictal and inter-ictal periods were examined and then randomly sampled to form a database of eigenvectors and correlation matrices according to the patient-seizure structure Ns_i. The overall distributions of entries for the patient (absolute) eigenvectors and (absolute) correlation matrix are displayed in Figure 6.1. For these curves and subsequent distribution plots for continuous data, the probability distributions were estimated from histogram data using a Gaussian kernel density estimation method (the "kde" function in Matlab). This allows for neater visualisation and easier visual comparison of these distributions.

Some general features of Figure 6.1 are apparent. Most notable are the larger absolute values of the correlation vector ("Cvec") in the ictal case as compared to the inter-ictal case. This is expected given the increased power at low frequencies during seizure periods, which leads to higher levels of correlation (Müller et al., 2008). Also interesting is that the mode of the distribution of absolute eigenvector entries ("Evec") is almost equivalent for the ictal and inter-ictal cases, although the distribution is considerably narrower for the ictal case, indicating preferred absolute eigenvector values in this case of absence seizure periods in general.
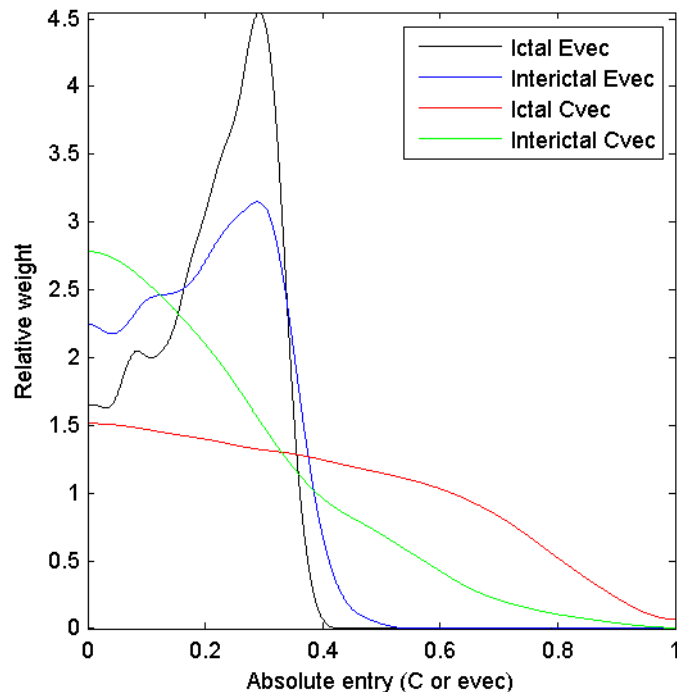

Figure 6.1: Distributions of absolute values of the principal eigenvector and absolute correlation matrix for all ictal and inter-ictal periods.

The distributions characterised in Figure 6.1 were sampled to form random absolute eigenvectors and random absolute correlation vectors in keeping with the

patient-seizure structure Ns_i. The distribution of distances for these vectors was then computed in the same way as for the actual patient data. Explicitly, "within patient" and "between patient" distance distributions were formed for the random data sets (we denote these distributions d_w^{rand} and d_b^{rand}, respectively). Comparing these randomly generated vectors also allows one to account for differences that might arise between d_w and d_b in the data due to the effects of asymmetry in the sizes of distributions $|d_w| \ll |d_b|$ where $|\cdot|$ indicates the order (size) of the set.

6.4.2 Cluster vector method

The approach described in this section is based on a method to identify correlation clusters using the eigenvector components of the correlation matrix (Rummel et al., 2007). Other methods of clustering time series require the pre-specification of either the number of clusters or arbitrary parameters and thus the output is not entirely driven by aspects of the data. The method of Rummel et al. (2007), however, is entirely data-driven and therefore its application can be interpreted as a map from time series space into the cluster vector space. As this map is derived from the equal-time correlation matrix, it is underpinned by aspects of the co-morphology of the time series.

Summary of the cluster identification method

Since the cluster identification method employed has been discussed elsewhere, readers are referred to Rummel et al. (2007), Rummel et al. (2008) and Rummel (2008) for a detailed explanation. We summarize the method below and in the flow chart in Figure 6.2.

For this method, the original segment under analysis was used to generate a set of 90 shift surrogate data per data window (Netoff and Schiff, 2002), for which the correlation matrices were also formed ($C_{surr}^n, 1 \leq n \leq 90$). This number of surrogates corresponds to the notion of a 0.1 significance level for the identification of clusters. The number of large eigenvalues of C significantly larger than those of the distribution from C_{surr}^n gave the estimate of number of clusters, K.

Once the number of clusters, K had been estimated, the K eigenvectors of C corresponding to the K largest eigenvalues (henceforth referred to as the K largest eigenvectors) were used to generate K cluster participation vectors (CPV) (Rummel et al., 2007). In short, the eigenvectors are rotated until their entries are maximally non-overlapping, which reveals the optimal block structure for correlations in C. The stochastic optimization procedure used to produce CPV was the great deluge algorithm (Dueck, 1993). Automatic attribution of clusters to channels was performed using the "ratio×difference" method of Rummel et al. (2007, 2008). This method automatically detects which groups of eigenvector entries can be separated into clusters.
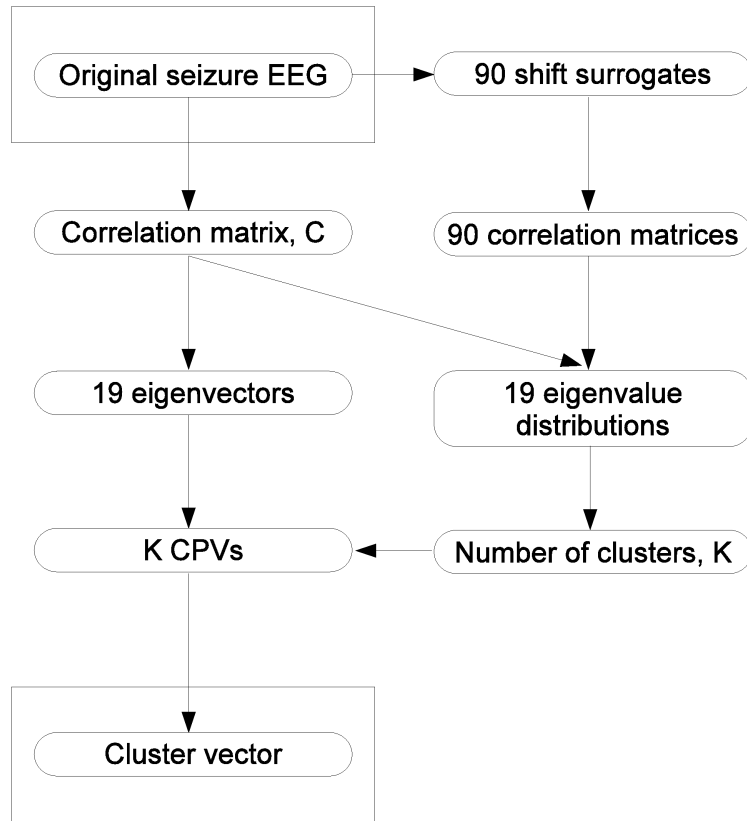
Figure 6.2: Flow chart of the map from a time series segment to a vector.

Relabelling of cluster vectors

The output of the map are cluster vectors, v, of dimension equal to the number of channels, M ($M = 19$ in our data). Each position, k, of this vector represents a channel with the cluster membership recorded by an integer value, v_k, $0 <= v_k <= K_{max} = 9$, where 0 indicates no cluster membership. Unfortunately, a consistent order of cluster allocation is not guaranteed by the CPV algorithm and therefore equivalent cluster structures may not be consistently labelled. A solution to this problem involves minimising the distance between vectors and therefore ensuring that common clusters in each vector are given the same label. An example of two vectors, u and v, that should be relabelled is shown below. The number of channels has been reduced here to 4 for ease of representation.

$$u = \begin{pmatrix} 1 \\ 2 \\ 2 \\ 3 \end{pmatrix}, \quad v = \begin{pmatrix} 2 \\ 3 \\ 3 \\ 1 \end{pmatrix} \tag{6.2}$$

Both vectors represent the same cluster structure with all channels involved in one of three clusters, though the labels are in different positions in each vector. The method for relabelling the second vector to match the first is now described.

Each vector is split into a binary matrix consisting of its substructures, where column j contains the binary representation of cluster j:

$$u^{bin} = \begin{pmatrix} 1 & 0 & 0 \\ 0 & 1 & 0 \\ 0 & 1 & 0 \\ 0 & 0 & 1 \end{pmatrix}, \quad v^{bin} = \begin{pmatrix} 0 & 1 & 0 \\ 0 & 0 & 1 \\ 0 & 0 & 1 \\ 1 & 0 & 0 \end{pmatrix} \tag{6.3}$$

We aim to reorder the columns of v^{bin}, $v_{\cdot j}^{bin}, 1 \leq j \leq K$ such that the sum of pair-wise distances with columns of u^{bin}, $H(u_{\cdot j}^{bin}, v_{\cdot j}^{bin}), 1 \leq j \leq K$, is minimised. In practice, the distribution of distances between column pairs is evaluated and the columns of v^{bin} closest to each successive column of u^{bin} are relocated.

The distance measure used here is the Hamming distance, calculated by:

$$H(u, v) = \frac{a}{n} \tag{6.4}$$

where a is the number of mismatches between vectors, and n is the length of each vector. In cases where v has more clusters than u, any remaining unmatched clusters are assigned the next smallest unused integers. The result of this relabelling process performed on v, above, is as follows:

$$u = \begin{pmatrix} 1 \\ 2 \\ 2 \\ 3 \end{pmatrix}, \quad v' = \begin{pmatrix} 1 \\ 2 \\ 2 \\ 3 \end{pmatrix} \tag{6.5}$$

It can be seen that the consistency in cluster structure is thus revealed.

Quantification of cluster vector variability

The CPV components are generated in a stochastic optimization procedure which is not unambiguously defined. In addition, there is an unavoidable uncertainty in the automatic attribution of CPV components to cluster labels. These two effects create a variability in the cluster output that is due to the method. We henceforth refer to this variability as "technical variability" as opposed to data-based variability in the output. In order to evaluate the technical variability in cluster calculation, ten iterations of the clustering algorithm were performed on each seizure with equal

settings, and the output examined. Variability was defined by the distribution of Hamming distances over all pairs of vectors in this output. The clustering of each data set therefore yielded ten separate estimates of the cluster vector, $v_n, 1 \leq n \leq 10$ and a distribution of $10 \times 9/2 = 45$ Hamming distances, $H_m, 1 \leq m \leq 45$, calculated according to the method described above after relabelling.

Figure 6.3 shows two extreme examples of technical variability. The two top panels of Figure 6.3 show ten realisations of cluster output for each seizure and the bottom panels of Figure 6.3 show the distribution of Hamming distances calculated for pairs of output within each seizure. It can be seen that on the one hand, the distribution in Figure 6.3 (c) (corresponding to output in Figure 6.3 (a) is dense at low values of H, meaning that large distances were not found and therefore in general only few corresponding labels in cluster vector pairs are different. On the other hand, the distribution in Figure 6.3 (d) (corresponding to output in Figure 6.3 (b)) shows increased density at larger distances with a modal value between 0.3 and 0.4 reflecting the higher degree of variability in cluster output. It can be seen that the apparent difference in consistency of output in these data sets is captured by the difference in their Hamming distance distributions.

Since technical variability is quantified by a distribution of distances $H_m(1 \leq m \leq 45)$, we can characterise the technical variability of each clustering by the median of this distribution, H_{med}. The distribution of H_{med}, over all data sets analysed, is shown in Figure 6.4 (a). The resulting distribution can in turn by characterised by a median Hamming distance of approximately 0.03 (Figure 6.4 (a)), a crude interpretation of which is that we might expect 1 out of 19 channels to be allocated to different clusters by this method, even though the underlying structure is the same. Figure 6.4 (b) shows the dependancy of this median on the median number of clusters over the 10 repeats. It can be seen that there is a general trend of increasing variability with increasing number of clusters, though the variability can still be high in data sets where the median number of clusters is low (e.g. see the case of $K = 3$). Variation in the estimate of number of clusters is a contributing factor to the measured technical variability and arises due to variability in the distribution of shift surrogates. The difference in estimate of number of clusters was rarely greater than 1 (data not shown) and hence this estimate was considered robust.

6.5 Results

6.5.1 Euclidean distance method

In order to illustrate the degree of conservation of correlation vectors and eigenvectors in EEG epochs from the same patient, examples are given in Figures 6.5 and 6.6. In Figure 6.5, top panel, the similarity between the red and black lines indicates the degree of conservation of patterns in 2 different seizures of the same
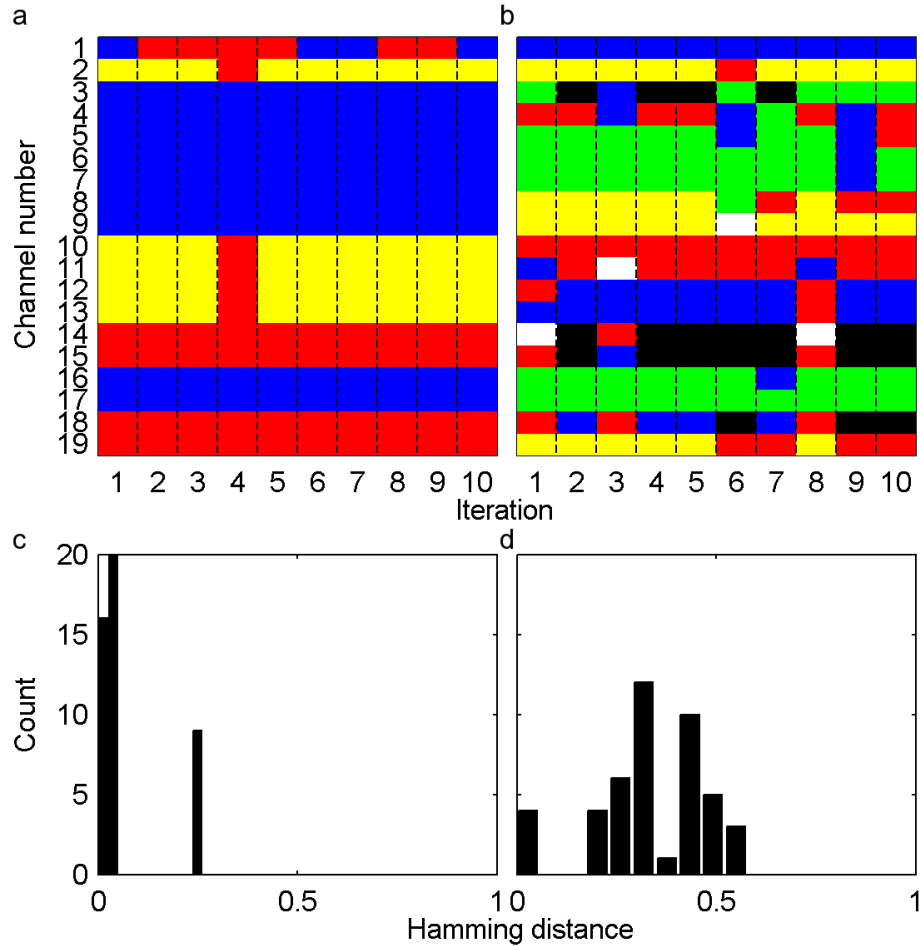
Figure 6.3: (a) and (b): Cluster output over 10 repeats for 2 different seizures. Clustered channels are coded by equivalent colours. The 10 repeats are organised on the x-axis and separated by vertical dashed lines. (c) and (d): Corresponding distributions of pairwise Hamming distances (n=45) for these output.

patient. The blue line which derives from a seizure of a different patient is shown to deviate from this pattern. In the inter-ictal case, shown in the bottom panel of Figure 6.5, a much reduced degree of conservation is apparent. Figure 6.6 shows vectorised correlation matrix entries across the same seizures as in Figure 6.5, top panel. The picture here is similar in that the correlation entries show a great degree of overlap for seizures of the same patient.

An examination of the distributions of Euclidean distance derived from the absolute eigenvectors and absolute vectorised correlation matrix are provided in Figure 6.7 and Figure 6.8, respectively. The median values for these distributions are displayed in Table 6.1.

Several interesting points emerge from Table 6.1 as well as by examining Figures 6.7 and 6.8. For each of the epochs examined, the within patient distribution of distances (in both eigenvectors and correlation vectors) was centred around a value lower than the distances calculated between patients indicating that spatio-temporal patterns are conserved for patient EEG. This effect was more pronounced for the
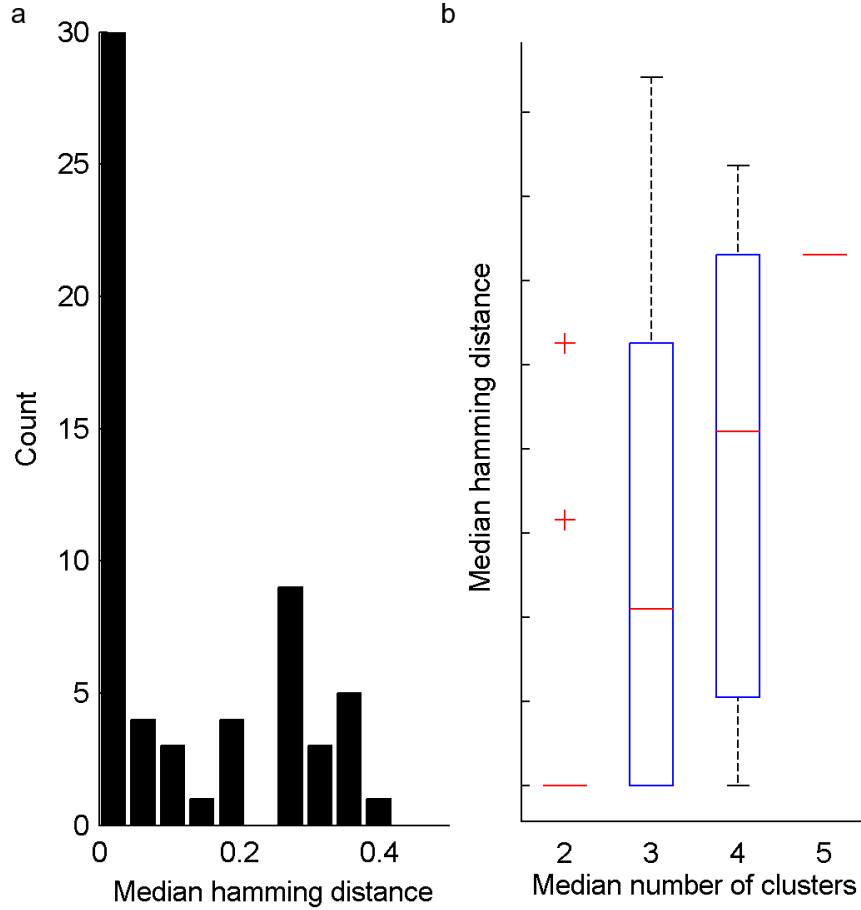
Figure 6.4: (a) Distribution of median technical variability (H_{med}) for n=60 absence seizures. (b) Dependancy of median variability on median number of clusters (with an integer median cluster number).

correlation vector than for the eigenvector measure. The largest separation of within patient and between patient distributions was seen in the ictal period which suggests an increased conservation of spatio-temporal patterns during seizures, as compared to background periods.

However, all of the randomly sampled vectors led to distance distributions centred at larger values than those observed in patient data. In the eigenvector measure, ictal and inter-ictal between patient comparisons were close to the random distributions. This suggests that when epochs of EEG from different patients are compared via the principal eigenvector, they are essentially unrelated. However, if the entries of the absolute correlation matrices are compared instead, one might expect some degree of conservation of patterns such that randomly sampled vectors cannot account for the observed distribution of vector distances.

Importantly, the "within" and "between" distributions as calculated from random data were very closely matched (see e.g. $d_b^{rand(ictal)} = 0.60$ and $d_w^{rand(ictal)} = 0.58$). This indicates that any differences observed in "within" versus "between" distributions in the patient data are not due solely to asymmetry in the distribution
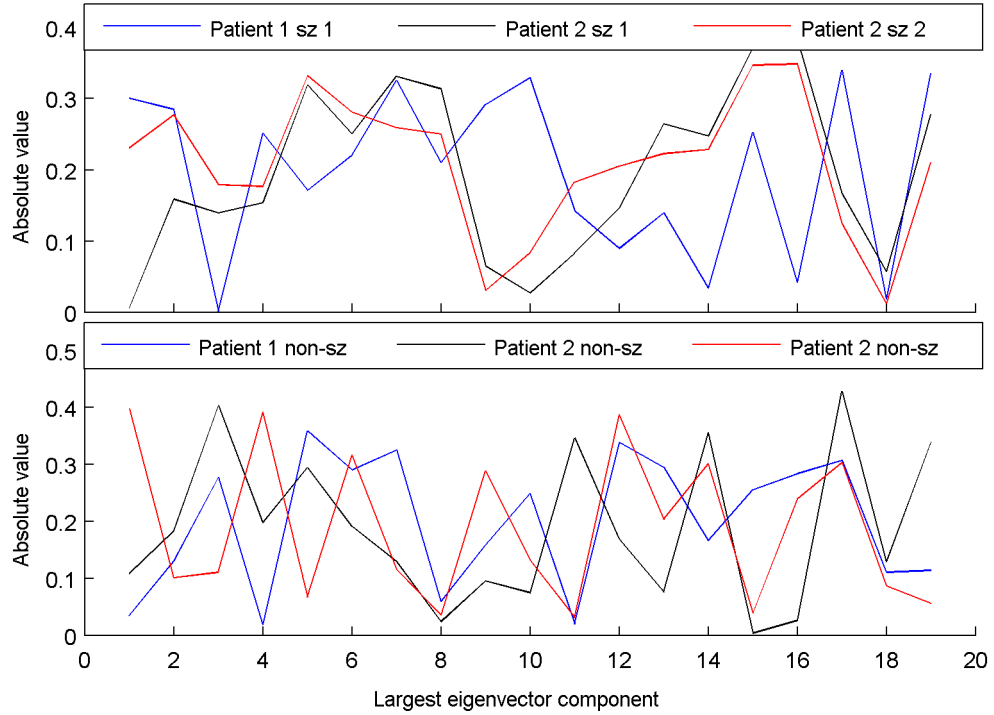
Figure 6.5: Example comparison of absolute entries of the principal eigenvector within and between patients. The top panel shows absolute eigenvector entries during seizure epochs for two seizures of patient 1 and one seizure of patient 2. The similarity between the eigenvectors of the same patient can be seen. The bottom panel shows a similar comparison for inter-ictal periods.

sizes. Thus, the distributions observed provide good evidence for the conservation of spatio-temporal patterns in seizures of the same patient. In addition, this is not simply a feature of the generic or synchronous properties of SWD since seizures of different patients are very different. Little evidence is presented for patient specific pre- or post- ictal states since the degree of conservation within patients in these epochs is similar to that observed in the inter-ictal state.

Since the distribution of distances can be quantified by the median value (see

Distribution	Median (Evec)	Median (Cvec)	Interpretation
d_b^{ictal}	0.56	3.91	Between patient distances: ictal
d_w^{ictal}	0.18	1.59	Within patient distances: ictal
$d_b^{rand(ictal)}$	0.60	4.47	Between random data distances: ictal
$d_w^{rand(ictal)}$	0.58	4.42	Within random data distances: ictal
d_b^{inter}	0.62	3.13	Between patient distances: inter-ictal
d_w^{inter}	0.44	1.85	Within patient distances: inter-ictal
$d_b^{rand(inter)}$	0.67	3.46	Between random data distances: inter-ictal
$d_w^{rand(inter)}$	0.64	3.40	Within random data distances: inter-ictal

Table 6.1: Median distances for the distributions in Figures 6.7 and 6.8
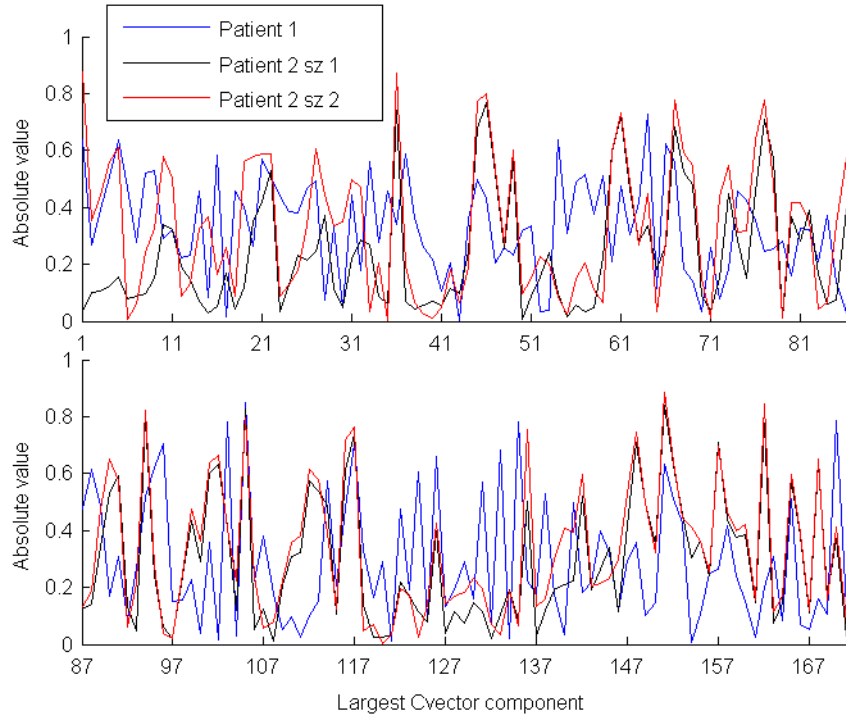
Figure 6.6: Example comparison of absolute entries of the vectorised correlation matrix within and between patients. Comparisons here are for the ictal period only. The 171 entry vector is split across the top and bottom panels.

Comparison			Absolute difference in medians	p-value
d_b^{ictal}	vs.	d_w^{ictal}	0.38	3.0×10^{-51}
$d_b^{rand(ictal)}$	vs.	$d_w^{rand(ictal)}$	0.019	0.03
d_b^{inter}	vs.	d_w^{inter}	0.18	1.5×10^{-22}
$d_b^{rand(inter)}$	vs.	$d_w^{rand(inter)}$	3.8×10^{-4}	0.63

Table 6.2: Selected comparisons of median eigenvector differences

Table 6.1), they can also be quantitatively compared by the difference in medians, the significance of which can be assessed using a Mann-Whitney type of statistical test. In Table 6.2 we present the quantification of distances for some important comparisons.

6.5.2 Cluster vector method

Cluster vectors were produced for each seizure period. Figure 6.9 shows one realisation of clustering for some exemplary seizures, arranged by patient. Visual inspection of Figure 6.9 shows striking variability in the output between patients, although some consistency is present in the sense that most channels are allocated to a cluster in all seizures. There is a suggestion of some degree of consistency between different seizures of the same patient. Four seizures of patient 1 are identical, for
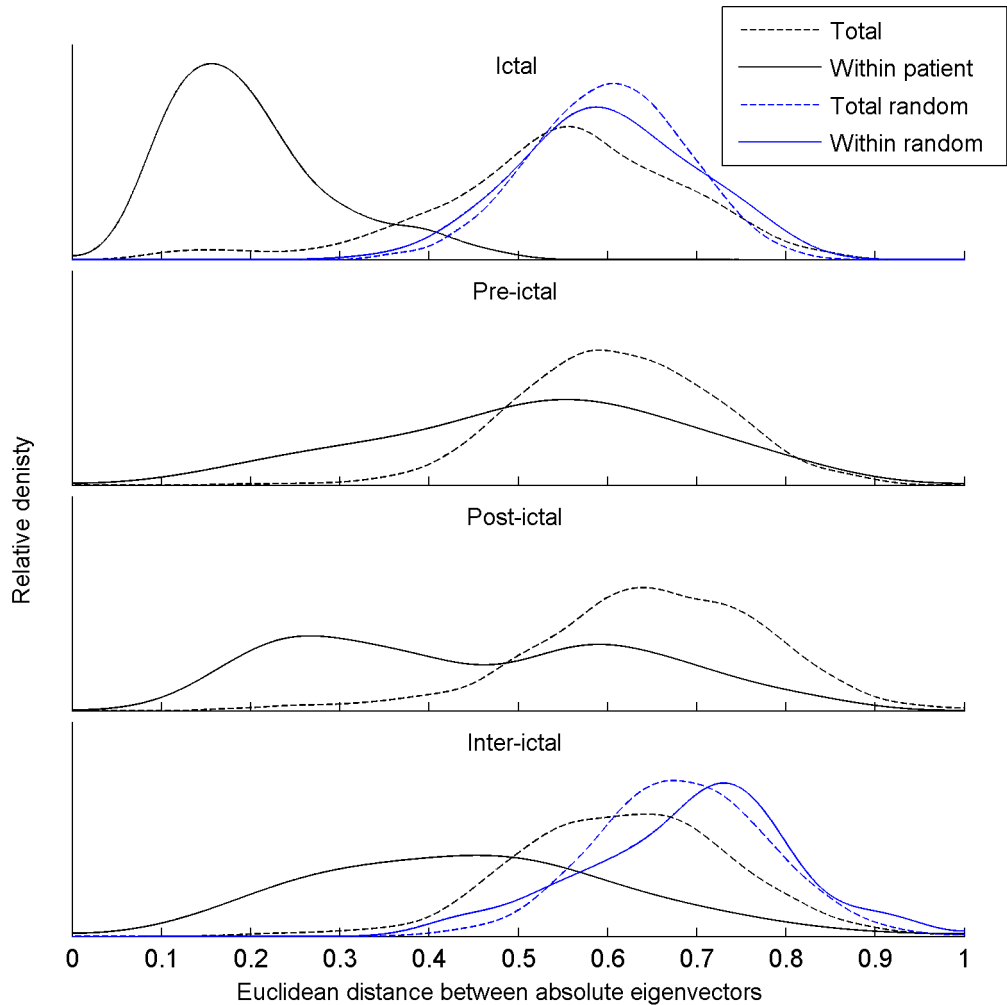
Figure 6.7: The distribution of distances between absolute eigenvectors. Distributions are compared for ictal, per-ictal and inter-ictal periods. In addition, the distances obtained from comparisons involving randomly sampled vectors are plotted.

example (Figure 6.9, patient 1). The seizures of patients 16, 17 and 22 appear to show within patient variability of the order of mild technical variability (cf. Figure 6.3 (a)). However, the seizures of patient 8 appear to show a greater degree of variability (cf. Figure 6.3 (b)).

The within- and between- patient variability of cluster output were quantified. Clearly the Hamming distance between two output vectors is insufficient for this task because two different seizures may represent the same cluster structure but map to different cluster vectors only as a result of the inherent technical variability. We account for this effect by considering Hamming distances only if they are greater than the maximum of those observed in the technical variability distributions of each seizure. The difference between two vectors, u and v, is therefore calculated as follows:
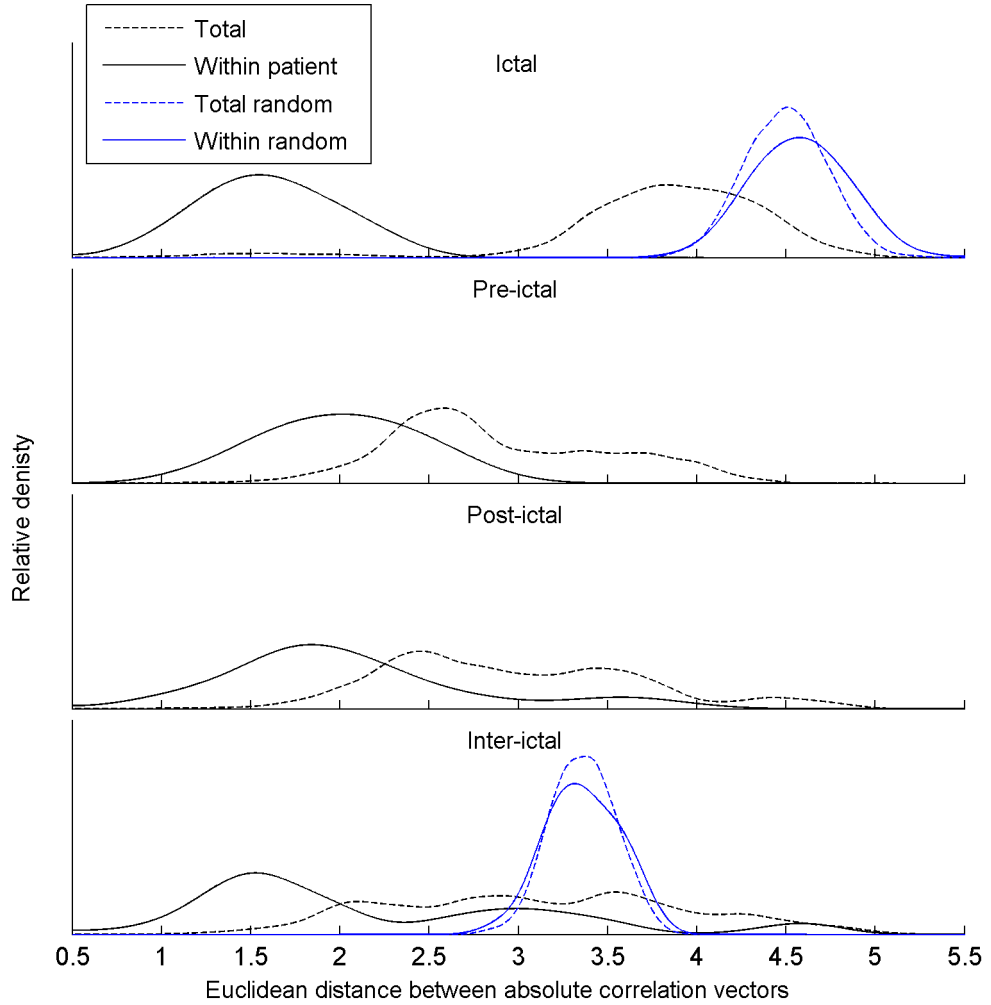
Figure 6.8: The distribution of distances between absolute correlation vectors. Distributions are compared for ictal, per-ictal and inter-ictal periods. In addition, the distances obtained from comparisons involving randomly sampled vectors are plotted.

$$d(u,v) =$$

$$\begin{cases} H(u,v') - max(\max_m(H_m^u), \max_m(H_m^v)), & H(u,v') > max(\max_m(H_m^u), \max_m(H_m^v)) \\ 0, & H(u,v') \le max(\max_m(H_m^u), \max_m(H_m^v)) \end{cases}$$

$$(6.6)$$

Figure 6.10 represents the quantification of within- and between- patient variability as calculated for 60 seizures. The proportion of comparisons that yielded a difference only of the order of the maximum technical variability is represented by the first bar of the histograms, centred at $d = 0.05$. Both histograms contain a large proportion of density in this bin, which would suggest a degree of consistency between cluster vectors in general, even when seizures of different patients
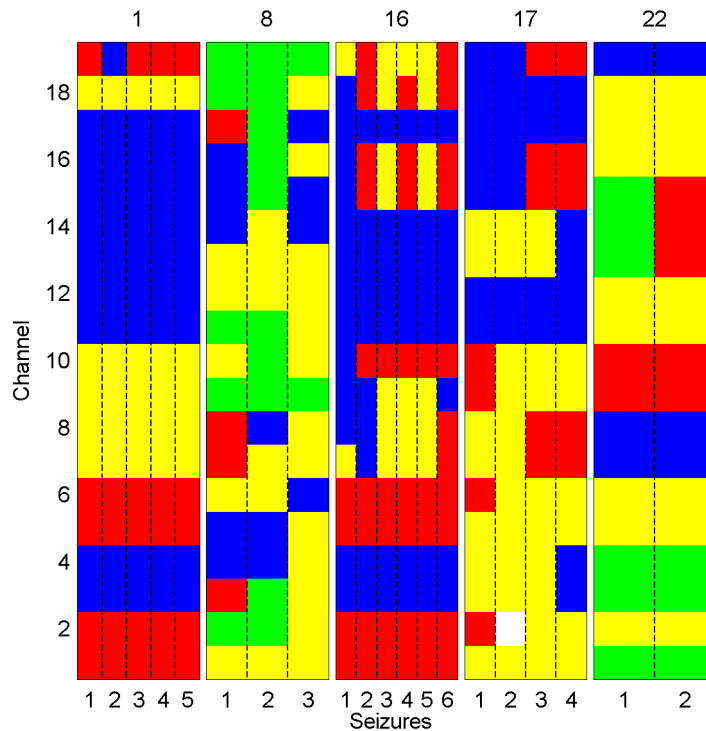
Figure 6.9: Cluster output for one run of the algorithm on a number of seizures in 5 patients. Multiple seizures (labelled on the x-axis) are separated by vertical dashed lines within patient. These are labelled according to patient number in our data base.

are compared. Around 88% of comparisons between seizures of the same patient lie in this region (Figure 6.10 (a)) and subsequently less than 15% of *within* patient comparisons display distances in excess of that explained by technical variability (Figure 6.10 (a)). In contrast, 53% of *between* patient comparisons display distances in excess of that explained by technical variability (Figure 6.10 (b)). Together, these results suggest a conservation of cluster vectors in seizures of the same patient.

6.6 Discussion

In this chapter, methods were introduced to quantify and quantitatively compare spatio-temporal patterns. The general method was a vectorisation of properties of inter-relation structures for quantification without reduction to a point measure, such as the mean inter-relation between channels. Quantitative comparison was introduced by means of vector distance measures. In applying these methods to EEG from patients with absence epilepsy we were able to demonstrate quantitatively the extent to which seizure patterns are conserved *within*, rather than *between*, patients.

Each method employed in the current chapter was based on properties of *inter-relations* in multi-variate time series, in this case quantified by the correlation matrix. This linear measure has been applied successfully to the analysis of bivariate properties in epileptic EEG and, in particular, absence seizures for a number of decades
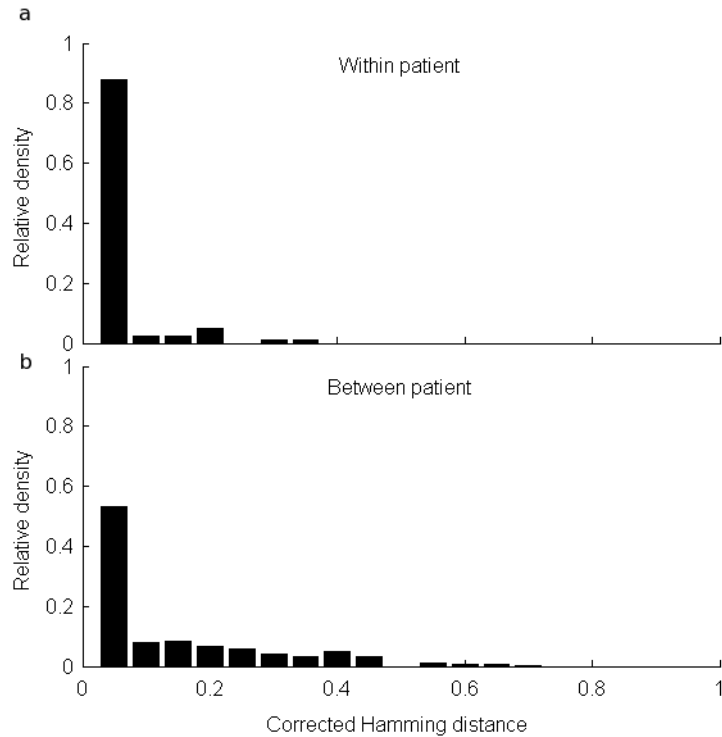
Figure 6.10: Distribution of (a) within and (b) between patient variability in correlation cluster vectors, corrected for technical variability as described in section 6.5.2. Calculation performed on the 60 seizures used in Figure 6.4.

(see e.g. Cohn and Leader (1967) for an early reference and Aarabi et al. (2008) for a more recent study). While during the last two decades nonlinear measures were widely studied and given preference, comparative studies of bivariate measures have found the correlation coefficient to perform no worse than the nonlinear measures under comparable conditions, e.g. in the prediction of epileptic seizures (Kreuz et al., 2007; Mormann et al., 2005).

The three methods applied to vectorise the correlation matrix relied on different abstractions from the distribution of pair-wise correlations. It was found that the vectorised correlation matrix and the principal eigenvector gave qualitatively similar results when applied to different EEG epochs. In addition, the preserved within-patient spatio-temporal patterns were verified by the cluster vector method. However, the clustering method sometimes suffered from high levels of technical variability and therefore its performance in quantifying data variability was deficient in comparison to the other methods. The problem of consistent labelling of clustered time series has been noted in attempts to visualise consistency of cluster vectors calculated at different time points. In the context of human EEG, one method used a symbolic approach to address this problem (Bialonski and Lehnertz, 2006). In contrast, our method, based on a binary vector expansion allows a consistent data-based labelling of seizures that avoids ad-hoc adjustments. Although we have used this relabelling for the purpose of whole seizure analysis in the present study, it also

126

facilitates the representation of dynamical changes in cluster vectors.

In examining distances between vectors derived from different methods we have demonstrated a general framework for the comparison of features of spatio-temporal patterns. Clearly in future expansions to the methods presented here other important features should be incorporated such as frequency and amplitude. Importantly, these can be introduced within the *vector distance* framework. An example of a more thorough approach might be to characterise spatio-temporal patterns by *three* vectors in $\mathbb{R}^M$ accounting for vectorised frequency, amplitude and inter-relations. In this case the distance between two spatio-temporal patterns will be a point in $\mathbb{R}^3$.

The comparison of cluster vectors relied on our being able to account for technical variability, which arises due to a combination of two factors; (i) differences in the estimate of the number of clusters and (ii) subtle differences in the components of the CPV. The observed trend of increasing variability with increasing median number of clusters is therefore to be expected; as more CPV are taken into account, more subtle variability in their components is translated into variable cluster memberships. Technical variability of the method was seen to be low in 100 trials of the algorithm for certain test conditions when clusters are accurately identified (Rummel, 2008). It could be the case with absence seizure data that a poorly defined block structure of correlations leads to competing optimal solutions for the CPV vectors. Such hypotheses can be investigated in future studies and are made possible by the introduction of the methods in this chapter. However, the occurrence of technical variability is unavoidable in a method that uses a discretisation and an optimisation step to characterise complex spatio-temporal patterns.

Various studies have been devoted to the investigation of variability in absence seizures both in terms of univariate and bivariate properties. The morphology of SWD have been shown to be variable, even within seizure, and the spatial distribution of its components have been observed to be particularly variable in seizures of different patients (Weir, 1965; Lemieux and Blume, 1986; Rodin and Ancheta, 1987; Hughes et al., 1990; Ferri et al., 1995; Rodin, 1999), with Rodin and Ancheta remarking that their study of field maps of SWD "clearly showed that even the most classic 3/sec spike-wave pattern is neither truly generalised nor bilaterally symmetrical or synchronous" (Rodin and Ancheta, 1987) . Despite this massive variability in SWD, a few studies have also noted a reproducibility of certain properties of SWD dynamics between seizures of the same patient (McKeown et al., 1999; Aarabi et al., 2008; Amor et al., 2005) but no generally applicable quantification of the reproducibility were provided.

In this chapter we aimed to provide this quantification. To this end, the "distance" between seizures of the same patient and seizures of different patients were quantified by the methods introduced, and their distributions compared. In all three methods it was observed that the distribution of *within* patient distances resided at

lower values of d. The comparison of these distributions was more robustly made in the case of the vectorised correlation matrix and the principal eigenvector, than for cluster vectors. This is due to issues of technical variability, and also due to the continuous nature of the distribution derived from the Euclidean distance, as opposed to the discrete Hamming distance. The quantification of preserved patterns of seizure activity within patients is an important verification of the notion of *stereotypy* (Schindler et al., 2011). This term pertains to the repeatability of aspects of seizure evolution within patients and is an important correlate to the presence of epileptic activity (Schindler et al., 2011). Thus it will be interesting in future studies to apply the methods presented in this chapter to different types of epileptic seizure. In general, the finding of conserved, or repeatable, patterns during seizure evolution adds weight to the notion of determinism in the evolution of brain dynamics (Schindler et al., 2011) and therefore provides important evidence for the validity of the dynamical systems approaches employed in Chapters 3 and 4.

Interestingly, the differences in distributions were not restricted to seizure periods, with inter-ictal epochs also displaying a degree of within-patient similarity (e.g. third entry in Table 6.2), although these were less pronounced than the seizure epochs. Thus, we have presented evidence for the conservation of EEG patterns in inter-ictal periods. An interesting future investigation will be to examine if this degree of conservation is also present in control subjects without absence epilepsy. Evidence to the contrary could support an ongoing pathological spatio-temporal dynamics for absence seizure patients. Also of interest was the deviation of these distributions from the random case, which was shown not to be due to the asymmetry in distribution sizes. This suggests that scalp EEG patterns in general are somehow constrained. This could be due, for example, to reference effects or consistent head geometry. It will be interesting to test these hypotheses further in future studies.

The methods presented, which enable the quantitative comparison of spatio-temporal patterns in epileptic multivariate time series are of general importance in epilepsy research for a number of reasons. Firstly, they facilitate a meaningful comparison between complex spatio-temporal patterns in different seizures and thus reveal their degree of consistency or difference (McKeown et al., 1999). While traditionally comparisons in the morphology of univariate properties are employed in the classification of epilepsy syndromes, quantitative comparisons based on bivariate properties have also been shown to be potentially useful (Dondey, 1983). Secondly, the proposed multivariate method allows the quantitative comparison between ictal spatio-temporal patterns in clinical EEG data and simulation output from spatially extended models of brain activity. Current models are typically univariate and make comparisons to clinical data using the qualitative properties of single channels (for absence seizure modelling see e.g. Suffczynski et al. (2004), Breakspear et al. (2006),

Marten et al. (2009a) and references therein). Although these models provide much insight into temporal brain dynamics, information derived from spatially extended models is required to appreciate the full extent of spatio-temporal diversity in the epileptic domain.

Absence seizures are characterised by the appearance on the EEG of spike and slow wave discharges, a feature that has been the object of representation of various mean field computer models, e.g. (Breakspear et al., 2006; Marten et al., 2009a). However, the conservation of spatio-temporal patterns reported in Figure 6.10 additionally suggests a manifestation of the underlying mechanisms in the spatial distribution of the SWDs (not only in their univariate morphology). Similar considerations hold for the so-called partial seizures where epileptic activity only appears in a subset of scalp channels. Apart from epileptic EEG, other research dealing with spatio-temporal aspects of the EEG, e.g. the study of sleep patterns and its disorders, might benefit from the present approach.

In extracting and visualising spatio-temporal patterns from clinical EEG, the choice of reference is known to affect the patterns observed. Indeed, the problem of referencing in analysis of spatio-temporal EEG data is well known. A particular problem is that of contamination of electrode recordings by common reference effects or long range activity. Nunez estimated that only half of the contribution to a scalp electrode recording comes from within a $3cm$ local region (Nunez et al., 1997). Laplacian methods (such as the Hjorth montage used here) aim to extract a time series at each electrode more closely related to proximal sources (Nunez and Pilgreen, 1991), and therefore give a better spatial resolution of activity. The effects of choice of reference have been investigated in a number of studies in relation to seizures with SWD. Rodin and Cornellier (1989), for example, examined seizure data in linked earlobes, common average and source derivation (Hjorth) montage. The source derivation approach was shown to reveal more complex spatio-temporal patterns, and there was a clear difference in SWD patterns between the three methods.

Traditionally, in EEG analysis, measures of channel association are used to investigate the degree of "functional connectivity" between regions from which they are recorded. We must therefore stress that although we have employed an interrelation measure in the method presented, our aim is not to use the results to make direct inference regarding associations between underlying brain activity. The use of the correlation measure in this context is purely to extract spatio-temporal patterns in order for them to be more succinctly represented and quantitatively compared. In this sense, the correlation measure we use is solely a means of quantifying the degree of co-morphology of waveforms. It is also important to note that the estimate of number of clusters is reliant on the correlation structure of the surrogate data sets, which have previously been described as embodying "random correlations" (Müller et al., 2005). We must therefore remember that both the correlation structure and

the channel auto-correlation contribute to the outcome of the map in the case of cluster estimation.

For these reasons we make no inference from the number of clusters found or the allocation of channels to clusters in terms of underlying brain function or connectivity. However, it is interesting to note that not one of the seizures analysed resulted in a single cluster, as would be expected in an event that is perfectly synchronised across the cortex. While the fact that more than one cluster is found in absence seizures may appear surprising at first glance it is entirely consistent with the previously reported observations of time delays between SWD time series from linear measures (Cohn and Leader, 1967; Aarabi et al., 2008). Also using a correlation matrix approach, evidence for the presence of more than one correlation cluster in absence EEG has been reported (Baier et al., 2007). However, our estimation of the number of clusters based on surrogate correlations is free of any arbitrary choice of reference interval and avoids comparison of patterns with drastically different Fourier spectral properties.

6.7   Summary

In this chapter we described methods by which spatio-temporal patterns in EEG data can be vectorised and quantitatively compared. Applying these methods to EEG recordings from patients with absence seizures enabled the visualisation and quantification of the degree to which these patterns are conserved within-patient. In particular we offered further evidence that spatio-temporal patterns during absence seizures display patient-specific spatio-temporal dynamics. The methods presented in this chapter will allow the future comparison of simulated spatio-temporal patterns with empirical data and therefore assist in our search for deeper insight into the mechanisms underlying the generation of epileptic seizures.

Chapter 7

Conclusions

7.1 Summary of findings

The aim of the current thesis was to advance our understanding of the patho-physiological mechanisms that lead to the production of abnormal spatio-temporal EEG dynamics in human epilepsy. In the spirit of systems biology and the physical sciences it was assumed that these mechanisms can be investigated within the framework of dynamical systems. That is, the assumption was made that the generation of abnormal rhythms can be formulated in terms of mathematical evolution equations derived from relevant interactions and processes in the brain. Currently this is the best method by which to relate underlying mechanisms to the production of measurable brain activity (Breakspear and Jirsa, 2007). The approach taken in the thesis was to model the interaction between networks of neural masses, which represent the mechanisms of spatially extended interactions in the cortex. To summarise, the main important results were as follows:

Stimulus response dynamics (Chapter 3)

It was demonstrated that long lasting and space dependent, transient response to perturbation could be produced in networks of nearest neighbour coupled neural masses with spatial heterogeneities. This provides a first mechanistic account of the observation of differential responses to spatially varying perturbations. The hypothesis generated in this study is that regions of functional abnormality exist (here diminished inhibition) which imbue certain regions of tissue with the capability to produce prolonged oscillations by direct stimulation. It is proposed that these "abnormal" regions posses different dynamics in relation to equivalent input levels, as received to the EPSP of populations of principal neurons. In the backdrop of "normal" excitable media, this can cause the persistent activation of neural tissue.

Dynamic intermittency for rhythmic transitions (Chapter 4)

It was demonstrated that a model with "background" and "seizure" dynamics could make autonomous transitions between these two states in spatially extended systems. The mechanism in the model relates to the transient synchronisation of excitable neural masses and subsequent de-synchronisation by invasion of the "noisy" background rhythm. Thus it is proposed that spontaneous transitions to seizure activity from background can be caused by the activation of intrinsic excitability dynamics in "normally" functioning regions due to the persistent activation of certain dynamics in other neural masses. This model therefore predicts the importance of spatially distributed masses which are more prone to abnormal oscillations. This is verified by the presence of "microseizures" in human epilepsy (Stead et al., 2010).

Uni-modal firing can underpin SWD (Chapter 5)

It was demonstrated that, when the laminar distribution of neural mass activity is taken into account, the uni-modal dynamics presumed to underlie surface SWD can produce a multi-modal waveform. This highlights important problems in the macroscopic modelling of EEG rhythms and offers some initial solutions to a specific problem in relation to modelling SWD.

New tools for comparing spatio-temporal patterns (Chapter 6)

The problem of comparison of spatio-temporal patterns was highlighted and new approaches tested on EEG data from patients with absence epilepsy. Using these methods, a conservation of patterns during seizure periods was found. The comparison of spatio-temporal patterns by feature vector distance will be important in future for verification of spatially extended models of clinical data.

7.2 General considerations on the modelling approach

The modelling approach employed in Chapters 3 and 4 proceeded from several important simplifying assumptions, which therefore must be examined in light of the results obtained. Firstly, the *level* of formulation of these mechanisms was chosen to be at the macroscopic scale in order for the system to be tractable in terms of computation and the exploration of parameter sets, and so that the measurable output of the system resided at the same level as the production of clinical data. Secondly, a spatially extended formulation was found to be important in this framework. The approach in this direction was also a simplified or abstracted one in which EEG generation was assumed to be underpinned by coupled local units.

Regarding the first point, it is the author's opinion that lumped or macroscopic models of brain activity are currently an essential means of interrogating the dynamics of brain activity recorded in clinical scenarios. Perhaps the most crucial reason for this is that the processes must be abstracted to a degree that enables a conceptual formulation to be made of the processes under question. The alternative and often employed tools with which to understand brain activity are microscopic models containing single neuronal elements. In reality, addressing the problem of rhythm generation at either of these scales has its advantages and disadvantages, which are summarised in Table 7.1. It is important to note that these advantages and disadvantages also exist in the context of understanding treatment in the clinical setting. The models referred to in Table 7.1 are those which embody a notion of physiologically relevant parameters or variables. Many other more abstract models can be used to address specific problems in epilepsy such as the distribution of seizure events, or the theoretical modes for intervention via stimulation, for example (Kalitzin et al., 2010).

Clearly the choice of scale for modelling studies depends on the questions to be addressed and the observable data to be investigated. In the case of clinical epilepsy data, and with questions regarding the role of connectivity in spatially extended systems for the production of EEG rhythms, the macroscopic scale provides an essential starting point. However, clear disadvantages in this setting are i) the lack of direct mechanistic interpretations of the effects of treatment and ii) the lack of a direct and completely understood link between the output of activity based macroscopic models and the EEG. Regarding the first point, the models are still useful as abstract and relativistic inference on the important components of the system can be made. The second point is an important shortcoming of the approach currently, and is an important direction for future research. Recent exposure of this problem has been given by Truccolo et al. (2011), in which the link between firing activity of neuronal populations and observed EEG rhythms were shown to be non-trivial in human epilepsy. The details of this link will be crucial to ascertain in future applications of population firing rate based models for the production of EEG.

Given the choice of macroscopic models to model the generation of spatio-temporal rhythms we must address the relevance of the coupled network node approach. Clearly this is a crude approximation to the dynamics of spatially extended nervous tissue, given that the latter is formed by spatially continuous synaptic interactions. However, the conceptual model of the cortical column provides a hint that certain functional oscillatory units may exist (Mountcastle, 1997), although the accuracy of this assumption is unknown (da Costa and Martin, 2010). Despite the potential shortcomings, there are clear questions that can be addressed within this framework. For example, abnormal oscillations have been observed in human epilepsy in recordings from electrodes of the order of 40 μm diameter which suggests

Microscopic		Advantages	Disadvantages
Components	Single neurons.	Fundamental network communication unit.	Often unmeasurable clinically. Require $O(10^6)$ for EEG generation. This is intractable computationally and conceptually.
Parameters	Membrane electrical properties and synaptic mechanisms.	Detailed pharmacological effects. Measurable and interpretable parameters.	Unmeasurable in humans (*in vivo*). Variability in space unknown (though can distribute probabilistically).
Networks	Coupled neurons	Detailed information transfer mechanisms and dynamics.	Omitted details become important when inference is made on emergent network properties due to detailed models

Macroscopic		Advantages	Disadvantages
Components	Neuronal populations.	Closer to EEG generation (which is clinically measurable). Good coverage of clinically relevant sizes of nervous tissue.	Link between population activity and EEG is not trivial and is incompletely understood.
Parameters	Lumped parameters. Abstract representations of synaptic time courses, gains and connectivities.	Relative exploration of parameters enabled by reduced complexity of the model.	No mechanistic link to fundamental processes. Only relativistic interpretation of the effects of parameter changes e.g. by intervention.
Networks	Coupled oscillators	Good coverage of clinically relevant sizes of nervous tissue. Effect of coupled oscillators directly investigated. Can investigate large scale network connectivity.	Synchronisation properties within the neural mass are unmodelled. Connectivity is lumped between separate nodes

Table 7.1: Comparison of the microscopic and macroscopic modelling approaches.

that functionally isolated rhythms do emerge. One can then ask, within this framework of the emergence of abnormal rhythms, how do these synchronise or spread to produce visible abnormalities at a larger spatial scale. Essentially, these are the questions asked in Chapters 3 and 4. In answering these questions importance was placed upon the mechanism of dynamic excitability at the macroscopic scale.

7.3   Neural mass excitability

The autonomous transitions observed in our two models rely on the principle of excitability in spatially extended systems. Crucially, in the systems presented here, the excitable components are neural masses. The idea of neural mass excitability is a natural cross-scale extension of the paroxysmal depolarisation shift (PDS), which led to the coining of the term population PDS (pPDS) in Chapter 3. This is the very principle that is thought to underlie the production of inter-ictal spikes, which are considered an archetypal feature of abnormal synchronisation in epileptic tissue (McCormick and Contreras, 2001) (although it is assumed that the mechanisms of inter-ictal spikes are not directly related to seizure mechanisms). The transmission of the excitation response between neural masses makes use of the conceptualisation of a neural mass as an input to output converter. The formalism employed usually takes input into a dendritic pulse-to-wave conversion and therefore provides a useful theoretical link between the micro- and macro- scales (see Chapter 2). This has allowed, in the current thesis, to examine the effect of neural mass output in spatially extended systems, via connection of mass output to the input of other masses.

Exploring macroscopic rhythms generated by excitable neural masses leads to new avenues of research into epileptiform EEG. Firstly, it suggests that one should seek the neuronal and neural network properties that imbue a local population of neurons with the capability to give a non-linear threshold response. Traditionally, single neural mass populations are formulated as linear systems, for example as second order linear impulse responses (Freeman, 1975; Robinson et al., 1997). Since each component of the neural mass model of Jansen and Rit (1995) is linear, the excitability of this model, and its interesting non-linear dynamics, arises due to non-linear coupling in the excitatory/inhibitory feedback network. Excitability in mathematical models residing at the macroscopic scale has not been ubiquitously reported, though perhaps this is because neural mass models have not been investigated in this context. Since we consider here that the properties of neural mass excitability is important, future experimental work should aim to investigate which neuronal and neural network properties are responsible for these dynamics in nervous tissue. This defines a truly multi-scale research endeavour, in which the small scale mechanisms responsible for the emergence of macroscopic level properties (mass excitability) are sought. Indeed, we might suppose that excitability is a

truly multi-scale phenomenon, and that the current work puts this into the context of dynamical systems. In addition, the presence of certain oscillatory modes within a neural mass may be important. One should then examine, within the neural mass, which microscopic properties, for example the neural network connectivity, the presence of certain membrane currents, "pacemaker neurons", or simply external forcing, can lead to the production of these rhythms.

The latter point has relevance for multi-scale investigation in systems biology in general. The question of the relative benefits of top down or bottom up modelling is an important one in this field (Noble, 2002). Clearly different insights are obtained at different scales, and the scale at which to approach a problem is an important consideration. In the above discussion we have highlighted a potential multi-scale approach to the problem of epilepsy. The notion is that one can identify, at the macroscopic scale, important properties of the system under investigation for the production of high-level observations. In the case presented here, one such property is neural mass excitability, which has consequences for rhythm generation in spatially extended models of epilepsy. On identification of important macroscopic properties, one can proceed to investigate, at a smaller spatial scale, the components that lead to their emergence. Thus one can define an iterative scheme for the investigation of complex, multi-scale biological systems in the spirit of "middle-out" systems biology (Noble, 2002).

7.4 The importance of network connectivity and spatial heterogeneity

Another important new direction in the work undertaken in this thesis is that *heterogeneities* in macroscopic formulations of brain dynamics were modelled, and their effects on rhythm emergence investigated. This is clearly an important advance as it allows many important new questions regarding epilepsy to be investigated, such as the role of spatially varying functional and structural abnormalities and the modes of transition from isolated, sub-clinical microseizures to full clinical seizures. It also allows one to reframe the emergence of rhythms from single neural mass dynamics to self-organising dynamics in networks of connected brain regions. Perhaps most crucially we present new conceptual frameworks for *icto-* and *epilepto-genesis*. In particular, these concepts, in the spatially extended neural mass model framework, are no longer restricted to the *time* domain, in that nervous tissue should become more likely to seize over time. In the new frameworks proposed in this thesis, these are now also rendered into the spatial domain, such that one may begin to think of a distribution of epileptogenic locations in space. This is demonstrated in the model of absence seizure generation by a spatially distributed system parameter which places certain network nodes into dynamics more likely to be "abnormal".

The intermittency model permits the possibility that these spatial abnormalities might be ever-present in the epileptic brain. This is in contrast to inference gleaned from previous models in which temporal changes in local excitatory or inhibitory efficacy (Wendling et al., 2002), or changes in the communication between the thalamus and cortex (Breakspear et al., 2006) are necessary for the onset of pathological rhythms. A further possibility is that *spatial ictogenesis* presents a hybrid of these two approaches in which the pre-ictal state is defined by certain spatially localised regions of nervous tissue changing parameters in the pathological direction, which imbues the locally connected network with self-organising, seizure generation potential. Much evidence exists for the spatial ictogenesis model. For example in WAG/Rij (Lüttjohann et al., 2011) and GAERS (Polack et al., 2007) models of absence seizures, some deep cortical layers of the somatosensory cortex are thought to be ictogenic. In addition, abnormal spatially restricted activity has been observed in human epilepsy at small spatial scales (Stead et al., 2010).

In this thesis, epileptiform rhythm generation is placed firmly in the domain of network dynamics. A major implication of this is that one should clearly address the following two mechanistic components, namely i) the network connectivity structure and ii) the (heterogeneous) distribution of intrinsic node dynamics. Clearly in evaluating the role of these components, one should aim to conduct validating experiments *in vitro* and *in vivo*. Thus, future experimental direction in epilepsy research should be placed upon i) evaluating intra-cortical and cortico-cortical connectivity and ii) evaluating the repertoire of intrinsic neural mass dynamics. The first point is currently being addressed at large scales by diffusion tensor imaging, whilst at the local level, studying the response of neurons to photo-stimulation of their counterparts can be utilised to map the probability of connectivity with respect to distance (Boucsein et al., 2011). Regarding the second point, emphasis should be placed on determining the extent to which local neural masses are excitable to stimuli and how this varies across nervous tissue and across normal and epileptic brains. Work in this direction has been undertaken recently (Lüttjohann et al., 2011). In general we should explore the oscillatory repertoire and stimulus responses of local masses, i.e. at the mesoscopic scale. This will ensure that our models of node dynamics are relevant for investigation of network connectivity in epilepsy. This clearly puts emphasis on the active probing of tissue rather than the passive observation of rhythms in different states (Suffczynski et al., 2008; Kalitzin et al., 2010), and in turn has implications for our models of ictogenisis, as expanded below and discussed by Lopes da Silva et al. (2003a) and Milton (2010), for example.

7.5 Modes of transition to seizure activity

A further implication of the current thesis is in relation to our abstract conceptualisation of dynamic models of transition in epilepsy. Two predominant models in this context are i) the presence of a normal and a pathological attractor (bistability) and ii) the formation of new attractors due to shifts in underlying parameters (bifurcations). These models have been examined in single location neural mass formulations (Suffczynski et al., 2004; Breakspear et al., 2006) as well as in spatially extended models (Kramer et al., 2005; Shusterman and Troy, 2008; Kim et al., 2009). An important finding in the current thesis was the presence of intermittency in a physiologically motivated neural mass model. This mode of transition had previously been alluded to for seizures though was proposed not to be present in models of neural interactions (Kalitzin et al., 2010). One of the appealing properties of the intermittent mode of transition proposed in Chapter 4 is that it relies on mechanisms of synchronisation and excitability. The former is often assumed for large amplitude rhythmic activity seen on the EEG and is often explicit in definitions of epileptic activity as being underpinned by abnormal synchrony. In this context, the findings of Chapter 4 give new conceptual foundations for studying the mechanisms of ictogenesis.

Combined with the model of Chapter 3, new emphasis is placed upon *transient* dynamics as a model for epileptiform rhythms. In the case of Chapter 4 these rhythms are transient excursions into a certain region of the brain attractor, whereas Chapter 3 supposes a transient deviation between rest states. The latter is therefore an example of a case in which stable phase space entities will not inform completely on the waveform generated by this transient excursion. From the dynamical systems perspective, the current thesis suggests a shift in emphasis from the study of stable structures to also include transient phase space trajectories and separatrices (unstable manifolds). These will explain the excitability of the nodes and the waveforms of transient rhythms that are expected to emerge due to transient self-organisation.

The idea that epileptiform activity could be underpinned by transient dynamics, rather than stable attractors has also recently been proposed by Milton et al. (2011). In this case, the mechanism for transient dynamics is based on the presence of metastability in neuronal systems with delays (Milton et al., 2010). In particular, this mechanism has been used to describe seizures which occur at the transition between macroscopic states (Milton et al., 2011). In an abstract formulation, a transient limit cycle could be observed when the system switched between two fixed points. In the context of epilepsy, a general dynamical mechanism might be the emergence of bistability at the cusp of evolution of a new stable state, and the emergence of metastable dynamics around the burgeoning separatrix.

The idea that epileptiform events can be modelled as complex transients has important implications. First of all it suggests that we might have to fundamentally

re-structure our analysis of dynamical systems with respect to inference regarding the mechanisms of epilepsy. In particular, it would no longer be sufficient to show that a certain stable structure in phase space exists. Rather, one would have to demonstrate the existence of a transient phase space trajectory with relevant features in comparison to clinical or experimental data. Thus, a numerical continuation approach in which stable structures are mapped over changing parameters, or the use of prolonged numerical simulation to demonstrate the long-term behaviour of a system will not be sufficient. An additional property of interest will be to map the response of a system to perturbation. Interestingly, this brings the study of dynamical systems more closely into line with our experimental and human systems of interest wherein the observation of complex transient responses to stimulation are ubiquitous (Penfield and Jasper, 1954; Lüttjohann et al., 2011).

Indeed, this shift in emphasis will also require changes in the way in which experiments into, and observation of, epilepsy are conducted. It may become apparent that the analysis of spontaneous transitions might not give enough information to characterise system dynamics in epilepsy. The transients present in real epilepsy systems will need to be explored by stimulation. Crucially, since we are motivated by the use of spatially extended neural mass models, the spatio-temporal dynamics of stimulus responses will need to be analysed and catalogued. This is in line with recent model based suggestions that active stimulation paradigms might be more appropriate for predicting the onset of seizure activity (Suffczynski et al., 2008).

7.6 The analysis of spatio-temporal patterns

Finally, we also addressed the problem of the quantitative comparison of spatio-temporal patterns. If it is accepted that seizures can be defined in terms of changes in spatio-temporal patterns our models and data analysis should exist in the spatio-temporal domain. In future it will not be sufficient to demonstrate the emergence of a certain uni-variate rhythm in models of epileptiform activity. In addition to the aforementioned investigations of the stimulation response dynamics, it will also be required to classify these rhythms in the spatio-temporal domain. To this end, we have demonstrated the application of measures derived from the eigenvectors of the correlation matrix. In reality, this analysis represents just one important feature of these patterns, which derives from the interrelations between channels. In future, a more comprehensive description of epileptiform spatio-temporal patterns will be given by at least one other feature, namely the distribution of frequencies. Together with the amplitude of waveforms, these features represent the fundamental aspects of epileptiform rhythms. Thus, in future the characterisation of EEG rhythms by these features and their quantitative comparison in 2 or 3 dimensional feature vector distance space should be explored.

Bibliography

Aarabi, A., Wallois, F., Grebe, R., 2008. Does spatiotemporal synchronization of EEG change prior to absence seizures? Brain Res. 1188, 207–221.

Adhikari, M. H., Heeroma, J. H., di Bernardo, M., Krauskopf, B., Richardson, M. P., Walker, M. C., Terry, J. R., 2009. Characterisation of cortical activity in response to deep brain stimulation of ventral-lateral nucleus: modelling and experiment. J Neurosci Methods 183 (1), 77–85.

Akman, O., Demiralp, T., Ates, N., Onat, F. Y., 2010. Electroencephalographic differences between WAG/Rij and GAERS rat models of absence epilepsy. Epilepsy Research 89 (2-3), 185–193.

Amari, S., 1977. Dynamics of pattern formation in lateral-inhibition type neural fields. Biol Cybern 27 (2), 77–87.

Amor, F., Rudrauf, D., Navarro, V., N'diaye, K., Garnero, L., Martinerie, J., Le Van Quyen, M., 2005. Imaging brain synchrony at high spatio-temporal resolution: application to meg signals during absence seizures. Signal Process. 85 (11), 2101–2111.

Anderson, W. S., Kudela, P., Cho, J., Bergey, G. K., Franaszczuk, P. J., 2007. Studies of stimulus parameters for seizure disruption using neural network simulations. Biol Cybern 97 (2), 173–94.

Anderson, W. S., Kudela, P., Weinberg, S., Bergey, G. K., Franaszczuk, P. J., 2009. Phase-dependent stimulation effects on bursting activity in a neural network cortical simulation. Epilepsy Res 84 (1), 42–55.

Avitan, L., Teicher, M., Abeles, M., 2009. EEG generator–a model of potentials in a volume conductor. J Neurophysiol 102 (5), 3046–59.

Babajani-Feremi, A., Soltanian-Zadeh, H., 2010. Multi-area neural mass modeling of EEG and MEG signals. NeuroImage , 1–19.

Bai, L., Huang, X., Yang, Q., Wu, J.-Y., 2006. Spatiotemporal patterns of an evoked network oscillation in neocortical slices: coupled local oscillators. J Neurophysiol 96 (5), 2528–38.

Baier, G., Müller, M., Stephani, U., Muhle, H., 2007. Characterizing correlation changes of complex pattern transitions: The case of epileptic activity. Phys Lett A 363 (4), 290–296.

Bao, W., Wu, J.-Y., 2003. Propagating wave and irregular dynamics: spatiotemporal patterns of cholinergic theta oscillations in neocortex in vitro. J Neurophysiol 90 (1), 333–41.

Bär, M., Hildebrand, M., Eiswirth, M., Falcke, M., Engel, H., Neufeld, M., 1994. Chemical turbulence and standing waves in a surface reaction model: the influence of global coupling and wave instabilities. Chaos 4, 499–508.

Bazhenov, M., Timofeev, I., Fröhlich, F., Sejnowski, T. J., 2008. Cellular and network mechanisms of electrographic seizures. Drug Discov Today Dis Models 5 (1), 45–57.

Berge, P., Pomeau, Y., Vidal, C., 1987. Order within chaos: Towards a deterministic approach to turbulence. Wiley-Interscience .

Bialonski, S., Lehnertz, K., 2006. Identifying phase synchronization clusters in spatially extended dynamical systems. Phys Rev E 74 (5).

Binzegger, T., Douglas, R. J., Martin, K. A. C., 2004. A quantitative map of the circuit of cat primary visual cortex. J Neurosci 24 (39), 8441–53.

Blume, W. T., Jones, D. C., Pathak, P., 2004. Properties of after-discharges from cortical electrical stimulation in focal epilepsies. Clin Neurophysiol 115 (4), 982–9.

Blumenfeld, H., 2005. Cellular and network mechanisms of spike-wave seizures. Epilepsia 46, 21–33.

Boucsein, C., Nawrot, M. P., Schnepel, P., Aertsen, A., 2011. Beyond the cortical column: abundance and physiology of horizontal connections imply a strong role for inputs from the surround. Front Neurosci 5, 32.

Breakspear, M., Jirsa, V., 2007. Neuronal dynamics and brain connectivity. In: Jirsa, V., McIntosh, A. (Eds.), Handbook of Brain Connectivity. Vol. 12 of Understanding Complex Systems. Springer Berlin / Heidelberg, pp. 3–64.

Breakspear, M., Roberts, J. A., Terry, J. R., Rodrigues, S., Mahant, N., Robinson, P. A., 2006. A Unifying explanation of primary generalized seizures through nonlinear brain modeling and bifurcation analysis. Cereb Cortex 16, 1296–1313.

Bub, G., Tateno, K., Shrier, A., Glass, L., 2003. Spontaneous initiation and termination of complex rhythms in cardiac cell culture. J Cardiovasc Electrophysiol 14 (10 Suppl), S229–36.

Charpier, S., Leresche, N., Deniau, J., Mahon, S., Hughes, S., Crunelli, V., 1999. On the putative contribution of GABA$_B$ receptors to the electrical events occuring during spontaneous spike and wave discharges. Neuropharmacology 38 (11), 1699–1706.

Chate, H., Manneville, P., 1987. Transition to turbulence via spatio-temporal intermittency. Phys Rev Lett 58 (2), 112–115.

Chervin, R. D., Pierce, P. A., Connors, B. W., 1988. Periodicity and directionality in the propagation of epileptiform discharges across neocortex. J Neurophysiol 60 (5), 1695–713.

Coenen, A. M., Drinkenburg, W. H., Inoue, M., van Luijtelaar, E. L., 1992. Genetic models of absence epilepsy, with emphasis on the WAG/Rij strain of rats. Epilepsy Res 12 (2), 75–86.

Coenen, A. M. L., Van Luijtelaar, E. L. J. M., 2003. Genetic animal models for absence epilepsy: a review of the WAG/Rij strain of rats. Behav Genet 33 (6), 635–55.

Cohn, R., Leader, H. S., 1967. Synchronization characteristics of paroxysmal EEG activity. Electroencephalogr Clin Neurophysiol 22 (5), 421–8.

Coombes, S., Sep 2010. Large-scale neural dynamics: simple and complex. Neuroimage 52 (3), 731–9.

Cope, D. W., Di Giovanni, G., Fyson, S. J., Orbán, G., Errington, A. C., Lorincz, M. L., Gould, T. M., Carter, D. A., Crunelli, V., 2009. Enhanced tonic GABA$_A$ inhibition in typical absence epilepsy. Nat Med 15 (12), 1392–8.

Cosandier-Rimélé, D., Badier, J.-M., Chauvel, P., Wendling, F., 2007. A physiologically plausible spatio-temporal model for EEG signals recorded with intracerebral electrodes in human partial epilepsy. IEEE Trans Biomed Eng 54 (3), 380–8.

Cosandier-Rimélé, D., Merlet, I., Badier, J. M., Chauvel, P., Wendling, F., 2008. The neuronal sources of EEG: modeling of simultaneous scalp and intracerebral recordings in epilepsy. NeuroImage 42 (1), 135–46.

Cosandier-Rimélé, D., Merlet, I., Bartolomei, F., Badier, J.-M., Wendling, F., 2010. Computational modeling of epileptic activity: from cortical sources to EEG signals. J Clin Neurophysiol 27 (6), 465–70.

Crampin, E. J., Halstead, M., Hunter, P., Nielsen, P., Noble, D., Smith, N., Tawhai, M., 2004. Computational physiology and the physiome project. Exp Physiol 89 (1), 1–26.

Creutzfeldt, O., Houchin, J., 1974. Neuronal basis of EEG-waves, in Remond, A. (Ed.). Handbook of Electroencephalography and Clinical Neurophysiology, Volume 2, Part C , 3–54.

da Costa, N. M., Martin, K. A. C., 2010. Whose cortical column would that be? Front Neuroanat 4, 16.

David, O., Bastin, J., Chabardès, S., Minotti, L., Kahane, P., 2010. Studying network mechanisms using intracranial stimulation in epileptic patients. Front Syst Neurosci 4, 148.

David, O., Cosmelli, D., Friston, K. J., 2004. Evaluation of different measures of functional connectivity using a neural mass model. NeuroImage 21, 659 – 673.

David, O., Friston, K. J., 2003. A neural mass model for MEG/EEG: coupling and neuronal dynamics. Neuroimage 20 (3), 1743–55.

David, O., Harrison, L., Friston, K. J., 2005. Modelling event-related responses in the brain. NeuroImage 25 (3), 756–770.

Deco, G., Jirsa, V. K., Robinson, P. A., Breakspear, M., Friston, K., 2008. The dynamic brain: from spiking neurons to neural masses and cortical fields. PLoS Comput Biol 4 (8), e1000092.

Destexhe, A., 1998. Spike-and-wave oscillations based on the properties of $GABA_B$ receptors. J Neurosci 18 (21), 9099.

Dondey, M., 1983. Transverse topographical analysis of petit mal discharges: diagnostical and pathogenic implications. Electroencephalogr. Clin. Neurophysiol. 55 (4), 361–371.

Douglas, R. J., Martin, K. A. C., 2004. Neuronal circuits of the neocortex. Annu Rev Neurosci 27, 419–51.

Douglas, R. J., Martin, K. A. C., 2007. Recurrent neuronal circuits in the neocortex. Curr Biol 17 (13), R496–500.

Dueck, G., 1993. New optimization heuristics. J. Comput. Phys. 104 (1), 86–92.

Elger, C., Speckmann, E., 1985. Mechanisms controlling the spatial extent of epileptic foci. John Libbey, Ch. 4, pp. 45–58.

Fauser, S., Schulze-Bonhage, A., 2006. Epileptogenicity of cortical dysplasia in temporal lobe dual pathology: an electrophysiological study with invasive recordings. Brain 129 (Pt 1), 82–95.

Fauser, S., Sisodiya, S. M., Martinian, L., Thom, M., Gumbinger, C., Huppertz, H.-J., Hader, C., Strobl, K., Steinhoff, B. J., Prinz, M., Zentner, J., Schulze-Bonhage, A., 2009. Multi-focal occurrence of cortical dysplasia in epilepsy patients. Brain 132 (Pt 8), 2079–90.

Ferri, R., Iliceto, G., Carlucci, V., 1995. Topographic EEG mapping of 3/s spike-and-wave complexes during absence seizures. Ital J Neurol Sci 16 (8), 541–547.

Fisher, R. S., van Emde Boas, W., Blume, W., Elger, C., Genton, P., Lee, P., Engel, Jr, J., 2005. Epileptic seizures and epilepsy: definitions proposed by the international league against epilepsy (ILAE) and the international bureau for epilepsy (IBE). Epilepsia 46 (4), 470–2.

Fitzhugh, R., 1961. Impulses and physiological states in theoretical models of nerve membrane. Biophys J 1 (6), 445–66.

Flanagan, D., Valentín, A., García Seoane, J. J., Alarcón, G., Boyd, S. G., 2009. Single-pulse electrical stimulation helps to identify epileptogenic cortex in children. Epilepsia 50 (7), 1793–803.

Freeman, 1975. Mass action in the nervous system. Examination of the Neurophysiological Basis of Adaptive Behavior through the EEG. Academic Press, New York.

Garcia Dominguez, L., Wennberg, R. A., Gaetz, W., Cheyne, D., Snead, O. C. r., Perez Velazquez, J. L., 2005. Enhanced synchrony in epileptiform activity? local versus distant phase synchronization in generalized seizures. J Neurosci 25 (35), 8077–8084.

Gerstner, W., Kistler, W. M., 2002. Spiking neuron models: single neurons, populations, plasticity. Cambridge University Press, Cambridge, U.K.

Giaretta, D., Avoli, M., Gloor, P., 1987. Intracellular recordings in pericruciate neurons during spike and wave discharges of feline generalized penicillin epilepsy. Brain Res 405 (1), 68–79.

Gloor, P., Pellegrini, A., Kostopoulos, G. K., 1979. Effects of changes in cortical excitability upon the epileptic bursts in generalized penicillin epilepsy of the cat. Electroencephalogr Clin Neurophysiol 46 (3), 274–89.

Gloor, P., Quesney, L. F., Zumstein, H., 1977. Pathophysiology of generalized penicillin epilepsy in the cat: the role of cortical and subcortical structures. ii. topical application of penicillin to the cerebral cortex and to subcortical structures. Electroencephalogr Clin Neurophysiol 43 (1), 79–94.

Goodfellow, M., Schindler, K., Baier, G., 2011a. Intermittent spike-wave dynamics in a heterogeneous, spatially extended neural mass model. Neuroimage 55 (3), 920–32.

Goodfellow, M., Schindler, K., Baier, G., 2011b. Self-organised transients in a neural mass model of epileptogenic tissue dynamics. NeuroImage DOI: 10.1016/j.neuroimage.2011.08.060, –.

Grimbert, F., Faugeras, O., 2006. Bifurcation analysis of jansen's neural mass model. Neural Comput 18 (12), 3052–68.

Heagy, J., Platt, N., Hammel, S., 1994. Characterization of on-off intermittency. Phys Rev E Stat Nonlin Soft Matter Phys 49 (2), 1140–1150.

Hodgkin, A., Huxley, A., 1952. A quantitative description of membrane current and its application to conduction and excitation in nerve. J Physiol 117 (4), 500–544.

Hodgkin, A. L., 1948. The local electric changes associated with repetitive action in a non-medullated axon. J Physiol 107 (2), 165–81.

Holmes, M. D., Brown, M., Tucker, D. M., Dec 2004. Are "generalized" seizures truly generalized? Evidence of localized mesial frontal and frontopolar discharges in absence. Epilepsia 45 (12), 1568–79.

Holmes, M. D., Quiring, J., Tucker, D. M., 2010. Evidence that juvenile myoclonic epilepsy is a disorder of frontotemporal corticothalamic networks. Neuroimage 49 (1), 80–93.

Hrachovy, R. A., Frost, Jr, J. D., 2006. The EEG in selected generalized seizures. J Clin Neurophysiol 23 (4), 312–32.

Hramov, A., Koronovskii, A. A., Midzyanovskaya, I. S., Sitnikova, E., van Rijn, C. M., 2006. On-off intermittency in time series of spontaneous paroxysmal activity in rats with genetic absence epilepsy. Chaos 16 (4).

Huang, X., Troy, W. C., Yang, Q., Ma, H., Laing, C. R., Schiff, S. J., Wu, J.-Y., 2004. Spiral waves in disinhibited mammalian neocortex. J Neurosci 24 (44), 9897–902.

Hughes, J., Miller, J., Hughes, C., 1990. Topographic mapping of different types of bilateral spike-and-wave complexes. J Epilepsy 3 (2), 67–74.

Hunter, P., Nielsen, P., 2005. A strategy for integrative computational physiology. Physiology (Bethesda) 20, 316–25.

Hutt, M., Neff, R., 2001. Quantification of spatiotemporal phenomena by means of cellular automata techniques. Physica A 289 (3-4), 498–516.

ILAE, 1981. Proposal for revised clinical and electroencephalographic classification of epileptic seizures. from the commission on classification and terminology of the international league against epilepsy. Epilepsia 22 (4), 489–501.

ILAE, 1989. Proposal for revised classification of epilepsies and epileptic syndromes. commission on classification and terminology of the international league against epilepsy. Epilepsia 30 (4), 389–99.

Inoue, M., Duysens, J., Vossen, J. M., Coenen, A. M., 1993. Thalamic multiple-unit activity underlying spike-wave discharges in anesthetized rats. Brain Res 612 (1-2), 35–40.

Izhikevich, E. M., 2006. Dynamical Systems in Neuroscience: The Geometry of Excitability and Bursting (Computational Neuroscience), 1st Edition. The MIT Press.

Jain, A. K., Dubes, R. C., 1988. Algorithms for clustering data. Prentice-Hall, Inc., Upper Saddle River, NJ, USA.

Jansen, B., Zouridakis, G., Brandt, M., 1993. A neurophysiologically-based mathematical model of flash visual evoked potentials. Biol Cybern 68 (3), 275–283.

Jansen, B. H., Rit, V. G., 1995. Electroencephalogram and visual evoked potential generation in a mathematical model of coupled cortical columns. Biol Cybern 73, 357–366.

Jirsa, Haken, 1996. Field theory of electromagnetic brain activity. Phys Rev Lett 77 (5), 960–963.

Jung, P., Mayer-Kress, G., 1995. Noise controlled spiral growth in excitable media. Chaos 5 (2), 458–462.

Kaiser, M., Goerner, M., Hilgetag, C. C., 2007. Criticality of spreading dynamics in hierarchical cluster networks without inhibition. New J Physics 9, 110.

Kalitzin, S. N., Velis, D. N., da Silva, F. H. L., 2010. Stimulation-based anticipation and control of state transitions in the epileptic brain. Epilepsy & Behavior 17 (3), 310–323.

Kandel, A., Buzsáki, G., 1997. Cellular-synaptic generation of sleep spindles, spike-and-wave discharges, and evoked thalamocortical responses in the neocortex of the rat. J Neurosci 17 (17), 6783–97.

Kim, J. W., Roberts, J. A., Robinson, P. A., 2009. Dynamics of epileptic seizures: evolution, spreading, and suppression. J Theor Biol 257 (4), 527–32.

Kostopoulos, G., Avoli, M., Pellegrini, A., Gloor, P., 1982. Laminar analysis of spindles and of spikes of the spike and wave discharge of feline generalized penicillin epilepsy. Electroencephalogr Clin Neurophysiol 53 (1), 1–13.

Kostopoulos, G., Gloor, P., Pellegrini, A., Gotman, J., 1981. A study of the transition from spindles to spike and wave discharge in feline generalized penicillin epilepsy: microphysiological features. Exp Neurol 73 (1), 55–77.

Kramer, M. A., Kirsch, H. E., Szeri, A. J., 2005. Pathological pattern formation and cortical propagation of epileptic seizures. J R Soc Interface 2 (2), 113–27.

Kreuz, T., Mormann, F., Andrzejak, R. G., Kraskov, A., Lehnertz, K., Grassberger, P., 2007. Measuring synchronization in coupled model systems: A comparison of different approaches. Physica D 225 (1), 29 – 42.

Labyt, E., Uva, L., de Curtis, M., Wendling, F., 2006. Realistic modeling of entorhinal cortex field potentials and interpretation of epileptic activity in the guinea pig isolated brain preparation. J Neurophysiol 96, 363–377.

Laing, C., 2005. Spiral waves in nonlocal equations. Siam J Appl Dyn Syst 4 (3), 588–606.

Lemieux, J., Blume, W., 1986. Topographical evolution of spike-wave complexes. Brain Res. 373 (1-2), 275–287.

Lesser, R. P., Lee, H. W., Webber, W. R. S., Prince, B., Crone, N. E., Miglioretti, D. L., 2008. Short-term variations in response distribution to cortical stimulation. Brain 131 (Pt 6), 1528–39.

Liley, D., Cadusch, P., Dafilis, M., 2002. A spatially continuous mean field theory of electrocortical activity. Network: Computation in Neural Systems 13 (1), 67–113.

Llinás, R. R., Dec 1988. The intrinsic electrophysiological properties of mammalian neurons: insights into central nervous system function. Science 242 (4886), 1654–64.

Lopes da Silva, F., Blanes, W., Kalitzin, S. N., Parra, J., Suffczynski, P., Velis, D. N., 2003a. Epilepsies as dynamical diseases of brain systems: basic models of the transition between normal and epileptic activity. Epilepsia 44 Suppl 12, 72–83.

Lopes Da Silva, F., Hoeks, A., Smits, H., Zetterberg, L., 1974. Model of brain rhythmic activity the ralpha-rhythm of the thalamus. Kybernetik 15, 27–37.

Lopes da Silva, F. H., Blanes, W., Kalitzin, S. N., Parra, J., Suffczynski, P., Velis, D. N., 2003b. Dynamical diseases of brain systems: different routes to epileptic seizures. IEEE Trans Biomed Eng 50 (5), 540–548.

Lopour, B. A., Szeri, A. J., 2010. A model of feedback control for the charge-balanced suppression of epileptic seizures. J Comput Neurosci 28 (3), 375–87.

Lüttjohann, A., Zhang, S., de Peijper, R., van Luijtelaar, G., 2011. Electrical stimulation of the epileptic focus in absence epileptic WAG/Rij rats: assessment of local and network excitability. Neuroscience 188, 125–34.

Lytton, W. W., Stewart, M., Hines, M., 2008. Simulation of large networks: Technique and progress. In: Soltesz, I., Staley, K. (Eds.), Computational Neuroscience in Epilepsy. Academic Press, San Diego, pp. 3 – 17.

Mackey, M. C., Glass, L., 1977. Oscillation and chaos in physiological control systems. Science 197 (4300), 287–288.

Marescaux, C., Vergnes, M., 1995. Genetic absence epilepsy in rats from strasbourg (GAERS). Ital J Neurol Sci 16 (1-2), 113–8.

Marescaux, C., Vergnes, M., Depaulis, A., 1992. Genetic absence epilepsy in rats from strasbourg–a review. J Neural Transm Suppl 35, 37–69.

Markram, H., 2006. The blue brain project. Nat Rev Neurosci 7 (2), 153–60.

Marreiros, A. C., Daunizeau, J., Kiebel, S. J., Friston, K. J., Aug 2008. Population dynamics: variance and the sigmoid activation function. Neuroimage 42 (1), 147–57.

Marten, F., Rodrigues, S., Benjamin, O., Richardson, M. P., Terry, J., 2009a. Onset of polyspike complexes in a mean-field model of human electroencephalography and its application to absence epilepsy. Philos. Transact. A Math. Phys. Eng. Sci. 367 (1891), 1145–1161.

Marten, F., Rodrigues, S., Suffczynski, P., Richardson, M. P., Terry, J. R., 2009b. Derivation and analysis of an ordinary differential equation mean-field model for studying clinically recorded epilepsy dynamics. Phys Rev E Stat Nonlin Soft Matter Phys 79 (2 Pt 1), 021911.

McCormick, D. A., Contreras, D., 2001. On the cellular and network bases of epileptic seizures. Annu Rev Physiol 63, 815–46.

McKeown, M., Humphries, C., Iragui, V., Sejnowski, T., 1999. Spatially fixed patterns account for the spike and wave features in absence seizures. Brain Topogr 12 (2), 107–116.

Meeren, H. K. M., Pijn, J. P. M., Van Luijtelaar, E. L. J. M., Coenen, A. M. L., Lopes da Silva, F. H., 2002. Cortical focus drives widespread corticothalamic networks during spontaneous absence seizures in rats. J Neurosci 22 (4), 1480–95.

Meeren, H. K. M., Veening, J. G., Möderscheim, T. A. E., Coenen, A. M. L., van Luijtelaar, G., 2009. Thalamic lesions in a genetic rat model of absence epilepsy: dissociation between spike-wave discharges and sleep spindles. Exp Neurol 217 (1), 25–37.

Milton, J., Naik, P., Chan, C., Campbell, S. A., 2010. Indecision in neural decision making models. Math Model Nat Phenom 5 (2), 125–145.

Milton, J. G., 2010. Epilepsy as a dynamic disease: a tutorial of the past with an eye to the future. Epilepsy Behav 18 (1-2), 33–44.

Milton, J. G., Quan, A. R., Osorio, I., 2011. Nocturnal frontal lobe epilepsy: Metastability in a dynamic disease? in. Osorio, I. and Zaveri, H. and Frei, M.G. and Arthurs, S. (Eds.) Epilepsy: The Intersection of Neurosciences, Biology, Mathematics, Engineering, and Physics, Chapter 38 , 501–510. CRC Press.

Moeller, F., Siebner, H. R., Wolff, S., Muhle, H., Boor, R., Granert, O., Jansen, O., Stephani, U., Siniatchkin, M., 2008. Changes in activity of striato-thalamo-cortical network precede generalized spike wave discharges. Neuroimage 39 (4), 1839–49.

Moran, R. J., Kiebel, S. J., Stephan, K. E., Reilly, R. B., Daunizeau, J., Friston, K. J., 2007. A neural mass model of spectral responses in electrophysiology. Neuroimage 37 (3), 706–20.

Morgan, R. J., Soltesz, I., 2008. Nonrandom connectivity of the epileptic dentate gyrus predicts a major role for neuronal hubs in seizures. Proc Natl Acad Sci U S A 105 (16), 6179–84.

Mormann, F., Kreuz, T., Rieke, C., Andrzejak, R. G., Kraskov, A., David, P., Elger, C. E., Lehnertz, K., 2005. On the predictability of epileptic seizures. Clin Neurophysiol 116 (3), 569–87.

Mountcastle, V. B., 1997. The columnar organization of the neocortex. Brain 120 (Pt 4), 701–22.

Müller, M., Baier, G., Galka, A., Stephani, U., Muhle, H., 2005. Detection and characterization of changes of the correlation structure in multivariate time series. Phys. Rev. E 71 (4).

Müller, M., Baier, G., Rummel, C., Schindler, K., 2008. Estimating the strength of genuine and random correlations in non-stationary multivariate time series. Europhys. Lett. 84 (1).

Nagumo, J., Arimoto, S., Yoshizawa, S., 1962. Active pulse transmission line simulating nerve axon. P IRE 50 (10), 2061–2070.

Neckelmann, D., Amzica, F., Steriade, M., 1998. Spike-wave complexes and fast components of cortically generated seizures. iii. synchronizing mechanisms. J Neurophysiol 80 (3), 1480–94.

Netoff, T., Schiff, S., 2002. Decreased neuronal synchronization during experimental seizures. J. Neurosci. 22 (16), 7297–7307.

Niedermeyer, E., Lopes da Silva, F. H., 2005. Electroencephalography: basic principles, clinical applications, and related fields, 5th Edition. Lippincott Williams and Wilkins, Philadelphia.

Noble, D., 2002. The rise of computational biology. Nat Rev Mol Cell Biol 3 (6), 459–63.

Nunez, P., 1995. Neocortical dynamics and human EEG rhythms. Oxford University Press,.

Nunez, P. L., 1981. Electric fields of the brain : the neurophysics of EEG / Paul L. Nunez ; with contributions by Ron D. Katznelson. Oxford University Press, New York :.

Nunez, P. L., Pilgreen, K. L., 1991. The spline-laplacian in clinical neurophysiology: a method to improve EEG spatial resolution. J Clin Neurophysiol 8 (4), 397–413.

Nunez, P. L., Srinivasan, R., Westdorp, A. F., Wijesinghe, R. S., Tucker, D. M., Silberstein, R. B., Cadusch, P. J., 1997. EEG coherency. i: Statistics, reference electrode, volume conduction, laplacians, cortical imaging, and interpretation at multiple scales. Electroencephalogr Clin Neurophysiol 103 (5), 499–515.

Ohayon, E., Kalitzin, S., Suffczynski, P., Jin, F., Tsang, P., Borrett, D., Burnham, W., Kwan, H., 2004. Charting epilepsy by searching for intelligence in network space with the help of evolving autonomous agents. J Physiol 98 (4-6), 507–529.

Olejniczak, P., 2006. Neurophysiologic basis of EEG. J Clin Neurophysiol 23 (3), 186–9.

Ortega, F., Sameith, K., Turan, N., Compton, R., Trevino, V., Vannucci, M., Falciani, F., 2008. Models and computational strategies linking physiological response to molecular networks from large-scale data. Philos Transact A Math Phys Eng Sci 366 (1878), 3067–89.

Otis, T. S., De Koninck, Y., Mody, I., 1993. Characterization of synaptically elicited $GABA_B$ responses using patch-clamp recordings in rat hippocampal slices. J Physiol 463, 391–407.

Parra, J., Kalitzin, S. N., Iriarte, J., Blanes, W., Velis, D. N., Lopes da Silva, F. H., 2003. Gamma-band phase clustering and photosensitivity: is there an underlying mechanism common to photosensitive epilepsy and visual perception? Brain 126 (Pt 5), 1164–72.

Penfield, W., Jasper, H. H., 1954. Epilepsy and the functional anatomy of the human brain. Little, Brown, Boston.

Pinault, D., Leresche, N., Charpier, S., Deniau, J. M., Marescaux, C., Vergnes, M., Crunelli, V., 1998. Intracellular recordings in thalamic neurones during spontaneous spike and wave discharges in rats with absence epilepsy. J Physiol 509 (Pt 2), 449–56.

Pinault, D., O'Brien, T. J., 2005. Cellular and network mechanisms of genetically-determined absence seizures. Thalamus Relat Syst 3 (3), 181–203.

Pinsky, C., Burns, B. D., 1962. Production of epileptiform afterdischarges in cat's cerebral cortex. J Neurophysiol 25, 359–79.

Pinto, D., Ermentrout, G., 2001. Spatially structured activity in synaptically coupled neuronal networks: I. traveling fronts and pulses. Siam J Appl Math 62 (1), 206–225.

Pinto, D. J., Patrick, S. L., Huang, W. C., Connors, B. W., 2005. Initiation, propagation, and termination of epileptiform activity in rodent neocortex in vitro involve distinct mechanisms. J Neurosci 25 (36), 8131–40.

Plerou, V., Gopikrishnan, P., Rosenow, B., Amaral, L., Guhr, T., Stanley, H., 2002. Random matrix approach to cross correlations in financial data. Phys Rev E Stat Nonlin Soft Matter Phys 65 (6), 066126.

Polack, P.-O., Guillemain, I., Hu, E., Deransart, C., Depaulis, A., Charpier, S., 2007. Deep layer somatosensory cortical neurons initiate spike-and-wave discharges in a genetic model of absence seizures. J Neurosci 27 (24), 6590–9.

Polack, P.-O., Mahon, S., Chavez, M., Charpier, S., 2009. Inactivation of the somatosensory cortex prevents paroxysmal oscillations in cortical and related thalamic neurons in a genetic model of absence epilepsy. Cereb Cortex 19 (9), 2078–91.

Ponten, S. C., Douw, L., Bartolomei, F., Reijneveld, J. C., Stam, C. J., 2009. Indications for network regularization during absence seizures: Weighted and unweighted graph theoretical analyses. Exp Neurol 217 (1), 197–204.

Prince, D. A., Parada, I., Scalise, K., Graber, K., Jin, X., Shen, F., 2009. Epilepsy following cortical injury: cellular and molecular mechanisms as targets for potential prophylaxis. Epilepsia 50 Suppl 2, 30–40.

Robinson, P., Rennie, C., Rowe, D., 2002. Dynamics of large-scale brain activity in normal arousal states and epileptic seizures. Phys Rev E 65 (4), 041924.

Robinson, P., Rennie, C., Wright, J., 1997. Propagation and stability of waves of electrical activity in the cerebral cortex. Phys Rev E 56 (1), 826–840.

Rodin, E., 1999. Decomposition and mapping of generalized spike-wave complexes. Clin. Neurophysiol. 110 (11), 1868–1875.

Rodin, E., Ancheta, O., 1987. Cerebral electrical fields during petit-mal abscences. Electroencephalogr. Clin. Neurophysiol. 66 (6), 457–466.

Rodin, E., Cornellier, D., 1989. Source derivation recordings of generalized spike-wave complexes. Electroencephalogr Clin Neurophysiol 73 (1), 20–9.

Rodin, E. A., Rodin, M. K., Thompson, J. A., 1994. Source analysis of generalized spike-wave complexes. Brain Topogr 7 (2), 113–9.

Rosenow, F., Lüders, H., Sep 2001. Presurgical evaluation of epilepsy. Brain 124 (Pt 9), 1683–700.

Rummel, C., 2008. Quantification of intra- and inter-cluster relations in nonstationary and noisy data. Phys. Rev. E 77 (1).

Rummel, C., Baier, G., Müller, M., 2007. Automated detection of time-dependent cross-correlation clusters in nonstationary time series. Europhys. Lett. 80 (6).

Rummel, C., Müller, M., Schindler, K., 2008. Data-driven estimates of the number of clusters in multivariate time series. Phys. Rev. E 78 (6), 066703.

Sadleir, L. G., Farrell, K., Smith, S., Connolly, M. B., Scheffer, I. E., 2006. Electroclinical features of absence seizures in childhood absence epilepsy. Neurology 67 (3), 413–8.

Sargsyan, A., Sitnikova, E., Melkonyan, A., Mkrtchian, H., van Luijtelaar, G., 2007. Simulation of sleep spindles and spike and wave discharges using a novel method for the calculation of field potentials in rats. J Neurosci Methods 164 (1), 161–76.

Schaul, N., 1998. The fundamental neural mechanisms of electroencephalography. Electroencephalogr Clin Neurophysiol 106 (2), 101–7.

Schevon, C. A., Goodman, R. R., McKhann, Jr, G., Emerson, R. G., 2010. Propagation of epileptiform activity on a submillimeter scale. J Clin Neurophysiol 27 (6), 406–11.

Schiff, S. J., Huang, X., Wu, J.-Y., 2007. Dynamical evolution of spatiotemporal patterns in mammalian middle cortex. Phys Rev Lett 98 (17), 178102.

Schindler, K., Gast, H., Stieglitz, L., Stibal, A., Hauf, M., Wiest, R., Mariani, L., Rummel, C., 2011. Forbidden ordinal patterns of periictal intracranial eeg indicate deterministic dynamics in human epileptic seizures. Epilepsia. 10.1111/j.1528-1167.2011.03202.x .

Shusterman, V., Troy, W. C., 2008. From baseline to epileptiform activity: a path to synchronized rhythmicity in large-scale neural networks. Phys Rev E Stat Nonlin Soft Matter Phys 77 (6 Pt 1), 061911.

Snead, 3rd, O. C., Feb 1995. Basic mechanisms of generalized absence seizures. Ann Neurol 37 (2), 146–57.

Sotero, R. C., Trujillo-Barreto, N. J., Iturria-Medina, Y., Carbonell, F., Jimenez, J. C., 2007. Realistically coupled neural mass models can generate EEG rhythms. Neural Comput 19 (2), 478–512.

Spiegler, A., Kiebel, S. J., Atay, F. M., Knösche, T. R., 2010. Bifurcation analysis of neural mass models: Impact of extrinsic inputs and dendritic time constants. Neuroimage 52 (3), 1041–58.

Stead, M., Bower, M., Brinkmann, B. H., Lee, K., Marsh, W. R., Meyer, F. B., Litt, B., Van Gompel, J., Worrell, G. A., 2010. Microseizures and the spatiotemporal scales of human partial epilepsy. Brain 133 (9), 2789–97.

Steriade, M., Amzica, F., 1994. Dynamic coupling among neocortical neurons during evoked and spontaneous spike-wave seizure activity. Journal of Neurophysiology 72 (5), 2051–2069.

Steriade, M., Amzica, F., Neckelmann, D., Timofeev, I., 1998a. Spike-wave complexes and fast components of cortically generated seizures. ii. extra- and intracellular patterns. J Neurophysiol 80 (3), 1456–79.

Steriade, M., Contreras, D., 1998. Spike-wave complexes and fast components of cortically generated seizures. i. role of neocortex and thalamus. J Neurophysiol 80 (3), 1439–55.

Strogatz, S. H., 1994. Nonlinear Dynamics And Chaos: With Applications To Physics, Biology, Chemistry, And Engineering (Studies in Nonlinearity), 1st Edition. Studies in nonlinearity. Perseus Books Group.

Suffczynski, P., Kalitzin, S., da Silva, F. L., Parra, J., Velis, D., Wendling, F., 2008. Active paradigms of seizure anticipation: computer model evidence for necessity of stimulation. Phys Rev E 78 (5 Pt 1), 051917.

Suffczynski, P., Kalitzin, S., Lopes Da Silva, F., 2004. Dynamics of non-convulsive epileptic phenomena modeled by a bistable neuronal network. Neuroscience 126 (2), 467–484.

Suffczynski, P., Lopes da Silva, F. H., Parra, J., Velis, D. N., Bouwman, B. M., van Rijn, C. M., van Hese, P., Boon, P., Khosravani, H., Derchansky, M., Carlen, P., Kalitzin, S., 2006a. Dynamics of epileptic phenomena determined from statistics of ictal transitions. IEEE Trans Biomed Eng 53 (3), 524–32.

Suffczynski, P., Wendling, F., Bellanger, J., Da Silva, F., 2006b. Some insights into computational models of (patho)physiological brain activity. P IEEE 94 (4), 784–804.

Tel, T., Lai, Y.-C., 2008. Chaotic transients in spatially extended systems. Phys Rep 460 (6), 245–275.

Thomson, A. M., Deuchars, J., 1997. Synaptic interactions in neocortical local circuits: dual intracellular recordings in vitro. Cereb Cortex 7 (6), 510–22.

Timofeev, I., Grenier, F., Steriade, M., 2004. Contribution of intrinsic neuronal factors in the generation of cortically driven electrographic seizures. J Neurophysiol 92 (2), 1133–43.

Traub, R., Wong, R., 1982. Cellular mechanism of neuronal synchronization in epilepsy. Science 216 (4547), 745–747.

Traub, R. D., Contreras, D., Cunningham, M. O., Murray, H., LeBeau, F. E. N., Roopun, A., Bibbig, A., Wilent, W. B., Higley, M. J., Whittington, M. A., 2005. Single-column thalamocortical network model exhibiting gamma oscillations, sleep spindles, and epileptogenic bursts. J Neurophysiol 93 (4), 2194–232.

Traub, R. D., Duncan, R., Russell, A. J. C., Baldeweg, T., Tu, Y., Cunningham, M. O., Whittington, M. A., 2010. Spatiotemporal patterns of electrocorticographic very fast oscillations (> 80 Hz) consistent with a network model based on electrical coupling between principal neurons. Epilepsia 51 (8), 1587–1597.

Trevelyan, A. J., Sussillo, D., Watson, B. O., Yuste, R., 2006. Modular propagation of epileptiform activity: evidence for an inhibitory veto in neocortex. J Neurosci 26 (48), 12447–55.

Troy, W. C., Shusterman, V., 2007. Patterns and features of families of traveling waves in large-scale neuronal networks. Siam J Appl Dyn Syst 6 (1), 263–292.

Truccolo, W., Donoghue, J. A., Hochberg, L. R., Eskandar, E. N., Madsen, J. R., Anderson, W. S., Brown, E. N., Halgren, E., Cash, S. S., 2011. Single-neuron dynamics in human focal epilepsy. Nat Neurosci 14 (5), 635–41.

Ursino, M., Cona, F., Zavaglia, M., 2010. The generation of rhythms within a cortical region: analysis of a neural mass model. Neuroimage 52 (3), 1080–94.

Valentín, A., Alarcón, G., García-Seoane, J. J., Lacruz, M. E., Nayak, S. D., Honavar, M., Selway, R. P., Binnie, C. D., Polkey, C. E., 2005. Single-pulse electrical stimulation identifies epileptogenic frontal cortex in the human brain. Neurology 65 (3), 426–35.

Valentin, A., Anderson, M., Alarcon, G., Seoane, J. J. G., Selway, R., Binnie, C. D., Polkey, C. E., 2002. Responses to single pulse electrical stimulation identify epileptogenesis in the human brain in vivo. Brain 125, 1709–1718.

Velazquez, J., Cortez, M., Snead, O., Wennberg, R., 2003. Dynamical regimes underlying epileptiform events: role of instabilities and bifurcations in brain activity. Physica D 186 (3-4), 205–220.

Velazquez, J. L., Khosravani, H., Lozano, A., Bardakjian, B. L., Carlen, P. L., Wennberg, R., 1999. Type iii intermittency in human partial epilepsy. Eur J Neurosci 11 (7), 2571–6.

Weir, B., 1965. The morphology of the spike-wave complex. Electroencephalogr Clin Neurophysiol 19 (3), 284–290.

Wendling, F., Bartolomei, F., Bellanger, J., Chauvel, P., 2002. Epileptic fast activity can be explained by a model of impaired GABAergic dendritic inhibition. Eur J Neurosci 15 (9), 1499–1508.

Wendling, F., Bartolomei, F., Bellanger, J. J., Chauvel, P., 2001. Interpretation of interdependencies in epileptic signals using a macroscopic physiological model of the EEG. Clin Neurophysiol 112 (7), 1201–18.

Wendling, F., Bellanger, J. J., Bartolomei, F., Chauvel, P., 2000. Relevance of nonlinear lumped-parameter models in the analysis of depth-EEG epileptic signals. Biol Cybern 83 (4), 367–78.

Westmijse, I., Ossenblok, P., Gunning, B., van Luijtelaar, G., 2009. Onset and propagation of spike and slow wave discharges in human absence epilepsy: A MEG study. Epilepsia 50 (12), 2538–48.

Wilson, H. R., Cowan, J. D., 1973. A mathematical theory of the functional dynamics of cortical and thalamic nervous tissue. Kybernetik 13 (2), 55–80.

Winfree, A. T., 2001. The Geometry of Biological Time, 2nd Edition. Springer.

Woermann, F., Free, S., Koepp, M., Sisodiya, S., Duncan, J., 1999. Abnormal cerebral structure in juvenile myoclonic epilepsy demonstrated with voxel-based analysis of MRI. Brain 122, 2101–2107.

Wright, J. J., Sergejew, A. A., Liley, D. T., May 1994. Computer simulation of electrocortical activity at millimetric scale. Electroencephalogr Clin Neurophysiol 90 (5), 365–75.

Wu, J.-Y., Huang, X., Zhang, C., 2008. Propagating waves of activity in the neocortex: what they are, what they do. Neuroscientist 14 (5), 487–502.

Yoshinaga, H., Kobayashi, K., Sato, M., Oka, E., Ohtahara, S., 1996. Investigation of bilateral synchronous spike-wave discharge by EEG topography. Brain Topogr. 8 (3), 255–260.

Zimmermann, M., Firle, S., Natiello, M., Hildebrand, M., Eiswirth, M., Bar, M., Bangia, A., Kevrekidis, I., 1997. Pulse bifurcation and transition to spatiotemporal chaos in an excitable reaction-diffusion model. Physica D 110 (1-2), 92–104.